



**Politecnico  
di Torino**

**Politecnico di Torino**

Master of Science in

Energy and Nuclear Engineering – Renewable Energy Systems

Academic Year 2022/2023

July 2023

**Aluminium redox cycles: modeling and  
preliminary experimental assessment of  
an innovative process for energy storage**

Supervisors:

Massimo Santarelli

Domenico Ferrero

Francesco Orsini

Candidate:

Christian Panero

*A mamma e papà,*

*per il supporto costante e incondizionato sempre dimostratomi*

*To my mother and father,*

*for the constant and full support always demonstrated to me*

# Contents

<b>CONTENTS</b> .....	<b>3</b>
<b>LIST OF FIGURES</b> .....	<b>6</b>
<b>LIST OF TABLES</b> .....	<b>10</b>
<b>ACRONYMS</b> .....	<b>11</b>
<b>ABSTRACT</b> .....	<b>12</b>
<b>1 INTRODUCTION</b> .....	<b>13</b>
1.1 GENERAL BACKGROUND .....	13
1.2 AIM OF THIS THESIS.....	14
<b>2 REACTIVE METALS AS ENERGY CARRIERS</b> .....	<b>16</b>
2.1 METALS AS ELECTROFUELS: THE CIRCULAR PERSPECTIVE .....	16
2.2 PROPERTIES OF METALS AS ENERGY CARRIERS.....	18
2.3 POSSIBLE ROUTES TO HARNESS ENERGY FROM METALS .....	20
2.3.1 <i>Wet cycle</i> .....	21
2.3.2 <i>Dry cycle</i> .....	23
2.4 ALUMINIUM AS A PROMISING ELECTROFUEL .....	24
2.4.1 <i>Advantages and applications</i> .....	24
2.4.2 <i>Current and future production methods</i> .....	25
2.4.3 <i>The REVEAL project</i> .....	27
<b>3 THERMODYNAMIC ANALYSIS</b> .....	<b>28</b>
3.1 REACTION OF ALUMINIUM WITH WATER .....	28
3.1.1 <i>Energy and mass balance</i> .....	28
3.1.2 <i>Kinetics and reaction mechanism</i> .....	32
3.2 ELECTROCHEMICAL PROCESSES .....	36
3.2.1 <i>Power-to-Al</i> .....	36
3.2.2 <i>Electrochemical oxidation of Al</i> .....	38
<b>4 FEASIBILITY ANALYSIS: A CASE STUDY</b> .....	<b>40</b>
4.1 ALUMINIUM-FUELED POWER PLANTS: POSSIBLE SCHEMES.....	41
4.1.1 <i>Some layouts from literature</i> .....	42
4.1.2 <i>Adopted layout</i> .....	44

## Contents

4.2	DISTRICT ANALYSIS.....	44
4.2.1	<i>Assumptions and methods</i> .....	45
4.2.2	<i>Results</i> .....	52
<b>5</b>	<b>AL-TO-POWER PLANT MODEL .....</b>	<b>57</b>
5.1	COMPONENTS DESCRIPTION.....	57
5.1.1	<i>Reactor</i> .....	57
5.1.2	<i>Steam Rankine cycle</i> .....	58
5.1.3	<i>Solid oxide fuel cell</i> .....	59
5.1.4	<i>Gas turbine section</i> .....	60
5.2	MODEL BUILDING.....	60
5.2.1	<i>Reactor model</i> .....	61
5.2.2	<i>Rankine cycle model</i> .....	62
5.2.3	<i>SOFC model</i> .....	63
5.2.4	<i>Gas turbine section</i> .....	65
5.2.5	<i>Operating parameters of the reference case</i> .....	65
5.3	RESULTS.....	67
5.3.1	<i>Efficiency metrics</i> .....	67
5.3.2	<i>Complete plant</i> .....	68
5.3.3	<i>Effect of water excess</i> .....	71
5.3.4	<i>Effect of reaction temperature</i> .....	75
5.3.5	<i>Comparison with simpler layout (SOFC-GT only)</i> .....	76
<b>6</b>	<b>EXPERIMENTAL ANALYSIS .....</b>	<b>79</b>
6.1	LITERATURE REFERENCES.....	79
6.2	EXPERIMENTAL SETUP.....	80
6.3	METHODS.....	83
6.4	PRELIMINARY TESTS IN MICROREACTOR.....	84
6.4.1	<i>Microreactor – 1<sup>st</sup> test</i> .....	84
6.4.2	<i>Microreactor: 2<sup>nd</sup> test</i> .....	86
6.4.3	<i>Microreactor: 3<sup>rd</sup> test</i> .....	87
6.5	TGA TESTS – OXIDATION IN AIR.....	90
6.5.1	<i>Temperature programmed oxidation (TPO) in air</i> .....	90
6.5.2	<i>Isothermal test in air</i> .....	93
6.6	TESTS IN MICROREACTOR.....	94
6.6.1	<i>Isothermal water oxidation - 900°C</i> .....	94
6.6.2	<i>TPO in water</i> .....	96

## Contents

6.6.3	<i>Isothermal water oxidation - 950 and 1000°C</i> .....	97
6.6.4	<i>TPO in water – sample with finer particle size</i> .....	99
6.7	DISCUSSION .....	99
6.7.1	<i>Effect of temperature in isothermal oxidation</i> .....	100
6.7.2	<i>Effect of particle size</i> .....	102
7	<b>CONCLUSIONS</b> .....	<b>106</b>
8	<b>REFERENCES</b> .....	<b>108</b>

## List of figures

Figure 1. Conceptual scheme of a recyclable electrofuel. ....	17
Figure 2. Conceptual scheme of a metal fuel redox cycle. ....	17
Figure 3. Possible metals that can be theoretically used as electrofuels. Elements in green are the most interesting in practical terms. ....	18
Figure 4. Volumetric energy density and gravimetric specific energy of different metals. ....	19
Figure 5. Classification of critical raw materials according to the EU. ....	20
Figure 6. Overview of the possible pathways to harness energy from metals. ....	21
Figure 7. Conceptual scheme of a metal-air battery. ....	24
Figure 8. Scheme of the aluminium seasonal energy storage cycle studied in REVEAL project. ....	27
Figure 9. Scheme of the stoichiometric masses involved in the reaction of aluminium with water and the corresponding energy stored. ....	31
Figure 10. Trend of $\Delta h$ , $\Delta s$ and $\Delta g$ with temperature for aluminium reactions to hydroxide and oxide. ....	31
Figure 11. Thermal stability of different aluminium oxides/hydroxides. ....	32
Figure 12. Hydration mechanism of an aluminium particle in water at ambient conditions [25]. ....	33
Figure 13. The different reactivity of aluminium powders in oxygen and in steam environments (experimental results from a TGA). ....	35
Figure 14. Theoretical minimum energy requirements for aluminium production, both if carbon anodes or inert anodes are used. ....	37
Figure 15. Hydrogen-based storage system vs aluminium-based one in a multi-family house scenario: system comparison of costs, volumes, GWP, size of PV needed. ....	41
Figure 16. The two concepts of plant provided by Vlaskin et al.: with fuel cell (a), without fuel cell (b). ....	43
Figure 17. The two concepts of plant provided by Yang et al.: 1-turbine layout (a), 2-turbines layout (b). ....	43
Figure 18. Conceptual scheme of the proposed case study: centralized energy storage in the smelter (production of aluminium), transport, and distributed consumption. ....	45

## List of figures

Figure 19. Mass and volume of the energy carrier (aluminium or hydrogen) that is produced with the same input electricity. ....	54
Figure 20. Comparison of transportation consumptions and RTE of aluminium-based and hydrogen-based storage systems. ....	54
Figure 21. RTE and specific emissions at different efficiencies of the Al-to-power generation unit. ....	55
Figure 22. Comparison of transportation consumptions with different sizes (radii) of the district. ....	56
Figure 23. Comparison of RTEs with different sizes (radii) of the district. ....	56
Figure 24. Schematic of the main sections of the Al-to-power plant. ....	57
Figure 25. Conceptual scheme of a water-cooled isothermal Al-steam reactor. 1: reactor; 2: vaporizer for reacting water; 3: steam generator for Rankine cycle water. ....	58
Figure 26. Schematic of a typical Rankine cycle. ....	59
Figure 27. Schematic representation of a SOFC. ....	60
Figure 28. Layout of the Al-fed power plant model in Aspen Plus. ....	61
Figure 29. Reactor section - model in Aspen Plus. ....	62
Figure 30. Rankine cycle section - model in Aspen Plus. ....	63
Figure 31. SOFC section - model in Aspen Plus. ....	64
Figure 32. Microturbine section - model in Aspen Plus. ....	65
Figure 33. Optimized SOFC+GT+ST plant: system diagram and results. ....	68
Figure 34. Contribution to the total power output of the three generation systems. ....	70
Figure 35. Dependence of the Nernst voltage with the concentration of H <sub>2</sub> O at the anode inlet. ....	72
Figure 36. Molar fraction of hydrogen at anode inlet and Nernst voltage depending on the water excess. ....	72
Figure 37. Electric power delivered by SOFC, GT and ST in function of the water excess. ....	73
Figure 38. Electrical and thermal power of SOFC+GT+ST plant in function of water excess. ....	74
Figure 39. Effect of reaction temperature on the power output of steam cycle and primary heat recovery. ....	75
Figure 40. Simpler layout: SOFC-GT plant. ....	76
Figure 41. Effect of water excess in SOFC-GT system. ....	77

## List of figures

Figure 42. Comparison of SOFC+GT system with SOFC+GT+ST system. ....	77
Figure 43. Experimental setup used for Al-steam reaction. ....	81
Figure 44. Experimental setup: 3-way valves and heated pipes (a) and outlet section of the microreactor (b). ....	81
Figure 45. Alumina spheres before (a) and after (b) the mixing with aluminium. ....	85
Figure 46. Tube-in-tube reactor – output section. ....	85
Figure 47. Results of the second test on aluminium in the reactor showing no significant hydrogen production. ....	86
Figure 48. Appearance of the sample at the end of the second test. ....	87
Figure 49. Sample of aluminium in the quartz wool for tube-in-tube reactor testing. ....	88
Figure 50. Results of the test in the reactor (Al-H <sub>2</sub> O) with temperature ramp. ....	89
Figure 51. Integrated flow of hydrogen during the test with respect to (corrected) temperature. ....	89
Figure 52. TGA results of aluminium oxidation in air (temperature ramp and % mass variation in time). ....	91
Figure 53. TGA results of aluminium oxidation in air (temperature vs mass variation). ..	92
Figure 54. DTA results of aluminium oxidation in air (negative values for exothermicity). ....	92
Figure 55. Aspect of aluminium sample before (a) and after (b) the air oxidation in TGA. ....	93
Figure 56. Temperature program and results of isothermal air oxidation in TGA. ....	94
Figure 57. Focus on isothermal oxidation section: TGA results. ....	94
Figure 58. Concentration and temperature in the isothermal water oxidation in microreactor. ....	95
Figure 59. Concentration and evolution of hydrogen volume produced in the isothermal water oxidation in microreactor. ....	96
Figure 60. TPO in microreactor: H <sub>2</sub> concentration and temperature ramp. ....	97
Figure 61. TPO in microreactor: produced volume of H <sub>2</sub> . ....	97
Figure 62. Results of isothermal oxidation in water at 950°C. ....	98
Figure 63. Results of isothermal oxidation in water at 1000°C. ....	98
Figure 64. TPO with the second batch, with finer aluminium powder. ....	99
Figure 65. Comparison of isothermal oxidation in water at 900°C, 950°C and 1000°C – full peak. ....	101

## *List of figures*

Figure 66. Comparison of isothermal oxidation in water at 900°C, 950°C and 1000°C – isothermal peak only.....	101
Figure 67. Comparison of isothermal oxidation in water at 900°C, 950°C and 1000°C – integral values of produced hydrogen volume.....	102
Figure 68. Appearance of the coarse powder (a) and fine powder (b). .....	103
Figure 69. Comparison of detected H <sub>2</sub> concentration from the TPO of coarse and fine powder.....	103
Figure 70. First (a) and second (b) stage of the TPO for the two different batches of Al powder.....	104
Figure 71. Comparison of calculated hydrogen volumetric yield from the TPO of coarse and fine powder. ....	105

# List of tables

Table 1. Possible oxidation reactions that a metal can undergo in the wet cycle with water.....	22
Table 2. General reactions happening at the anode and cathode of a metal-air battery in case of discharge.....	24
Table 3. Aluminium reaction with water: mass yields based on stoichiometry. ....	29
Table 4. Standard molar enthalpy of formation and standard molar entropy of species involved in aluminium wet oxidation.....	30
Table 5. Calculated enthalpy, entropy and Gibbs free energy of reaction for the two reactions giving $\text{Al}(\text{OH})_3$ (1) and $\text{Al}_2\text{O}_3$ (3), per unit mole and unit mass.....	30
Table 6. Case study: sizing and main parameters of the smelter. ....	47
Table 7. Case study: energy consumption and sizing of the users and their main parameters.....	48
Table 8. Case study: equivalent hydrogen P2P system sizing and main parameters.....	49
Table 9. Case study: dimensions of the served area. ....	49
Table 10. Case study: transport aspects analysis and energy consumptions.....	50
Table 11. Case study: transport aspects analysis and energy consumptions for the equivalent hydrogen P2P system.....	51
Table 12. Case study: emission analysis inputs and results. ....	52
Table 13. Input parameters for plant simulation. ....	69
Table 14. Results of the plant simulation. ....	70
Table 15. Integral results of isothermal oxidation in water at different temperatures.....	100

# Acronyms

<b>CRM</b>	Critical raw materials
<b>DTA</b>	Differential thermal analysis
<b>GT</b>	Gas turbine
<b>HT</b>	High temperature
<b>LCA</b>	Life cycle assessment
<b>LT</b>	Low temperature
<b>MtX</b>	Metal-to-X
<b>P2P</b>	Power-to-power
<b>PtM</b>	Power-to-metal
<b>PtX</b>	Power-to-X
<b>PV</b>	Photovoltaic
<b>RES</b>	Renewable energy sources
<b>RTE</b>	Round-trip efficiency
<b>SOFC</b>	Solid oxide fuel cell
<b>ST</b>	Steam turbine
<b>TPO</b>	Temperature-programmed oxidation
<b>TGA</b>	Thermogravimetric analysis
<b>VRE</b>	Variable renewable energy
<b>XtP</b>	X-to-power

# Abstract

The increasing share of Renewable Energy Sources (RES) in the energy mix brings the necessity to find innovative and efficient methods for long-term energy storage. Recyclable electrofuels are a promising solution, allowing to store electrical energy in a compact and safe way through energy-dense materials thanks to Power-to-Power cycles. Among them, aluminium shows many advantages such as safety, efficiency, and sustainability. In charging phase, pure electricity is exploited to produce aluminium thanks to electrochemical processes in centralized smelters; in the discharging phase the metal is oxidized in air or water, returning part of the energy previously stored. In this work, a comprehensive assessment of aluminium as energy vector is performed, starting from a theoretical thermodynamic analysis of the chemical redox reactions involved in the production and utilization of the metal, leading to a theoretical energy density of 23.3 kWh/l. The attention is focused on medium/high temperature aluminium-water reactions allowing the cogeneration of hydrogen and heat, that can be then converted efficiently to electricity. A case study on a district/regional level is proposed: the calculated round-trip efficiency of 30% is competitive with compressed hydrogen Power-to-Power systems, especially if the hydrogen consumed for transportation is taken into account. A model of a highly efficient Aluminium-to-Power plant was developed in Aspen Plus, including 3 generation units (steam turbine, gas turbine, and solid oxide fuel cell), that was optimized to reach an electrical efficiency up to 77.2%. Finally, an experimental section is included, in which the oxidation of Al is studied in TGA (thermo-gravimetric analysis) and in a microreactor. TGA, performed both in temperature ramp and in isothermal mode, confirmed the possibility of reaction of pure aluminium powders in air without activation methods, with full oxidation reached at 1500°C. Tests in microreactor show the possibility of hydrogen production during temperature ramps, while in isothermal mode (e.g., 900°C, above melting point) the oxidation of the sample appears slower, suggesting that the microstructural changes of the material at different temperatures could play an important role to overcome the passive external oxide layer and activate the reaction.

# 1 Introduction

## 1.1 General background

One of the most debated issues in the last few years, on a global level, is the climate crisis. Increasing attention has been paid to discuss possible pathways to mitigate the effects of greenhouse gases emissions, while satisfying the principles of sustainability and circular economy. In this context, the energy sector is expected to undergo huge changes, since it contributes to almost three-quarters of global CO<sub>2</sub> emissions [1]. Another driver of this evolution is the energy crisis related to Russo-Ukrainian War in 2022, that made prices of primary energy commodities increase in an unprecedented way. Even though the path may not be easy, the energy crisis of 2022 can be considered the probable historic turning point towards a cleaner and more secure energy system [2].

The most comprehensive aim of the transition is to substitute the current fossil-based energy system with a renewable-based one, to pursuit environmental sustainability. Embedded in the concept of sustainability is the idea of circular economy, reflecting the paradigm of reusing and recycling the primary materials of our planet, minimizing the extraction of natural resources and optimizing the value of an asset through its life cycle, even though in some cases it may not be trivial to build processes both circular and sustainable [3].

Renewable energy sources (RES) are already part of the answer to the need of sustainability and circularity in the energy sector. However, a RES-based energy system cannot be built instantaneously with the current technology and prices, and research is going on to face the challenges that such a system brings. Among them, the most crucial are intermittency and uncertainty: the majority of the modern RES (e.g., wind, solar, wave) cannot be predicted and modulated with the same ease of the current fossil-based power plant. This causes the need of new efficient energy storage systems and new energy conversion processes, that would allow the transformation of energy from RES into new forms of energy, for example electrical, thermal or chemical. The concept is realized in the so-called “multi-energy systems” [4], in which different vectors are used, together with different energy conversion processes, in order to allow a better

management of energy in time and space, increasing the flexibility of the system and, thus, the penetration of RES-based technologies in the different sectors.

## **1.2 Aim of this Thesis**

In this Thesis, the focus will be put on the use of reactive metals as energy carriers. This concept of energy conversion and storage has the potential to be both circular and sustainable though being still under research phase. These materials are studied since they can be potentially key in many different applications, such as metal-based batteries, chemical looping, combustion engines, electrochemical machines and many other, being at the same time circular and sustainable and can be produced by electrochemical processing of the waste materials, with an external input only made of electricity derived by RES. The field of application of metal-based technologies in energy conversion and storage is potentially similar to the one of hydrogen, that has been more and more discussed in the last few years as a possible green energy vector. In turn, many of the processes involving reactive metals will involve the production and utilization of hydrogen, therefore the two vectors are somehow linked. There are aspects in which metals could be more interesting than the direct use of hydrogen, like the much higher volumetric energy density, but many challenges are still present, starting from the selection of the correct metal for the processes, passing through the development of reaction models and, finally arriving to the construction of prototypes and commercial machines.

In **Section 2** an introduction on reactive metals is provided, with the focus on recyclable electrofuels for long-term compact energy storage, analyzing advantages and challenges of the possible processes to harness energy from them, and justifying why aluminium is probably the most interesting material in this regard.

In **Section 3** a thermodynamic analysis is provided on the processes of aluminium oxidation, deepening the reaction with water but also explaining the oxidation in air and the processes related to the production and recycling of the material.

Subsequently, in **Section 4** a feasibility analysis is carried out studying the scenario of a district/region using aluminium as seasonal energy storage medium in synergy with renewables for industrial users.

In the following **Section 5**, an aluminium-fueled cogenerative power plant layout is

proposed and modeled in Aspen Plus, evaluating the thermodynamic convenience of the inclusion an additional Rankine cycle to recover the reaction heat, and performing sensitivity analysis on some key parameters related to the reaction, such as water excess and temperature.

Finally, in **Section 6** the results of an experimental campaign on medium-high temperature aluminium-water steam reaction are reported and discussed, making use of a microreactor test bench and a TGA.

## 2 Reactive metals as energy carriers

### 2.1 Metals as electrofuels: the circular perspective

The urgent need of energy storage media requested by the energy transition has pushed the research to explore new technologies in the field, besides the traditional ones like hydro-pumped and electrochemical batteries. A concept that could be crucial in the coupling of various energy forms (mainly electrical, thermal, chemical) is the so-called “power to X” (PtX) and “X to power” (XtP) paradigm [5]. According to this idea, electrical power can be stored in other forms of energy, like thermal energy (power to heat) or chemical energy, for example as a gas (power to gas), thanks to processes that only make use of RES electricity and, possibly, some abundant molecules easy to find, to capture and to recycle, such as water or CO<sub>2</sub>.

In particular, the storage of electric power in form of chemical species seems very promising also in the coupling of energy sector and industrial sector, since it allows to produce green gases or liquids (e.g., green hydrogen, methane or liquid organic molecules) that are then available not only to produce energy again, but also to be exploited in industrial processes. The energy vector X that has been produced in the PtX stage can be eventually used in the XtP stage to produce electrical power or other forms of energy in the moment of need, resulting to be an effective energy storage process, particularly convenient for long-term storage.

The chemical energy vector used in this paradigm is usually called “electrofuel” [6], [7]. Recyclable electrofuels are based on redox cycles, conceptually reported in Figure 1. Clean primary energy is injected into the system to permit the reduction of an oxide (fuel reduction stage), producing the fuel F and releasing oxygen as by-product. The fuel F can be now stored and transported, until it is finally used to produce clean secondary energy, thanks to the reaction with oxygen (fuel oxidation stage). This last stage produces a by-product in form of an oxidized fuel F<sub>2</sub>O<sub>y</sub>, that can be captured and transported to the fuel reduction stage, to start the cycle again in the framework of a circular process.

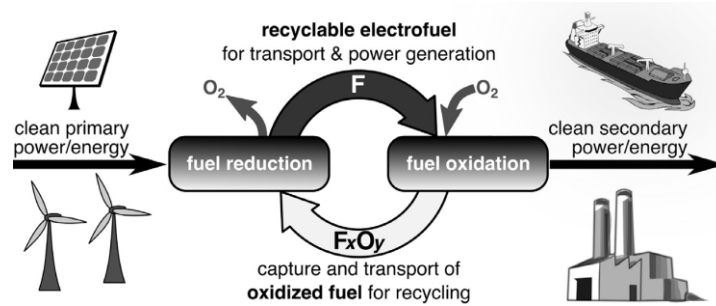


Figure 1. Conceptual scheme of a recyclable electrofuel.

A typical example of an electrofuel is green hydrogen, that can be produced for instance from electrolysis of water ( $\text{H}_2\text{O}$  is the oxidized form of hydrogen) thanks to RES electricity, stored, and finally exploited in different final uses, like power generation, transportation or as a precursor of other species. For example, thanks to the combination of hydrogen and  $\text{CO}_2$  it is possible to construct synthetic hydrocarbons and many molecules used in the industrial sector, not only considered as a fuel but also as a final product.

Even though typically the electrofuels are in the form of gases, or possibly liquids at room temperature, the idea can be easily extended to solid materials like metals. The concept is, again, to perform a redox cycle in which a metal oxide ( $\text{M}_x\text{O}_y$ ) is reduced in an electrochemical way to produce the pure metal ( $\text{M}$ ), that can be stored, transported and eventually oxidized in the final use (Figure 2), to produce secondary energy [7]. The fuel reduction stage is also called “Power-to-Metal” (PtM), while the oxidation stage can be considered a “Metal-to-X” (MtX) process [8], where “X” can be power, heat or a chemical species.

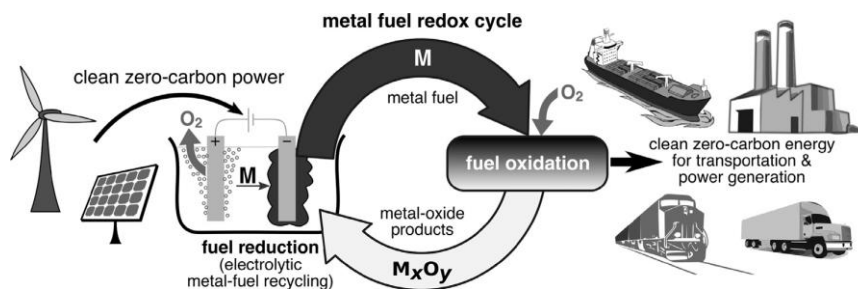


Figure 2. Conceptual scheme of a metal fuel redox cycle.

The use of metals to produce secondary energy is a quite well studied process. Among the options, it is possible to employ metals as anode of batteries (electrochemical utilization), to directly burn the metal to produce heat, or to perform reactions in which

thermal energy and/or a chemical species (typically hydrogen) are released. All these processes are different forms of fuel oxidation, and do not emit any greenhouse gases or pollutants.

The inverse process, that is to convert the metal oxide into pure metal (recycling), is instead more problematic to be performed in a completely sustainable manner. Many technologies are available for the production of metals by means of electricity, but most of the traditional pathways either foresee the use of non-sustainable primary sources and methods (e.g., the use of a coal distillate to produce Iron) or anyway the emission of CO<sub>2</sub>. Nevertheless, numerous zero-carbon processes of PtM are being studied, and some of them could be used at industrial scale, even if the prices are still high.

## 2.2 Properties of metals as energy carriers

The necessary condition of a material to be considered an electrofuel is that it can undergo a redox reaction cycle with atmospheric oxygen. Moreover, to guarantee a sufficient specific energy, materials with relatively low nuclear mass for a given number of electrons are needed. On the periodic table, the first condition restricts the possible field to groups 1-14, while the second one reduces the possible periods to 1-4. Keeping these constraints in mind, in Figure 3 the possible metals that theoretically can be considered electrofuels are reported [7].

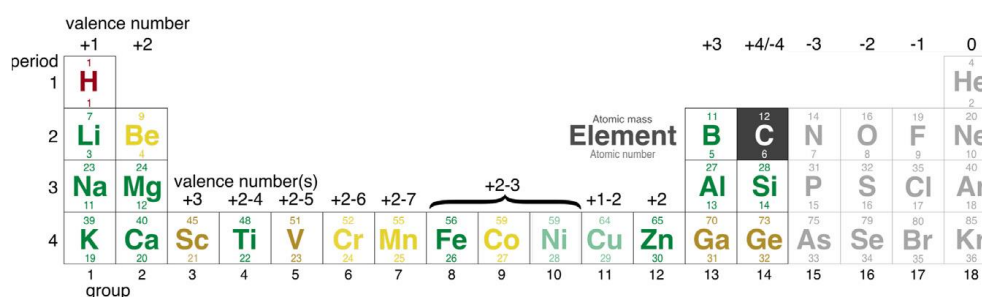


Figure 3. Possible metals that can be theoretically used as electrofuels. Elements in green are the most interesting in practical terms.

Anyway, not all of them are of practical interest, because the element must not show any toxicity and must be sufficiently affordable in economic terms; the only elements of practical interest are colored in green in Figure 3. Hydrogen and Carbon are included in the options but will not be considered in this Thesis, since they already have their own

well-known research field and applications. The focus will be put on metals and metalloids colored in green, to which we will refer as “reactive metals” from now on.

Among all elements, metals are the ones showing the highest amount of volumetric heat production if burned in air. Therefore, their main advantage is that they possess a very high theoretical energy density (stored energy per unit volume), even higher than the one of fossil fuels like Diesel or gasoline. In terms of specific energy (stored energy per unit mass), their performance is usually slightly worse than fossil fuels, but not so different, so that the advantages on the energy density are often higher than the slight decrease in specific energy. An overview of the energy density and specific energy of the main metals, also compared to fossil fuels and hydrogen, is reported in Figure 4.

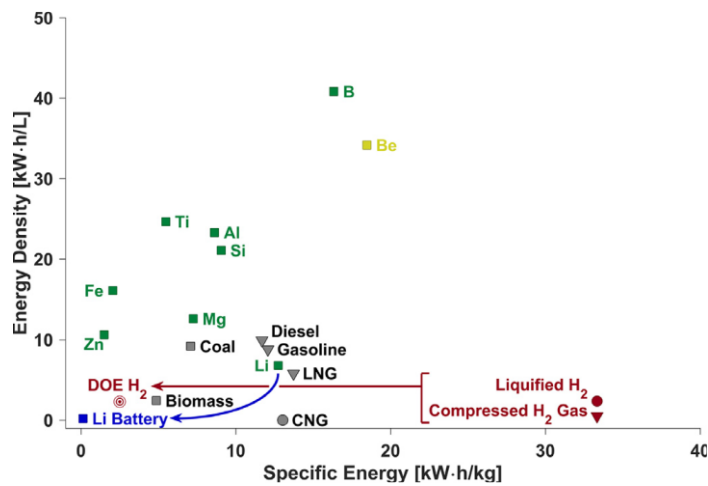


Figure 4. Volumetric energy density and gravimetric specific energy of different metals.

Another rule to respect in the selection of the best candidates is to avoid rare materials. Fortunately, among the options reported above, some are related to very abundant materials: silicon, aluminium and iron are respectively the 2<sup>nd</sup>, 3<sup>rd</sup> and 4<sup>th</sup> most abundant elements in the Earth’s crust; in general, most of the metals in the list do not show any major criticalities in terms of abundance.

Renewable energy and storage sector anyway are problematic in the use of critical raw materials. In the selection of the suitable metals in our application, it is advisable to avoid the materials in the list reported in Figure 5, in which from the “very high” to “low” risk they are considered critical raw materials (CRM) for the EU [9]. For example, even if Silicon is a very abundant element, it is considered a CRM because it is used in different competing sectors, like electronics and photovoltaic (PV); the main fear is price volatility

and the domination of the market by China. These aspects (geopolitical and economic) are also very important in the definition of a CRM, and so they must be taken in account.

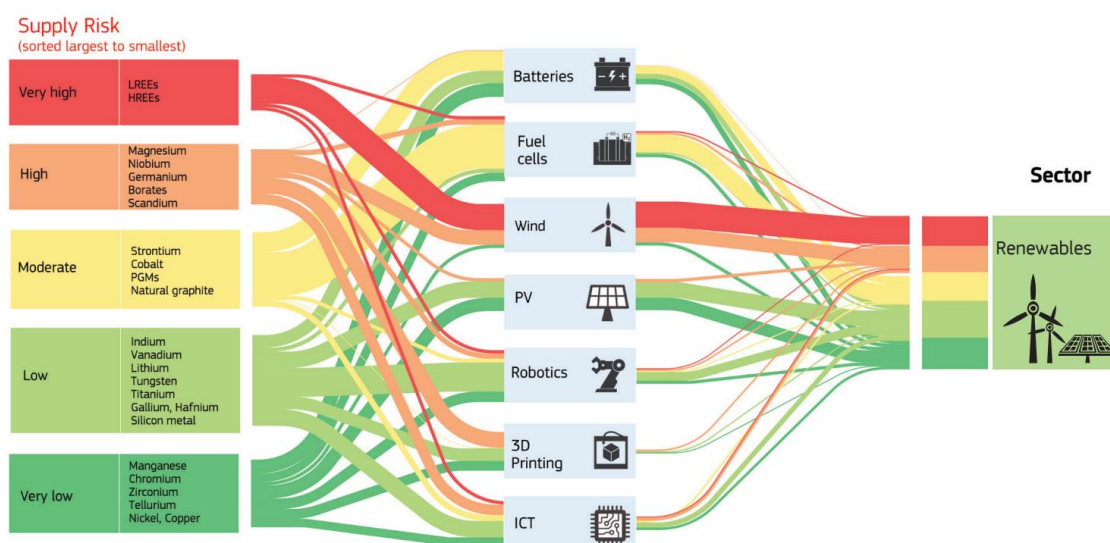


Figure 5. Classification of critical raw materials according to the EU.

The most used metal today in industrial processes is iron, that is also a good candidate to be an electrofuel. Silicon is also very interesting, since it can be produced from sand (silica), water and solar energy, even if currently it is considered a CRM. Magnesium and especially aluminium are considered promising thanks to their high energy density, relatively low cost and the possibility to exploit low-carbon technologies for recycling already now. Boron is the metal with the highest energy density, and also in terms of specific energy it shows values higher than fossil fuels; until now, it has been proposed in studies to produce hydrogen on demand for power production. Regarding alkali metals, like lithium and sodium, they are already used electrochemically in batteries, but their exploitation can be optimized considering them as recyclable electrofuels [7].

## 2.3 Possible routes to harness energy from metals

In this section the focus is put on the “metal-to-X” part of the redox cycle, analyzing the different possibilities in order to harness energy from the metal fuel.

The possible routes can be classified in two large categories based on the chemical species that acts as oxidant in the redox reaction: in particular the metal fuel can react with water (metal-water reaction) or directly with atmospheric oxygen (metal-air reaction). The first one is also referred as “wet cycle”, while the second one as “dry cycle”. Starting from

them, further subdivisions can be noted, as reported in the schematic overview of Figure 6 [7].

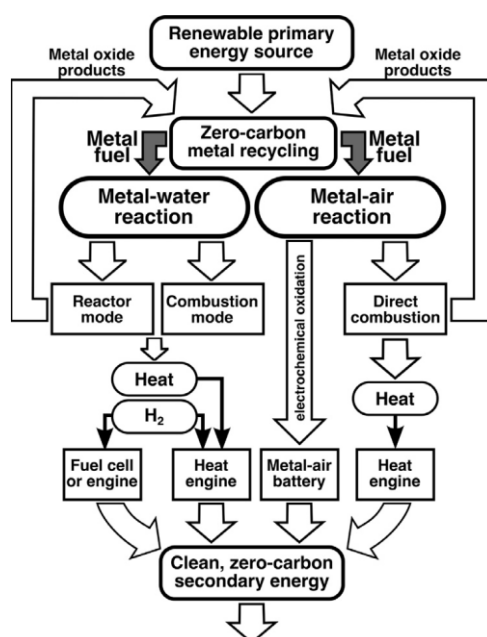


Figure 6. Overview of the possible pathways to harness energy from metals.

### 2.3.1 Wet cycle

The wet cycle is based on metal-water reactions: the products are hydrogen, heat and the metal oxide. The reaction can be performed at low or high temperature, respectively reported in the figure as “reactor mode” or “combustion mode”. Many different possibilities have been studied to take advantage of both the produced hydrogen and the heat, in order to maximize the efficiencies of the conversion. For instance, it is possible to use heat and hydrogen together in a heat engine, or the hydrogen can be considered the reactant in a fuel cell.

One of the biggest advantages of using metals through the wet cycle is the possibility to produce hydrogen on request. In fact, even though this gas is considered the energy carrier of the future, many challenges are still not solved, especially regarding its storage and transportation. Reactive metals are instead typically safer and easier to transport and store, since they are solid and possess an advantageous energy density; this allows to keep using hydrogen in the final uses, thanks to the reaction metal-water that will produce it on demand but avoiding its problem in storage and transportation [10].

The reactions that a metal undergoes in the wet cycle can be summarized in two steps, and a thermodynamically equivalent reaction can be expressed as reported in Table 1.

Table 1. Possible oxidation reactions that a metal can undergo in the wet cycle with water.

Step	Possible reactions
1. Oxidation of metal	a) $xM + yH_2O \rightarrow M_xO_y + yH_2 + Q_1$
	b) $xM + 2yH_2O \rightarrow xM(OH)_{2y/x} + yH_2 + Q_1$
2. Oxidation of the $H_2$ produced in step 1	$yH_2 + \frac{y}{2}O_2 \rightarrow yH_2O + Q_2$
Thermodynamic equivalent reaction	a) $xM + \frac{y}{2}O_2 \rightarrow M_xO_y + Q_3$
	b) $xM + \frac{y}{2}O_2 + yH_2O \rightarrow xM(OH)_{2y/x} + Q_3$

In the phase of oxidation of the metal, two pathways are possible, the first producing a metal oxide and the second producing a metal hydroxide, but always releasing a certain quantity of useful heat  $Q_1$ , thanks to the exothermicity of the reaction. The oxidation of hydrogen, besides useful energy  $Q_2$ , produces water that can theoretically be recycled and used as reactant in the next step.

Performing the sum of reactants and products of step 1 and 2, it is possible to write the global reactions that act as thermodynamically equivalents. In the pathway a), the reaction is equivalent to a dry air oxidation, and both  $H_2$  and  $H_2O$  do not appear in the balance (this means that theoretically water can be completely recycled internally, and hydrogen is both produced and consumed). In this sense, the wet cycle can be considered as a chemical looping system in which hydrogen acts as an intermediate to facilitate the overall process of metal oxidation [10]. In the pathway b), the metal is not completely oxidized (hydrogen is still present in the hydroxide) and it is not possible to self-sustain the reaction recycling all the water (some  $H_2O$  must be injected in the cycle). The heat  $Q_3$  is formally the sum of the heat produced in the two steps:  $Q_3 = Q_1 + Q_2$ , with the two heats of reaction being similar for most metals.

The metal-water reaction can be performed at high temperature (HT) or low temperature (LT).

Temperatures of reaction can go over 1000°C (HT) in a metal-water flame in which

usually the main purpose is to deliver the highest amount of high-grade heat possible, referred as “combustion mode” in Figure 6. In this case, the typical applications are using the metal-water combination as propellants or in internal/external combustion engines for high-density compact power production.

Instead, with LT (“reactor mode” in Figure 6) we consider temperatures that do not exceed 200-300°C, but most of the research and of the interest in LT metal-water reaction is in the realization of an efficient room temperature (RT) reaction. Since the heat  $Q_1$  in the first oxidation of the metal is produced at low temperature, it is not always considered as useful product of the reaction in this case. Usually, in fact, the aim is to produce the highest amount of hydrogen, that then can react to deliver electric power, for example in a fuel cell, that is the most efficient method to exploit hydrogen reactivity.

Another possibility is to perform the reaction at intermediate temperatures (around  $300 < T < 1000^\circ\text{C}$ ), combining the advantages of LT and HT: in this temperature range in principle it is technologically possible to recover both hydrogen and heat at a sufficient temperature level, without incurring in the formation of a flame, therefore it could be an advantageous solution to analyze.

### **2.3.2 Dry cycle**

Dry cycle is a term used to describe the reaction of the metal with oxygen or dry air, without the use of water as a reactant and without the production of hydrogen. Therefore, the overall reaction of a dry process is one of the equations reported in Table 1 as thermodynamically equivalent. Two pathways are available for the exploitation of the dry air oxidation reaction: the electrochemical one and the direct combustion one.

The first pathway is the utilization of the metal in an electrochemical battery. Metal-air batteries are of particular interest to increase the energy density of the current standard solutions for energy storage, reaching 3-30 times higher energy density than Li-ion batteries [11]. In fact, the redox reaction of a metal with oxygen is much more profitable than the reaction with other species.

A metal-air battery consists in mainly three elements: a metal anode, a porous cathode allowing the supply of oxygen, and an electrolyte layer separating the two electrodes. Currently there is not a single winning solution, and many materials have been studied both for anode (Li, Na, Fe, Zn, Al, K), electrolyte (aqueous, non-aqueous, hybrid, and

solid-state) and catalysts. A generic scheme of a metal-air battery, operating in an aqueous (a) and non-aqueous (b) electrolyte is depicted in Figure 7 [12]. In the two situations it is possible to write the general chemical reactions happening at the anode and cathode during the process of discharge, as reported in Table 2.

Table 2. General reactions happening at the anode and cathode of a metal-air battery in case of discharge.

	Anode	Cathode
Aqueous electrolyte	$M \rightarrow M^{n+} + ne^{-}$	$O_2 + 4e^{-} + 2H_2O \rightarrow 4OH^{-}$
Non-aqueous electrolyte	$M \rightarrow M^{+} + e^{-}$	$xM^{+} + O_2 + xe^{-} \rightarrow M_xO_2$ ( $x = 1$ or $2$ )

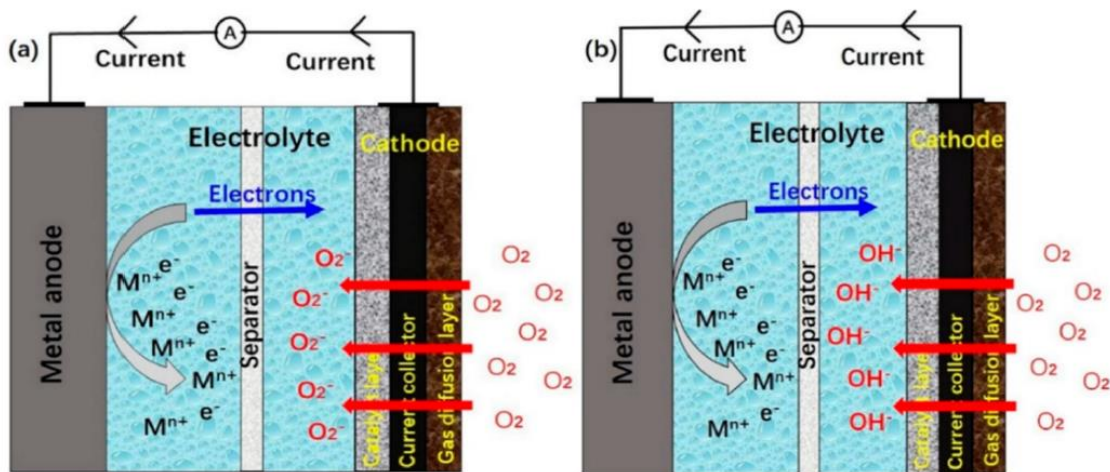


Figure 7. Conceptual scheme of a metal-air battery.

The second pathway is the production of high-grade heat driving a high-temperature combustion reaction between the metal and air, with the main aim to supply a heat engine [13]. These last pathways will not be considered in the work, and the focus will be put on wet cycle, in which also hydrogen is involved.

## 2.4 Aluminium as a promising electrofuel

### 2.4.1 Advantages and applications

Most of the research on reactive metals for power and hydrogen production has been focused on aluminium. Some of the reasons of the selection of this metal are the following [14]:

- Safe handling, storage and transportation thanks to the protective film of alumina naturally produced on the surface of Al when exposed to air.
- High calorific value and theoretical energy density (oxidation of Al is highly exothermic).
- Very abundant in the Earth's crust, and high current industrial production rates.
- Possibility to take advantage of Al scrap.
- Possibility to produce it with carbon-free processes.

The Al<sub>2</sub>O<sub>3</sub> (alumina) film on the surface provides safety, but at the same time hampers the contact of the material with the oxidizing agent, so that many different strategies are being studied to improve its reactivity, like thermal methods (increase temperature), mechanical (production of very small-size powders), chemical (use of alkaline solutions or alloying with other elements).

For some applications, like Al-air batteries, high purity is needed: this causes some issues in the sustainability assessment, since the production process of high-purity Al is very energy-intensive. However, many studies have shown that also low-grade Al or even scrap Al can be of interest in energy production, to the point that many commercial alloys have been tested so far, with contrasting results.

The perspectives of Al usage as energy carrier range from automotive, propulsion systems, lightweight batteries for portable devices, to the production of hydrogen and large-scale energy storage for stationary application. These last two applications provide the best approach if combined, when a wet cycle is used in which hydrogen is then reacted to produce electric power, and plant concepts should be optimized in order to harness energy also from the heat produced in the different stages.

#### **2.4.2 Current and future production methods**

Primary aluminium resource is extracted by bauxite, an abundant mineral mainly containing oxides and hydroxides of Al (in a fraction of 50-80%), besides other metal oxides. Most of the bauxite extracted is then used to produce metallurgical alumina, thanks to Bayer process [14]. Once alumina is obtained, metallurgical aluminium is produced thanks to a smelting process, in an electrolytic cell. This last process is the one of interest in our applications, since the utilization of Al for energy purposes will lead to the production of alumina, that must be treated again to re-form the metal. In the circular

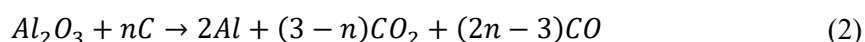
perspective, no more bauxite is needed to produce “fresh”  $Al_2O_3$ , and the latter is completely recycled in an electrochemical way.

The electrolysis of alumina, also called smelting process or Hall-Héroult process, could be carried out with the following simple global reaction:



The electrolyte cannot be an aqueous solution, since in this case hydrogen would be reduced at the cathode instead of aluminium, because it is more electronegative. Therefore, the current solution is to employ cryolite ( $Na_3AlF_6$ ), that at the operating temperatures of 950-1000°C dissociates in  $3Na^+$  and  $AlF_6^{3-}$  ions. Theoretically, cryolite is not consumed in the process, however practically it is, with the addition of 20 kg of cryolite for each kg of Al produced.

Even if the global reaction reported above is feasible, current industrial processes of Al production are based on consumable carbon anodes. The global reaction of the process in this case is the following:



that, as can be seen, leads to the production of the unwanted  $CO_2$ . The use of bio-based anodes could minimize the impact of  $CO_2$  emissions [15], but currently the anodes are made of calcinated coke and pitch. The research is going on to study methods to make possible the exploitation of the reaction (1), avoiding any direct  $CO_2$  emissions, thanks to the use of inert anodes. Attempts have been done using metallic anodes like Fe-Ni, Cu-Ni-Fe, Fe-Ni-Al alloys and many others, but the corrosion and oxide layer growth are important barriers to overcome [16].

According to the current best practice, around 12 kWh/kg<sub>Al</sub> of electricity are consumed in the Hall-Héroult process, and the direct emissions of  $CO_2$  are about 1.7 kg<sub>CO2</sub>/kg<sub>Al</sub> if carbon electrodes are used. Of course, the electricity needed for the smelting must be generated from RES to avoid additional indirect emissions. In the traditional smelting process, an additional greenhouse gas source is the emission of perfluorocarbons [17].

Taking all these considerations into account, we can conclude that the smelting process of alumina in the future must be carried out with inert anodes, otherwise it is practically impossible to avoid greenhouse gases emissions.

### 2.4.3 The REVEAL project

The huge attention paid to the aluminium-based systems is confirmed by the EU, that has launched the project “REVEAL storage” in the contest of the program Horizon Europe [18]. The project has the aim to study a carbon-free electrochemical production method for Al starting from alumina and the possible utilization pathways, especially as an energy carrier (the objective is to go over 15 MWh/m<sup>3</sup>) to produce heat and electricity in winter (Figure 8). The focus is put on the wet cycle, with Al-steam (high temperature) or Al-water (low temperature) reactions.

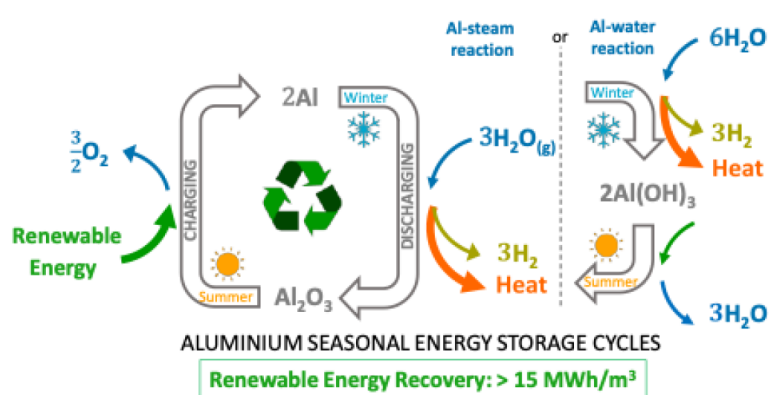


Figure 8. Scheme of the aluminium seasonal energy storage cycle studied in REVEAL project.

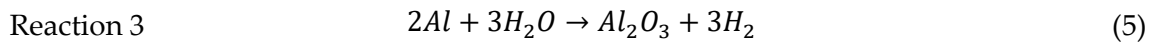
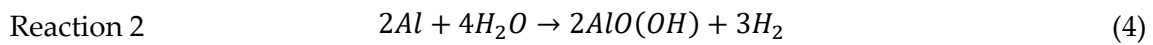
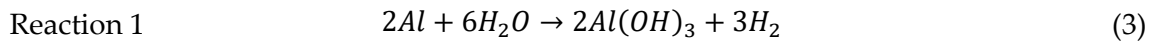
Such a system would “recharge” during summer thanks to surplus electricity from RES, producing carbon-free aluminium (one of the objectives is the elimination of CO<sub>2</sub> emissions during production) starting from its oxide, alumina. The “discharging” process can instead be performed in two possible paths, one reacting the metal with steam producing hydrogen and directly alumina, and the other reacting the metal with liquid water and producing hydrogen and aluminium hydroxide, that then can be turned into alumina thanks to solar energy.

## 3 Thermodynamic analysis

### 3.1 Reaction of Aluminium with water

#### 3.1.1 Energy and mass balance

The possible oxidation reactions involving aluminium and water are the following [19]:



The first possible product is aluminium hydroxide  $Al(OH)_3$ , also called bayerite/gibbsite, the second is an aluminium hydroxide oxide  $AlO(OH)$ , named boehmite, and the last one is the aluminium oxide  $Al_2O_3$ , also called alumina.

In all the three reactions the same quantity of  $Al$  (2 moles) will produce the same quantity of  $H_2$  (3 moles), therefore the hydrogen yield is the same in any case. Instead, the water or steam needed is different, being the minimum for the reaction 3, with 3 moles of water every 2 moles of  $Al$ .

Knowing the moles  $n$  and the molar masses  $\bar{M}$  of reactants and products, it is possible to calculate the hydrogen yield  $\varepsilon_{H_2}$  in  $kg_{H_2}/kg_{Al}$  and the masses involved for the other components, i.e., the water needed for the reaction  $\varepsilon_{H_2O}$  and the amount of oxide/hydroxide formed per kg of aluminium  $\varepsilon_{ox}$ :

$$\varepsilon_{H_2} = \frac{n_{H_2} \cdot \bar{M}_{H_2}}{n_{Al} \cdot \bar{M}_{Al}}; \quad \varepsilon_{H_2O} = \frac{n_{H_2O} \cdot \bar{M}_{H_2O}}{n_{Al} \cdot \bar{M}_{Al}}; \quad \varepsilon_{ox} = \frac{n_{ox} \cdot \bar{M}_{ox}}{n_{Al} \cdot \bar{M}_{Al}} \quad (6)$$

The same calculations can be done using as a reference the hydrogen produced, giving the results in  $kg_{Al}/kg_{H_2}$ ,  $kg_{H_2O}/kg_{H_2}$  and  $kg_{ox}/kg_{H_2}$ . The results are reported in Table 3.

Table 3. Aluminium reaction with water: mass yields based on stoichiometry.

Reaction	$\varepsilon_{H_2} \left( \frac{kg_{H_2}}{kg_{Al}} \right)$	$\varepsilon_{H_2O} \left( \frac{kg_{H_2O}}{kg_{Al}} \right)$	$\varepsilon_{ox} \left( \frac{kg_{ox}}{kg_{Al}} \right)$	$\varepsilon_{Al} \left( \frac{kg_{Al}}{kg_{H_2}} \right)$	$\varepsilon_{H_2O} \left( \frac{kg_{H_2O}}{kg_{H_2}} \right)$	$\varepsilon_{ox} \left( \frac{kg_{ox}}{kg_{H_2}} \right)$
1	0,111	2,003	2,891	8,923	17,873	25,796
2	0,111	1,335	2,223	8,923	11,915	19,838
3	0,111	1,002	1,889	8,923	8,937	16,860

For all the three reactions, around 9 kg of aluminium and 9-18 kg of water are needed to produce 1 kg of hydrogen, with the production of about 17-26 kg of subproduct. Taking as a benchmark the ideal electrolytic splitting of water, that needs 9 kg of water to produce 1 kg of hydrogen, it is possible to say that in terms of mass the aluminium-based reaction is comparable to the electrolysis of water if only the aluminium is considered as a fuel (in fact 9 kg<sub>Al</sub> per kg of hydrogen are needed), otherwise, if also water is considered as a fuel the result is that more than 18 kg (Al+H<sub>2</sub>O) are needed to produce 1 kg of hydrogen. Therefore, the availability of water at the point of use is a key aspect if a high specific energy has to be reached, making the exploitation of this reactions more promising in stationary applications. However, an additional energy term is added to the energy content of hydrogen, since the reaction also produces heat.

From the enthalpic balance, in fact, it results that the three reactions are spontaneous and highly exothermic. The heat of reaction  $\Delta \bar{h}_r$  can be calculated in standard conditions using the enthalpy of formation  $\Delta \bar{h}_f^o$  of each component and considering their stoichiometric coefficient  $\nu$ , using the formulation:

$$\Delta \bar{h}_r = \sum_{i=1}^{\# prod} \nu_i \Delta \bar{h}_{f,i}^o - \sum_{i=1}^{\# react} \nu_i \Delta \bar{h}_{f,i}^o \quad (7)$$

and analogous balances can be performed to find the molar entropy and Gibbs free energy of reaction. The enthalpy, entropy and free energy of formation of the species can be found in literature for standard conditions [20]–[23] (Table 4). Eventually, in standard conditions the enthalpy of reaction and Gibbs free energy of reaction of the two reactions 1 and 3 are reported in Table 5, normalized per unit mole and unit mass of aluminium.

Table 4. Standard molar enthalpy of formation and standard molar entropy of species involved in aluminium wet oxidation.

Chemical species	Standard molar enthalpy of formation $\Delta h_f^0$ (kJ/mol)	Standard molar entropy (J/mol·K)
<b>Al</b>	0	28
<b>H<sub>2</sub></b>	0	131
<b>H<sub>2</sub>O<sub>(l)</sub></b>	-285,8	70
<b>Al(OH)<sub>3</sub></b>	-1277	85
<b>AlO(OH)</b>	-1003	
<b>Al<sub>2</sub>O<sub>3</sub></b>	-1676	51

Table 5. Calculated enthalpy, entropy and Gibbs free energy of reaction for the two reactions giving Al(OH)<sub>3</sub> (1) and Al<sub>2</sub>O<sub>3</sub> (3), per unit mole and unit mass.

		Reaction 1 (to hydroxide)	Reaction 3 (to oxide)
unit mole	$\Delta \bar{h}_r$ (kJ/mol)	-419,5	-409,1
	$\Delta \bar{s}_r$ (J/mol·K)	27,0	87,3
	$\Delta \bar{g}_r$ (kJ/mol)	-427,3	-434,2
unit mass	$\Delta h_r$ (MJ/kg)	-15,55	-15,16
	$\Delta s_r$ (kJ/kg·K)	1,00	3,23
	$\Delta g_r$ (MJ/kg)	-15,84	-16,09

The energy released in the reaction Al-H<sub>2</sub>O can be split in the one directly emitted in the form of heat ( $Q_1$ ), and the one contained in the produced hydrogen. Since in all the reactions 1 kg of Al produces 0,111 kg of H<sub>2</sub>, the maximum energy content stored in hydrogen  $E_{H_2}$  can be found multiplying this mass for its calorific value:

$$E_{H_2} = \varepsilon_{H_2} \cdot HHV_{H_2} = 0,111 \text{ kg} \cdot 141,8 \frac{\text{MJ}}{\text{kg}} \cong 15,7 \text{ MJ} \quad (8)$$

The heat  $Q_1$  is related to the enthalpy of reaction and therefore is in the range of 15-16 MJ/kg, according to the data calculated in Table 5. The specific energy of 1 kg of Al therefore depends on the reaction considered but can be assessed to be the sum of  $Q_1$  and

$E_{H_2}$ , around 31 MJ/kg or 8.6 kWh/kg. The energy density can be evaluated knowing the density of Al ( $\rho_{Al} = 2700 \text{ kg/m}^3$ ), resulting in 23.3 kWh/l.

Thus, since the values of  $Q_1$  are very close to the value of  $E_{H_2}$ , it is possible to say that the energy released in the Al-water reaction is divided in two almost equal parts into heat and hydrogen. A summary of the products, in mass and energy, found so far is depicted in the scheme (Figure 9).

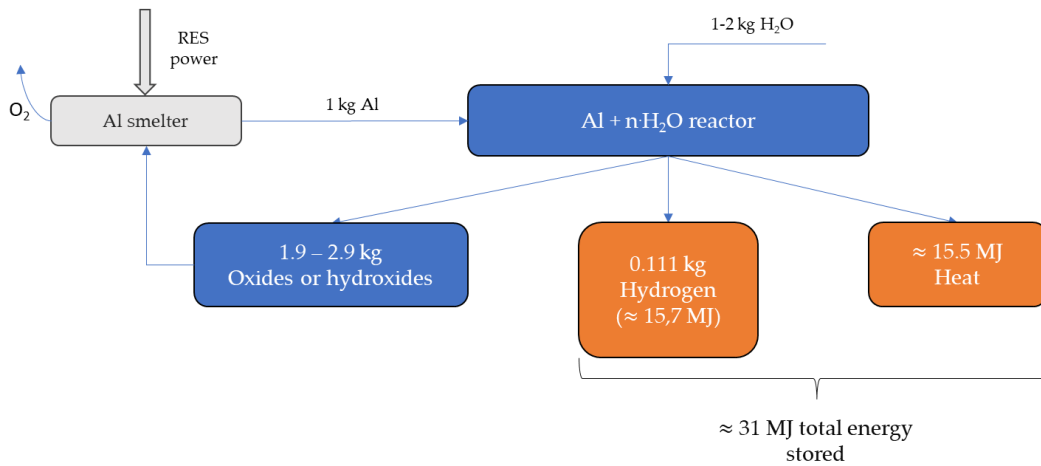


Figure 9. Scheme of the stoichiometric masses involved in the reaction of aluminium with water and the corresponding energy stored.

The dependance on the temperature of the thermodynamic quantities for the two reactions studied can be found in literature [19] and a graphical rearrangement is reported in Figure 10.

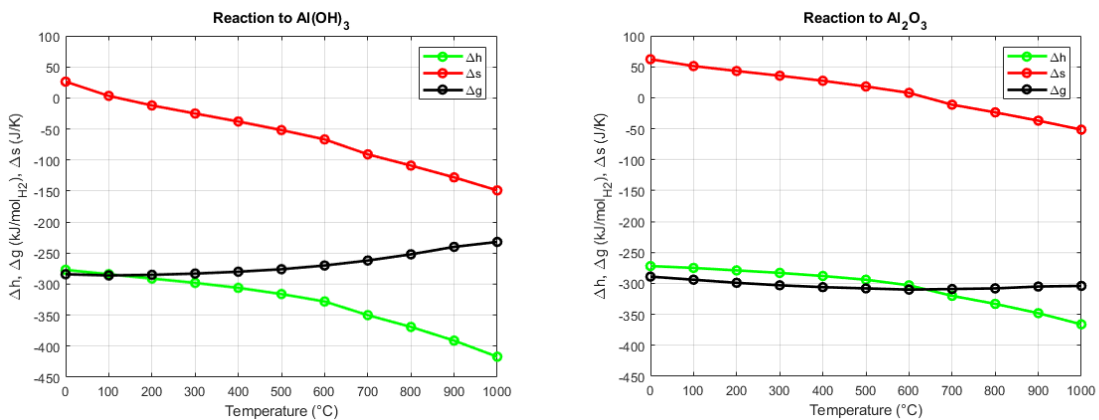


Figure 10. Trend of  $\Delta h$ ,  $\Delta s$  and  $\Delta g$  with temperature for aluminium reactions to hydroxide and oxide.

The stability of one Al compound with respect to another, that is, the reaction governing the process among the three initially written, depends on thermodynamics considerations. From the graphs in Figure 10 for example it is possible to assess that

alumina will be surely favored at higher temperature, because the Gibbs free energy is much lower than the one of the hydroxides at high temperature. In Figure 11 it is reported the relative Gibbs free energy of different aluminium hydroxides with respect to the Gibbs free energy of  $Al_2O_3$  ( $\alpha$ -alumina), taken as a reference [24]. At a given temperature, the Al-based compound that is favored is the one exhibiting the lowest Gibbs free energy. Therefore, at low temperatures, below  $280^\circ C$ ,  $Al(OH)_3$  (bayerite/gibbsite) is the most stable product. At high temperatures, above  $480^\circ C$ ,  $Al_2O_3$  (alumina) becomes the favored one, as expected. In between, from  $280^\circ C$  to  $480^\circ C$ , the favored product is boehmite,  $AlO(OH)$ .

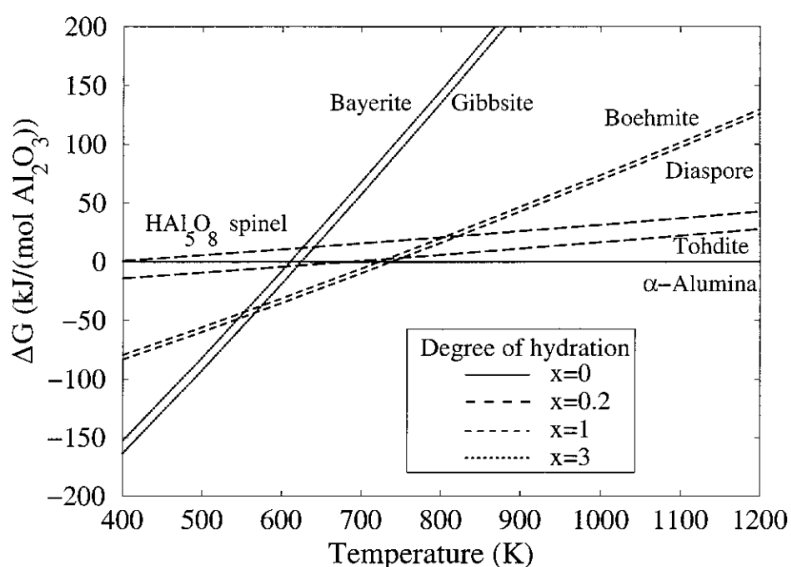


Figure 11. Thermal stability of different aluminium oxides/hydroxides.

### 3.1.2 Kinetics and reaction mechanism

The reactivity of aluminium as found in normal ambient conditions is very low: the metal cannot be directly oxidized in air or in water, and it is considered completely non-reactive. The reason is that in normal conditions the external layer of aluminium particles (or any possible shape) automatically oxidizes forming a passive layer of alumina ( $Al_2O_3$ ), that behaves as a completely inert material, for a thickness of 4-6 nm. Thus, it is not feasible to react a normal foil/rod/powder of aluminium with oxygen or water simply by putting in contact the two reactants, because the reaction will not take place. This fact can be seen as the main hurdle in the utilization of aluminium as a fuel, but at the same time it makes the handling of this metal very safe compared to other analogue materials.

Placing a pure aluminium metal powder in water at near-ambient conditions could trigger a hydration reaction on the surface oxide film. In the first stage, Al-O-Al bonds are broken via hydrolysis, to form hydroxide species like  $\text{Al}(\text{OH})_3$  or  $\text{AlOOH}$ . Hydroxyl ions  $\text{OH}^-$  have been found to represent the predominant mobile species inside the films, moving with rapid transport rates. Therefore,  $\text{OH}^-$  ions can migrate through the film to reach metallic aluminium, where the reaction between hydroxyl ions and Al makes possible the evolution of hydrogen in a bubble (Figure 12). If the reaction equilibrium pressure is higher than the external pressure, the bubble breaks, driven by the pressure gradient. External pressure depends on the ambient conditions and on the tensile strength of the material (the lower the strength, the higher the probability to break the bubble) [25].

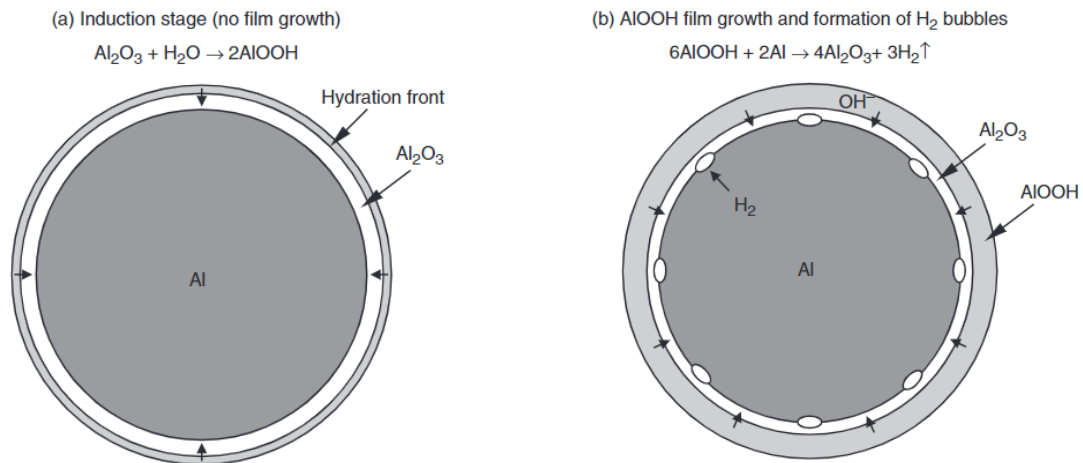


Figure 12. Hydration mechanism of an aluminium particle in water at ambient conditions [25].

Experimental tests show kinetic curves with usually more than one peak, in accordance with the step behavior of the reaction, including initial oxidation, induction and hydrogen production [26]. However, the feasibility of implementing the aforementioned mechanism is contingent upon boundary conditions, such as granulometry of the powder, temperature, and presence of catalysts.

### 3.1.2.1 Activation of Al-water reaction

To drive the reaction of aluminium with water it is necessary to overcome the passive oxide layer, performing an activation of the material [14]. Employing activator substances is the oldest and most studied method. Some of the most standard catalysts are NaOH and KOH, in an alkaline solution with water. In particular NaOH has been proved to be the most effective one, delivering the highest amount of hydrogen at temperatures of 70-

90°C and 5.75 M solution.

Another way is the mechanochemical activation of the material, adding to the metal other substances that influence the reactivity, thanks to the difference in properties of metal alloys compared to the pure metal. Some interesting alloying materials are Ga, In, Re, Bi, Mg, Ca, but also solutions with NaCl have been proposed.

The simply mechanical activation of the material is also possible, allowing the reaction of water with the metal without adding other species. One method is the wet cutting, where the water encounters non-oxidized fresh aluminium particles, thanks to the short time interval between their production and the reaction phase (therefore, the particle must be in contact with water in a time shorter than the one of the formation of the oxide layer). Also the manufacturing of nano-sized particles can be sufficient to drive the reaction without the need of activators in pure water, but the use of ultrafine particles increases the risks of explosions.

Using chemical, mechanochemical or mechanical activation techniques leads to higher costs due to the employment of additional materials (even rare ones) or to the need of more sophisticated production processes, nullifying the advantages of employing a standard and simple material like Al.

Reaction of micron-sized Al powders without other activators can be performed thanks to temperature-related effects. In particular, above the melting point of Al (660°C) the effect of temperature has been proved to be sufficient to drive the reaction of micron-sized industrial particles with no need of other substances.

The oxidation of pure aluminium powder in air or water has been deeply studied. One reference method to study such a reaction is to perform a temperature ramp in a thermogravimetric analysis (TGA) setup that allows to evaluate the mass variations of the sample as function of temperature.

According to thermodynamics and experimental literature, aluminium oxidizes in oxygen in different stages [27]. Until 550°C the reaction proceeds slowly, with the increasing of the natural protective oxide layer of amorphous alumina driven by outward diffusion of Al cations. At about 550°C a phase transition occurs in the external layers, transforming the amorphous Al<sub>2</sub>O<sub>3</sub> into  $\gamma$ -Al<sub>2</sub>O<sub>3</sub>. This last phase exhibits higher density than the previous one, hence the external structure shrinks, leaving some free spaces in which oxygen can reach metal aluminium with more ease. This phenomenon leads to an

increased reaction rate, with the reaction proceeding at high pace until the external layer grows to a point in which it is again difficult to reach the internal core. During and after this stage other phase transitions appears (to  $\theta$ - $\text{Al}_2\text{O}_3$  and to  $\alpha$ - $\text{Al}_2\text{O}_3$ , the latter very stable, almost impeding the reactions at about  $1000^\circ\text{C}$ ), until the final phase of  $\alpha$ -alumina is reached at  $1500^\circ\text{C}$ , point at which the oxidation phenomenon is considered completed. According to stoichiometry, the full oxidation of Al in oxygen leads to a mass increase of the sample of about 88%.

Oxidation in water shows a quite different trend in temperature ramp TGA tests. Two main differences are detectable: first, the oxidation is completed at a much lower temperature (around  $1000^\circ\text{C}$ ); second, a peak is present in correspondence to the melting point of the metal. Results from a study in TGA are visible in Figure 13 [28] and will be used as a benchmark in the experimental analysis.

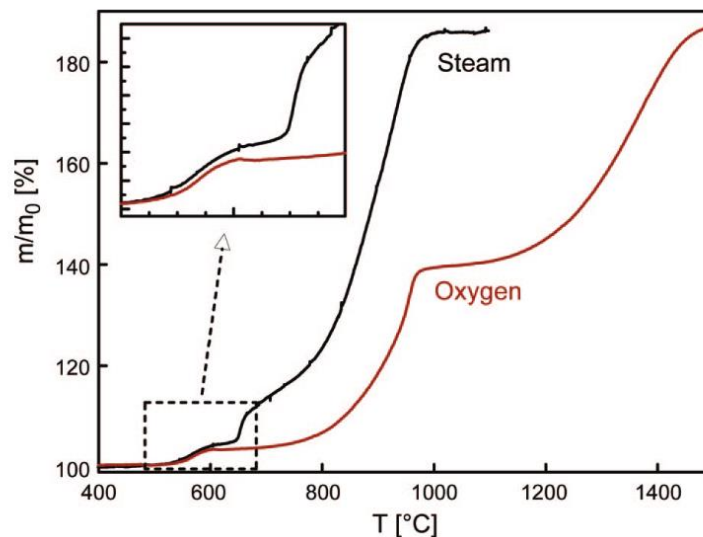


Figure 13. The different reactivity of aluminium powders in oxygen and in steam environments (experimental results from a TGA).

It is evident that near  $660^\circ\text{C}$  (melting point of aluminium) a very sharp increase of the reactivity is present. It is proposed that the presence of water stabilizes the  $\gamma$ - $\text{Al}_2\text{O}_3$  phase, delaying the transition to  $\alpha$ - $\text{Al}_2\text{O}_3$ , responsible to lowering the reaction rate. Moreover, it is assumed that the oxide layer around the molten particle could act as a semipermeable membrane, where OH ions are more prone to diffuse with respect to oxygen. Another model foresees that the external layer temporally increases its porosity. Each model could explain this step, but further work is requested to investigate the phenomenon.

## 3.2 Electrochemical processes

### 3.2.1 Power-to-Al

The production of aluminium from its oxide can be performed through electrochemical processes. If a hydroxide is the product of the Al-to-power process, common for low-temperature reactions, an additional preliminary step is requested to obtain  $Al_2O_3$  from  $Al(OH)_3$ , named calcination, happening at high temperatures ( $>1000^\circ C$ ) and following the reaction:



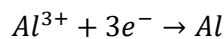
The reaction is endothermic, with a calculated  $\Delta \bar{h}_{calcination}^o = 185 \text{ kJ/mol}_{Al_2O_3}$ . Studies have demonstrated the possibility to perform the calcination only using concentrated solar energy [29].

Once alumina is available, it can be used to produce aluminium in an electrolytic cell. In the Hall-Héroult process, cryolite ( $Na_3AlF_6$ ) is used as electrolyte. Inside the cell, the dissociation of cryolite and alumina proceeds according to the reactions:

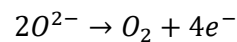


Cations  $Al^{3+}$  and  $Na^+$  are moved to the cathode to be reduced, but since Al is more electropositive than Na, mainly aluminium is discharged. Instead, anions  $AlF_6^{3-}$  and  $O^{2-}$  move to the anode, where oxygen is formed.

**Cathodic reaction**



**Anodic reaction**



Currently, carbon anodes are used in Hall-Héroult process as discussed in section 2.4.2, with the exploitation of another reaction that emits  $CO_2$ .

The necessary minimum charge needed to produce 1 g of Al can be calculated using Faraday's Law:

$$\dot{n} = \frac{I}{zF} \quad (12)$$

Thermodynamic analysis

$$n = \frac{Q}{zF} \rightarrow Q = zFn = zF \frac{m}{M} = 3 \cdot 96485 \cdot \frac{1 \text{ g}}{26,98 \frac{\text{g}}{\text{mol}}} = 10729 \text{ C} = 2,98 \text{ Ah/g}_{Al}$$

The minimum theoretical energy requested, without any losses, is made of the following contributions [30]:

- energy to drive the reaction forward ( $\Delta g$ );
- thermal energy needed to maintain equilibrium ( $\Delta h - \Delta g$ )
- thermal energy associated to the molten Al (960°C) with respect to room temperature.

If this equilibrium thermodynamic analysis is performed for both carbon anodes (following reaction in Eq. 2) and inert anodes (following reaction in Eq. 1), the results are different in the two cases: the minimum energy requirement for carbon anode method is 5,99 kWh/kg while for inert anode method it is 9,03 kWh/kg (Figure 14).

**Table J.1: Theoretical Minimum Energy for Hall Héroult Carbon Anode System**

Reactants Temp	Products Temp	Reaction Thermodynamics at 298 K				(products – reactants) cal/gm mole Al	
2 Al <sub>2</sub> O <sub>3</sub> 25°C	4 Al 960°C	( 2 Al <sub>2</sub> O <sub>3</sub> + 3 C )	to	( 4 Al + 3 CO <sub>2</sub> )	= Net		
		delta G	-756,358	0	0	-282,779	118,395
		delta H	-801,000	0	0	-282,155	129,711
		delta S	24.3	4.1	27.1	153.2	11,311
3 C 25°C	3 CO <sub>2</sub> 25°C						
						kWh/kg	
						Electrolytic Work Requirement (delta G)	5.11
						Thermal Energy for Temperature Maintenance (delta H - delta G)	0.49
						Thermal Energy for Al at 960°C	0.39
						<b>Theoretical Minimum</b>	<b>5.99</b>
						Thermal Energy for CO <sub>2</sub> at 960°C	0.17

Note: Thermodynamic values for G, H and S are from Table J.6. Heat capacity data are from Table J.9 and Appendix K

**Table J.2: Theoretical Minimum Energy for Hall Héroult Inert Anode System**

Reactants Temp	Products Temp	Reaction Thermodynamics at 298 K				(products – reactants) cal/gm mole Al	
Al <sub>2</sub> O <sub>3</sub> 25°C	2 Al 960°C	( Al <sub>2</sub> O <sub>3</sub> )	to	( 2 Al + 1.5 O <sub>2</sub> )	= Net		
		delta G	-378,179	0	0	189,089	
		delta H	-400,500	0	0	200,250	
		delta S	12	14	74	11,155	
1.5 O <sub>2</sub> 25°C							
						kWh/kg	
						Electrolytic Work Requirement (delta G)	8.16
						Thermal Energy for Temperature Maintenance (delta H - delta G)	0.48
						Thermal Energy for Al at 960°C	0.39
						<b>Theoretical Minimum</b>	<b>9.03</b>
						Thermal Energy for O <sub>2</sub> at 960°C	0.27

Note: Thermodynamic values for G, H and S are from Table J.6. Heat capacity data are from Table J.9 and Appendix K

Figure 14. Theoretical minimum energy requirements for aluminium production, both if carbon anodes or inert anodes are used.

However, the actual energy requirements for the power-to-Al process are higher than theoretical ones. Moreover, only carbon anodes are currently used at industrial scale. The final result is that for the state-of-the-art Hall-Héroult process the energy consumption is around 12,95 kWh/kg [17] but some applications lowered it to less than 12 kWh/kg.

According to these results, it is possible to assess the expected round-trip efficiencies (RTE) of an ideal Al-based energy storage system with current parameters considering that the term  $E_{out}$  is the specific energy of Al and  $E_{in}$  is the state-of-the-art energy requirement per kg of Al produced from alumina:

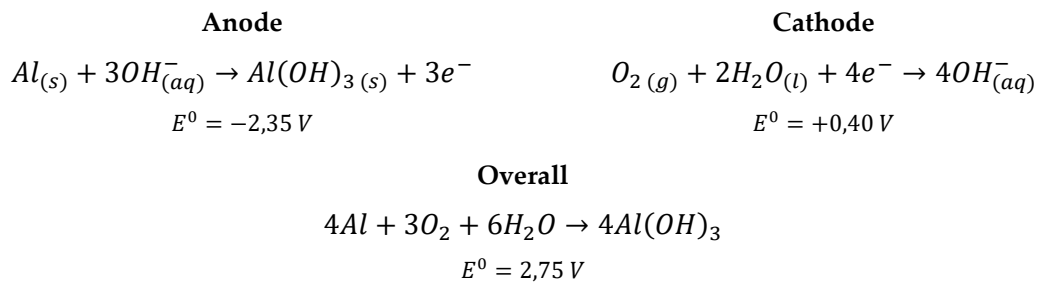
$$RTE_{max} = \frac{E_{out,delivered,max}}{E_{in,production}} = \frac{8,6 \text{ kWh/kg}}{12,95 \text{ kWh/kg}} \cong 0,66 \quad (13)$$

If only electricity is considered a useful product in the Al-to-power route, only a fraction of the potential energy of aluminium is valuable, and the delivered energy must be corrected of a term that, in first approximation, can be assumed around 45% considering that heat could be transformed into electricity in an engine and hydrogen can be exploited in a fuel cell. In this case, the RTE results around 30%. Additional energy consumption in the aluminium production has to be considered only if the process of calcination (1.6 kWh/kg) and consumption of carbon anodes (3.8 kWh/kg) are included.

### 3.2.2 Electrochemical oxidation of Al

So far in this work, the attention has been paid to Al-water reactions and production of hydrogen and heat, while these last two products can then be converted in electricity in a secondary step. Actually, a very attracting idea is to make aluminium to react directly in an electrochemical cell, in order to produce electricity in a direct manner. This concept is realized in the Al-air fuel cell/battery, in which the oxidant is atmospheric oxygen.

The electrolyte is usually an aqueous solution of KOH, NaOH or NaCl. Referring to alkaline electrolyte, the reactions at anode, cathode and overall are the following [11]:



An important aspect to consider is the possibility of the evolution of hydrogen. Indeed, aluminium in presence of water can react to produce  $H_2$ , as discussed before, when hydrogen was a desired product; in the direct electrochemical oxidation in batteries or fuel cells, instead, hydrogen production must be avoided. Additional challenges are avoiding corrosion of the anode due to the formation of impurities as  $Al(OH)_3$  and  $Al(OH)_4$ . An approach to improve the performance is using an alloy as anode, and many different other metals have been tested, such as Zn, Ga, In, Sn [31]. Some studies showed that, if the corrosion reactions are controlled, the battery anode could be exploited to cogenerate electricity and hydrogen [32].

## 4 Feasibility analysis: a case study

Keeping in mind the possible applications of Al as energy vector, in this section a single case study will be analyzed, providing an evaluation of the feasibility of an “energy hub” based on aluminium energy storage. In particular, the scenario considered is a district in which an aluminium smelter is present and can increase its capacity producing a surplus used for RES energy storage purposes. After the production from the smelter, the aluminium can be stored and delivered to the users in the district under request, exploiting an Al-to-power system that can generate electricity, heat and/or hydrogen. The paradigm can be summarized with “centralized production and distributed consumption”. In fact, it is very difficult to imagine a distributed production of aluminium, because the process of smelting increases in efficiency with increasing size of the plant and requires components that must be included in a specialized and well controlled plant.

The first step is to design a proper Al-to-power system, maximizing the extraction of power and heat from the aluminium fuel using the type of reactions discussed in the previous paragraph, in particular the Al-steam reaction performed at medium-high temperatures; then, the RTE of the unit can be estimated, and it can be used as input in a global energy/sustainability analysis at a district level, comparing the solution to another known P2P system, the hydrogen-based one. A comparison has already been done in literature stopping the analysis at the level of hydrogen production, evaluating the convenience of the use of aluminium (exploiting low-temperature reactions) with respect to the direct water electrolysis [33], showing similar economic indicators. However, it remains to be evaluated the convenience of aluminium with respect to hydrogen in a global context. The performance of a hybrid energy storage and hydrogen supply based on aluminium has been economically evaluated by Ersoy et al. [34], including the possibility of aluminium-fueled hydrogen refueling station for electric mobility, remarking possible economic benefits thanks to the exclusion of hydrogen transport from the global equation, substituting it with the dense aluminium.

A recent article [35] assessed the performance of an Al redox cycle in the framework of multi-family houses energy storage, in which the electricity is produced in compact fuel cells and including the thermal recovery. It shows interesting results in the coupling of

electrical and thermal needs of the houses with a global energy-to-energy efficiency of up to 69%, but with poor P2P efficiency (not higher than 19% in the best case), that instead will be the main focus of our study. It also provides a cost estimation that confirms the possible competitiveness of the metal-based storage compared to the hydrogen system, and a LCA (life cycle assessment) analysis that also confirms that the values are comparable and justifies keeping researching in the field (Figure 15).

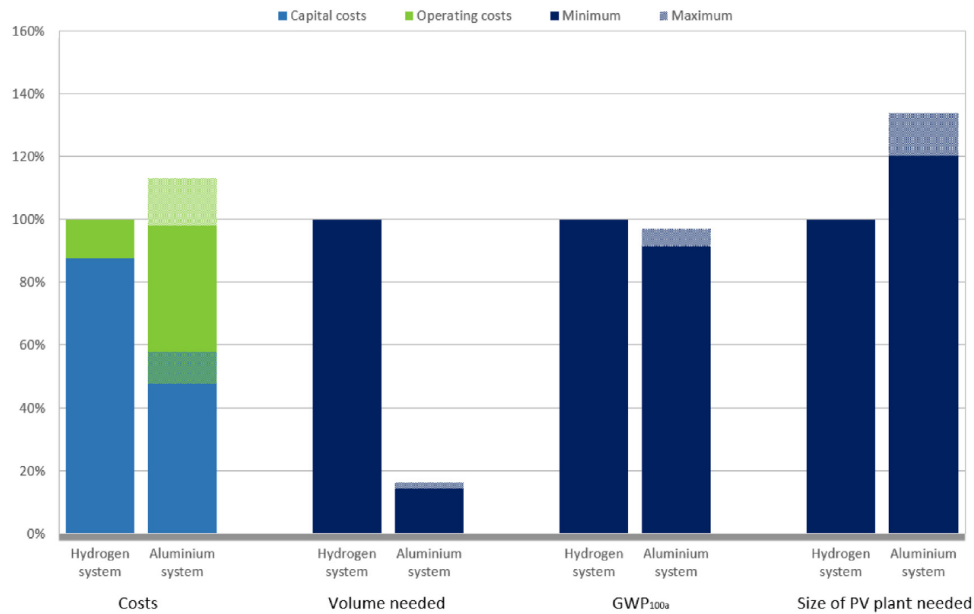


Figure 15. Hydrogen-based storage system vs aluminium-based one in a multi-family house scenario: system comparison of costs, volumes, GWP, size of PV needed.

## 4.1 Aluminium-fueled power plants: possible schemes

Most articles treating aluminium technology in energy applications focus on the production of hydrogen. In many cases then a single fuel cell is considered for the power production. However, if the aim is to produce power, a crucial step is to find an efficient layout to maximize the electrical yield of the system, because just the exploitation of hydrogen in the fuel cell does not provide satisfying P2P efficiencies, since the thermal power released by the reaction (that represents half of the energy content) cannot be converted in electricity. Thus, with this configuration the RTE usually is not higher than 20%, a value well below other proposed solutions. The aim of this section is to find possible integrated schemes to efficiently exploit Al-steam reaction at suitable temperature levels.

### **4.1.1 Some layouts from literature**

Franzoni et al. [36] studied the concept of a combined hydrogen production and power generation taking advantage of a high temperature aluminium combustion with water. According to this concept, the heat of reaction can be recovered vaporizing more water than the one requested by the reaction and expanding it into a steam turbine following a standard Rankine cycle; moreover, the hydrogen is reacted in a fuel cell. Efficiencies of such power plants according to the authors can reach 64% electrical and 85% global (including thermal one), values comparable to current standard gas-fired cogeneration systems. In the work also the energy consumption of an aluminium grinding machine is taken into account, powered by part of the electricity produced in the steam turbine. However, no plant schemes were provided in the reference, as the paper only explores the idea conceptually.

Vlaskin et al. [37] studied methods to exploit the enthalpy of the steam-hydrogen mixture exiting the reaction chamber, with medium-low temperature of reaction (600 K) and high pressure (15 MPa). The proposed layout foresees the installation of a steam-hydrogen turbine just after the reactor that converts the thermal energy of the flow into useful power, followed by a condenser and finally a secondary generation unit consisting either in an air-hydrogen fuel cell or in a hydrogen-fueled gas turbine (Figure 16). These configurations with reaction performed at this quite low temperature do not seem to be promising since the electrical efficiency is assessed in the range 25-30%, and steam-hydrogen turbines could not be the optimal solution due to their complexity.

Yang et al. studied the efficiency of two configurations based on a 1-turbine layout and a 2-turbine layout [38] coupled with a fuel cell and with a heat recovery system (Figure 17). The 1-turbine layout foresees a gas turbine after the reactor, followed by the fuel cell, while the 2-turbine layout includes a steam turbine that takes advantage of steam produced in the contact of cooling water with the walls of the reactor, with efficiencies up to around 50% (electrical) and 70% (total).

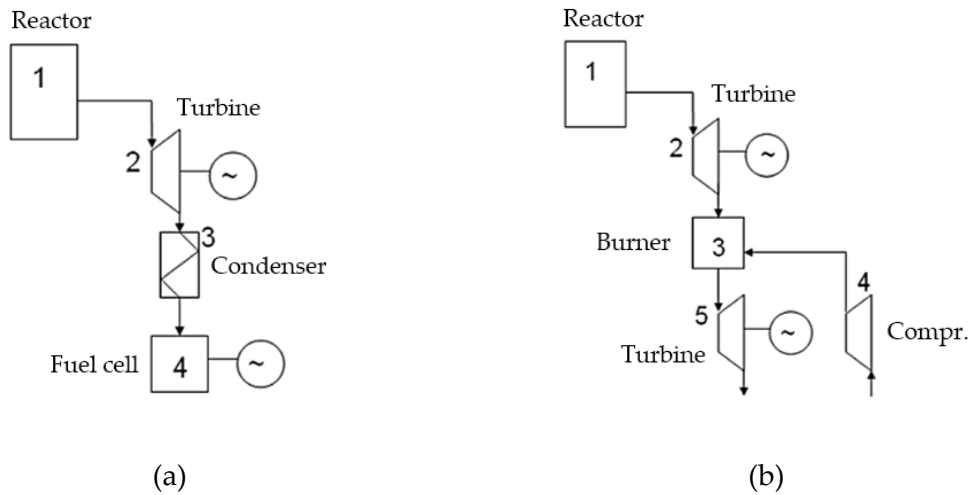


Figure 16. The two concepts of plant provided by Vlaskin et al.: with fuel cell (a), without fuel cell (b).

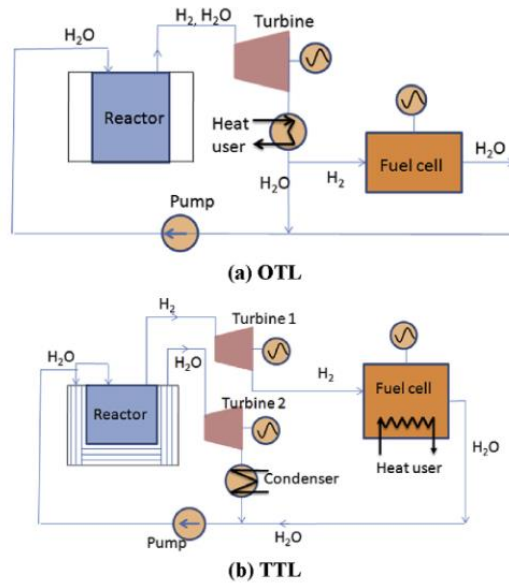


Figure 17. The two concepts of plant provided by Yang et al.: 1-turbine layout (a), 2-turbines layout (b).

A combination and integration of the previous ideas could lead to an improved solution. The exploitation of a Rankine cycle, a standard and well-known technology, appears to be the most interesting and simple path to recover part of the heat of reaction with a significant electrical production. Employing fuel cells is also promising, since they are the most efficient generators when a hydrogen flow is available; a high temperature fuel cell (i.e., solid oxide fuel cells, SOFC) would even improve the performance if the reaction temperatures are compatible. In this case, an additional section with a hydrogen-fueled gas turbine could be employed to extract more power from the flow of gases exiting the

SOFC. The system then can be optimized in order to recover thermal power. A layout concept of this type is well explained in the paper of Barelli et al. [17].

### **4.1.2 Adopted layout**

The solution that will be adopted in this section is the one proposed by Barelli et al. [17], therefore the configuration foresees the following main components:

- An isothermal (750°C) aluminium-steam reactor.
- A steam Rankine cycle section exploiting the heat of reaction and controlling the temperature of the reactor.
- A SOFC using the produced hydrogen.
- An afterburner and gas turbine system exploiting the enthalpy of the flow after the SOFC.

This configuration is the one that will be considered in the next case study for the Al-to-power plant, and a conceptual scheme will be reported in Figure 24 and Figure 28 in Section 5. Actually, this is a flexible layout in which the only necessary components are the reactor and the fuel cell; the other can be present or not depending on the aim of the plant, mainly to produce power or to cogenerate heat.

The explanation and simulation of a similar plant on Aspen Plus will be carried out in the next chapter. For now, it is sufficient to take the reference electrical efficiency of the layout proposed by Barelli et al., that is 71.2%. In the next case study, all the users are considered equipped with a plant of this kind, and the focus is put on electrical power, while thermal needs are not under consideration since they strongly depend on the type of user (industrial, tertiary, residential etc.).

## **4.2 District analysis**

In this section the energy sustainability of a hypothetical aluminium-based energy hub will be assessed in a simple way.

The considered hub is a district/region in which an aluminium smelter of a typical size is already present and it can increase its capacity up to a certain amount making use of excess renewable power (mainly photovoltaics), thus storing energy in aluminium. Since smelters are large and energy-consuming plants, this type of energy storage can be

assessed as “bulk” or large-scale storage, and it could be convenient if a large renewable plant is present near the smelter. The surplus aluminium is stored on site and delivered by truck to the users, placed in a certain radius around the smelter according to the amount of metal fuel available (Figure 18). Assuming a typical power consumption of the users and their density per unit area, it is possible to estimate the size of the district that can be served by this hub. Also transport energy consumptions are taken into account, considering hydrogen-fueled trucks. Finally, some key indicators are reported, such as the power-to-power efficiency (including transport) and the specific CO<sub>2</sub> emissions per kWh (considering current production methods for Al).

To provide a comparison the same district will be evaluated also based on a hydrogen P2P system with compressed H<sub>2</sub> storage, to assess the advantages and disadvantages of each technology.

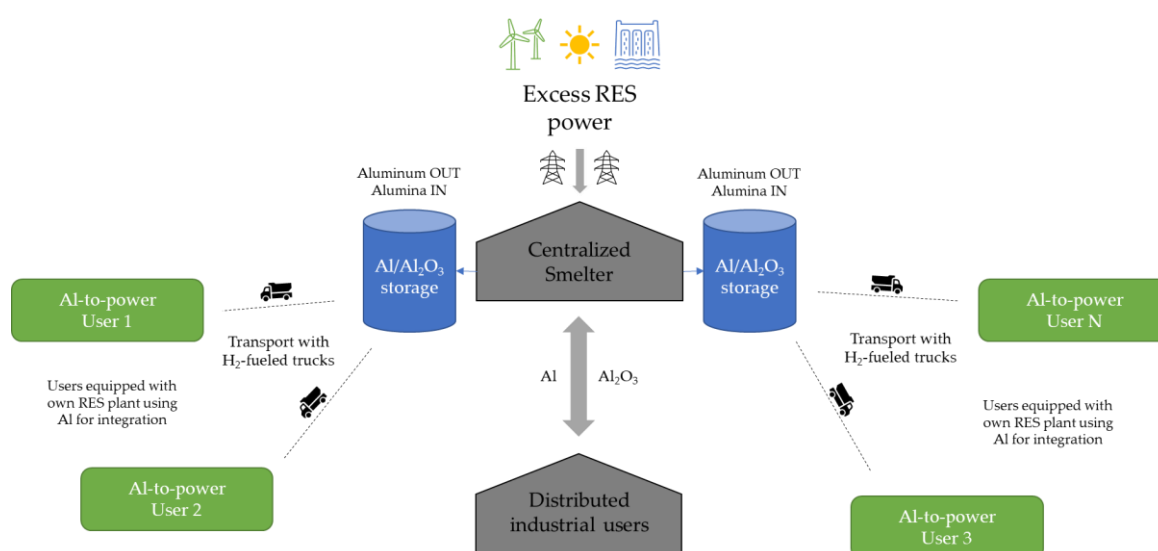


Figure 18. Conceptual scheme of the proposed case study: centralized energy storage in the smelter (production of aluminium), transport, and distributed consumption.

## 4.2.1 Assumptions and methods

### 4.2.1.1 Smelter

The size of the smelter, expressed in ton/year, is chosen in accordance with typical values for European plants, since the district has been considered placed in Italy, even if nowadays no smelting units are active in this country. As can be seen in an online list [39], the productivity ranges from 25000 to 1500000 ton/year worldwide (the biggest plants are located in Asian and Middle East countries), while in Europe a typical average value can be set to 150000 ton/year, that is the chosen size.

The next step is to estimate the nominal power consumption of the plant, assuming it is completely powered by renewables. It is first necessary to hypothesize the electrical energy intensity for the production of a unit mass of aluminium: the world average is 14.1 kWh/kg, but this value is influenced by many old and inefficient plants still running, and today the energy intensity of state-of-the-art smelters reaches values as low as 11.5 kWh/kg like in the case of Norwegian plant of Karmøy [40][41]. With these two parameters it is possible to evaluate the annual electricity consumption of the plant and, considering a steady state operation during the year, a nominal power rating, that results 197 MW.

Aluminium smelters are big and complex systems that usually show poor flexibility levels and should always work at constant power supply: the production lines should always operate in steady state conditions because their start and stop may require a huge amount of time. The main issue is that, increasing the current in a single unit of smelting, the heat produced by Joule effect increases very much as well, leading to an overheating of the cell; instead, if the current goes below the nominal value, the operating temperature of the cell drops down, to the point that the cryolite could solidify. As a consequence, it is currently difficult to integrate variable renewable energies (VRE) in an aluminium smelter without using energy storage, indeed they are typically powered by hydroelectric plants (mainly in Europe) or coal/gas fired plants (mainly outside Europe) that can guarantee a steady electric power input; practically it is not currently feasible to run a smelter only on PV or wind system without the use of very large storage systems near the plant, that can smooth out the intermittency.

One of the most interesting solutions to this problem is to integrate heat exchangers in the walls of the smelters, allowing to deal with the different heat fluxes due to different injected currents. This solution has proven to be feasible and quite economical with a payback time of 2.5 years and should allow a flexibility of the plant up to  $\pm 25\%$  for VRE integration [41]. TRIMET, one of the biggest companies in Europe dealing with aluminium, has already tested these heat exchangers in its facilities, with success [42].

Therefore, in the case study a conservative flexibility level of 20% is assumed, that means the plant can absorb up to 20% of its nominal rated power of variable RES in addition to the steady state nominal operation. In numbers, given a nominal power rating of 197 MW, the maximum amount of RES that can be stored is  $197 \cdot 0.2 \cong 39$  MW and the

maximum power input for the plant is  $197+39=236$  MW. The smelter, therefore, will work with power inputs between 197 and 236 MW depending on how much electricity must be stored, with a storing power capacity of 39 MW. The annual electricity stored by the smelter will depend on how long it will operate at each power input in this range, and can be estimated in a simple way by hypothesizing an annual parameter of “capacity factor of storage” that quantifies the percentage of used storing ability. It has been assumed 60%, considering a mix of PV and wind energy storage, in which during night the capacity of the smelter is not saturated. In this way the annual electricity stored can be estimated, as well as the corresponding aluminium produced and destined to the users (Table 6). The smelter will therefore produce metal powder in surplus, that will be destined to the energy storage, while the nominal aluminium (the amount linked to the nominal power consumption) will continue to be produced for the sale to manufacturers and secondary industries and will not be involved in this analysis.

Table 6. Case study: sizing and main parameters of the smelter.

Name	Description	Value	U.M.	Explanation
NS	Nominal size	150000	ton/year	hyp.
EI	Energy intensity	11.5	MWh/ton	hyp.
AEC	Annual electricity consumption	1725000	MWh/year	$NS \cdot EI$
$P_r$	Nominal power rating	197	MW	$AEC/8760$
FL	Flexibility level of the plant	0.2	-	hyp.
$P_{st}$	Storing capacity	39	MW	$FL \cdot P_r$
$P_{max}$	Maximum power rating	236	MW	$P_r + P_{st}$
$CF_s$	Capacity factor for storage	0.6	-	hyp.
AES	Annual electricity stored	207000	MWh/year	$CF_s \cdot FL \cdot AEC$
$M_{Al,pr}$	Aluminium powder produced	18000	ton/year	$AES/EI$

#### 4.2.1.2 User

The users are considered equipped with own RES power plant to self-produce electricity with an assumed self-sufficiency of 60%. The remaining part should be covered by the AI-based power generator. A nominal power consumption of 500 kW is assumed in order

to size the user, in accordance with the needs of medium-big industrial facilities. The annual amount of electricity needed from the Al-to-power system can be found (assuming constant consumption during the year) and, considering an efficiency of the Al-to-power plant of 71,2% (based on its lower heating value LHV) the aluminium needed by each user can be estimated (Table 7).

Table 7. Case study: energy consumption and sizing of the users and their main parameters.

Name	Description	Value	U.M.	Explanation
$P_{u,n}$	Nominal power of user	500	kW	hyp.
$F_{Al}$	Fraction needed from Al	0.4	-	hyp.
$AE_n$	Annual electricity needed from Al	1752	MWh/y	$P_{u,n} \cdot F_{Al} \cdot 8760 h$
$LHV_{Al}$	Lower heating value of Al	17.874	MJ/kg	known
$\eta_{g,Al}$	Efficiency of the Al generator	0.712	-	hyp.
$Y_{Al}$	Electrical yield of Al	3.54	MWh/ton	$\eta_{g,Al} \cdot LHV_{Al}/3.6$
$M_{Al,n}$	Amount of aluminium needed	495.6	ton/year	$AE_n/Y_{Al}$

#### 4.2.1.3 Equivalent H<sub>2</sub> P2P system

Hydrogen power-to-power systems are composed of an electrolyzer (production of H<sub>2</sub> from electricity), a storage system (in this case compressed gas in a tank) and a fuel cell (production of electricity from H<sub>2</sub>). The electrolysis energy intensity has been considered 50 kWh<sub>el</sub>/kgH<sub>2</sub>, the compression energy intensity 3.1 kWh/kg [43]. Assuming the same availability of electricity as the previous case (same parameter “AES”), it is possible to evaluate the amount of hydrogen that can be produced and the electricity used for compression. The users are the same as the previous case, but with different generation units, in this case fuel cells with an efficiency of 60%. Knowing the electrical need, the generator efficiency and the lower heating value of hydrogen (33,3 kWh/kg) the mass of hydrogen needed by each user can be found (Table 8).

Table 8. Case study: equivalent hydrogen P2P system sizing and main parameters.

Name	Description	Value	U.M.	Explanation
AEI	Annual electricity input	207000	MWh/year	Same as smelter
EP	Energy intensity for H <sub>2</sub> production	50	MWh/ton	hyp.
EC	Compr. energy intensity @350 bar	3.1	MWh/ton	hyp.
M <sub>H<sub>2</sub>p</sub>	Amount of H <sub>2</sub> produced	3898	ton/year	$AEI/(EP + EC)$
E <sub>comp</sub>	Annual electricity for compression	12085	MWh/year	$EC \cdot M_{H_2p}$
η <sub>FC</sub>	Efficiency of fuel cells	0.60	-	hyp.
LHV <sub>H<sub>2</sub></sub>	Lower heating value of H <sub>2</sub>	33.3	MWh/ton	known
M <sub>H<sub>2</sub>n</sub>	Mass of H <sub>2</sub> needed for 1 user	87.6	ton/year	$\frac{AE_n}{\eta_{FC} LHV_{H_2}}$

#### 4.2.1.4 Transport

To deal with transport aspects it is first needed the size of the district that can be served. The reasoning will be carried out for the case of Al storage but is the same for H<sub>2</sub> storage. Knowing the amount of aluminium needed by 1 user and the total aluminium powder produced by the smelter, the number of users that can be served is easily found, rounding down the result. A density of users per km<sup>2</sup> can be assumed in order to find the area served and finally the radius of this area, centered around the smelter. The average transport length has been considered as 80% of the radius (Table 9).

Table 9. Case study: dimensions of the served area.

Name	Description	Value	U.M.	Explanation
N <sub>u</sub>	Number of users served	36	users	$M_{Al,pr}/M_{Al,n}$
D <sub>u</sub>	Density of users	0.01	users/km <sup>2</sup>	hyp.
A	Area served	3600	km <sup>2</sup>	$N_u/D_u$
R	Radius of the area	33.9	km	$\sqrt{A/\pi}$
L	Average transport length	27.1	km	hyp. (0.8 · R)

The load of aluminium that can be transported on a truck is assumed 40 ton, in accordance with current values for large trucks transporting solids. With this assumption

the number of cycles of transport per year can be calculated, and hence the total length covered in 1 year linked to 1 user. Considering that both aluminium to the user and alumina to the smelter must be transported, and that for each kg of Al the production of alumina is 2 kg, the total length is the double compared to the case in which no alumina would be reported to the smelter.

For hydrogen fueled trucks, the fuel consumption is a function of the payload [44]. Current maximum payload for these trucks is about 25 tons, for which the fuel consumption is 10 kg/100 km; these values will be used for aluminium transport. Instead, for the transport of hydrogen a lower fuel consumption will be considered (7 kg/100 km) corresponding to the minimum payload. The values are used to calculate the hydrogen consumption for transport, then converted in terms of energy using its calorific value and, in the first scenario, in equivalent aluminium, considering that each ton of Al can produce 111 kg of hydrogen as discussed in 3.1.1. Results are reported in Table 10 and Table 11.

Table 10. Case study: transport aspects analysis and energy consumptions.

Name	Description	Value	U.M.	Explanation
$M_{tr}$	Maximum load for Al transport	25	ton	hyp.
$N_c$	Number of cycles needed per year	40	-	$2 \cdot M_{Al,n}/M_{tr}$
$D_y$	Distance travelled per year, 1 user	2167	km/year	$2 \cdot L \cdot N_c$
$f_{tr}$	Fuel consumption for H <sub>2</sub> trucks	10	kg/100km	hyp.
$TR_{H_2}$	Hydrogen for transport, 1 user	217	kg/year	$\frac{f_{tr}}{100} \cdot D_y$
$TR_E$	Energy for transport, 1 user	7.2	MWh/year	$TR_{H_2} \cdot LHV_{H_2}$
$\epsilon_{H_2}$	Hydrogen yield from aluminium	111	kg <sub>H<sub>2</sub></sub> /ton <sub>Al</sub>	thermodynamics
$M_{Al,tr}$	Equivalent aluminium for transport	1.95	ton/year	$TR_{H_2}/\epsilon_{H_2}$

Regarding the hydrogen P2P system, the same assumptions have been performed, except:

- The maximum load for transport in trucks in compressed form has been considered 300 kg [45], consequently the fuel consumption is the one corresponding to the minimum payload in ref. [44] (7 kg/100 km);

- The number of transport cycles is not the double, because the reaction product (water) can be managed directly by the user;
- It is not needed to calculate the aluminium equivalent.

Table 11. Case study: transport aspects analysis and energy consumptions for the equivalent hydrogen P2P system.

Name	Description	Value	U.M.	Explanation
$N_u$	Number of users served	45	users	$M_{H2p}/M_{H2n}$
$D_u$	Density of users	0.01	users/km <sup>2</sup>	hyp.
$A$	Area served	4500	km <sup>2</sup>	$N_u/D_u$
$R$	Radius of the area	37.9	km	$\sqrt{A/\pi}$
$L$	Average transport length	30.3	km	hyp. ( $0.8 \cdot R$ )
$M_{tr}$	Load for hydrogen transport	0.3	ton	hyp.
$N_c$	Number of cycles needed per year	292	-	$M_{H2n}/M_{tr}$
$D_y$	Distance travelled per year, 1 user	17687	km/year	$2 \cdot L \cdot N_c$
$f_{tr}$	Fuel consumption for H <sub>2</sub> trucks	7	kg/100km	hyp.
$TR_{H2}$	Hydrogen for transport, 1 user	1238	kg/year	$\frac{f_{tr}}{100} \cdot D_y$
$TR_E$	Energy for transport, 1 user	41.3	MWh/year	$TR_{H2} \cdot LHV_{H2}$

#### 4.2.1.5 Emissions

In this scenario all the electrical energy is derived from renewables and transport is performed with hydrogen fueled trucks. Thus, no greenhouse gases are emitted during these processes. In particular, hydrogen-based P2P system is completely CO<sub>2</sub>-free. Instead, for aluminium this can be said only in the case of utilization of inert anodes or “clean” production processes: up to now (and realistically for the next years) the Hall-Héroult process gives unavoidable emissions due to the consumption of the carbon anode. Even though they are very limited compared to other metal production processes, they must be considered. A value of 1.6 kg<sub>CO2</sub>/kg<sub>Al</sub> is considered [46].

Table 12. Case study: emission analysis inputs and results.

Name	Description	Value	U.M.	Explanation
e	Specific emissions in smelting	1.6	kg <sub>CO2</sub> /kg <sub>Al</sub>	hyp.
EM	Annual emissions	28800	ton <sub>CO2</sub> /year	$e \cdot M_{Al,pr}$

## 4.2.2 Results

### 4.2.2.1 Volume of fuel needed

The first aspect that will be analyzed is the volume of fuel needed in 1 year by 1 user in both cases, to satisfy the same needs. The calculation is quite simple since, having the mass of Al or H<sub>2</sub> requested by 1 user, it is sufficient to divide by the density of the fuel. For Al the density is 2700 kg/m<sup>3</sup>, for hydrogen at 300 bar it is 20 kg/m<sup>3</sup>. Therefore, even if the mass of aluminium needed is much higher (496 ton<sub>Al</sub> vs 87.6 ton<sub>H2</sub>), the resulting volume is only 183.6 m<sup>3</sup> for Al compared to 4380 m<sup>3</sup> for H<sub>2</sub>, with a clear and expected advantage for the Al-based system in terms of volumetric energy density.

### 4.2.2.2 Impact of transport

The impact of transport can be assessed by comparing the amount of fuel needed to power the trucks with the total amount, always referring to one user. For aluminium system, 1.95 tons of Al-equivalent are wasted for transport with respect to a total of 496 tons, corresponding to 0.39%. For hydrogen system, 1.24 tons of H<sub>2</sub> are wasted for transport compared to a total of 87.6 tons, corresponding to 1.41%. Therefore, the impact of transport is about 4 times higher for the hydrogen scenario, mainly due to the much lower maximum load of trucks carrying compressed gas with respect to solid metals.

### 4.2.2.3 Round trip efficiency

The round trip efficiency (RTE) of the system is one of the most important parameters, summarizing the power-to-power energy performance in a single number considering also the transport losses; it has been defined in this case as the ratio between the total annual energy need ( $AE_n$ ) subtracted by the equivalent energy for transport ( $TR_E$ ) for all users ( $N_u$ ) and the annual energy stored in the smelter ( $AES$ ):

$$RTE = \frac{N_u \cdot (AE_n - TR_E)}{AES} \quad (14)$$

The parameters  $AES$  and  $AE_n$  are the same in the two cases since the same smelter and users are considered as baseline. The parameters changing are the number of users served, higher for hydrogen system (because more hydrogen can be produced with the same input electricity, thanks to higher production efficiency) and the transport energy (higher for hydrogen system as well).

The results are a RTE of 30.3% for Al system and 37.2% for H<sub>2</sub> system.

#### *4.2.2.4 Emissions per kWh*

To assess the specific emissions per useful kWh in the Al-based system it is sufficient to divide the total annual emissions in smelting (EM) by the total electric energy consumed by the users (subtracting transport energy). The outcome is 0.458 kg<sub>CO2</sub>/kWh.

This value is practically not acceptable since it is comparable to the world's average carbon intensity of electricity generation, that for 2021 was 0.441 kg<sub>CO2</sub>/kWh [47]. Therefore, in order to obtain advantages from the point of view of CO<sub>2</sub> emissions, aluminium production must reduce in a strong way its carbon intensity, otherwise the process adds to the clean renewable energy a contribution of CO<sub>2</sub> that cancels out the expected benefits. The pathway is to invest in new carbon-neutral technologies, like for example inert anodes.

Actually, many studies focus on the utilization of aluminium as electrofuel in perspective, with zero CO<sub>2</sub> emissions supposed, but if current values are taken into account this study demonstrate that aluminium would still not be a reasonable solution for a carbon-free electrofuel.

#### *4.2.2.5 Comparative graphs*

In the graphs here reported, it is possible to visually see the difference in mass and volume yield of the two cases (Figure 19) and the fuel used for transportation and RTE (Figure 20).

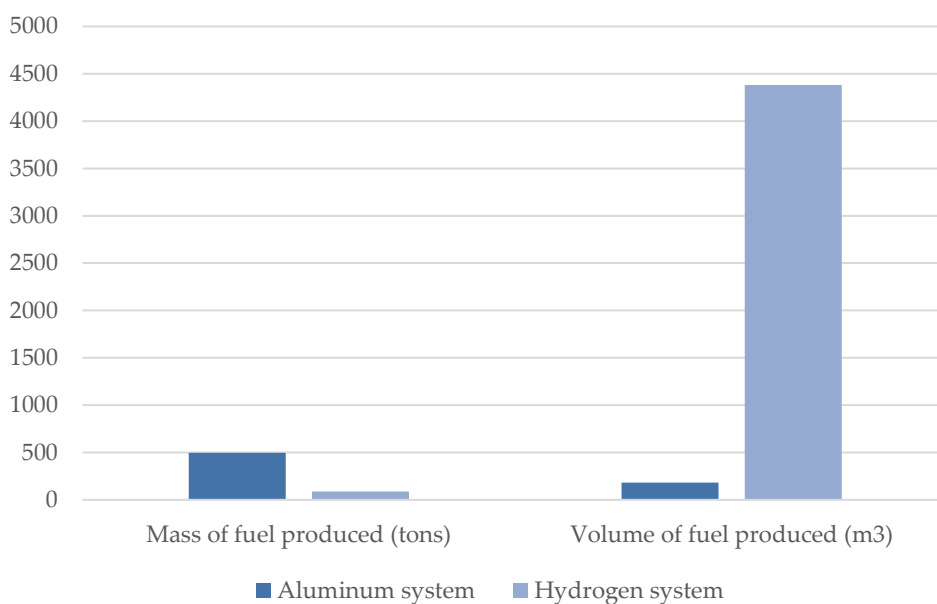


Figure 19. Mass and volume of the energy carrier (aluminium or hydrogen) that is produced with the same input electricity.

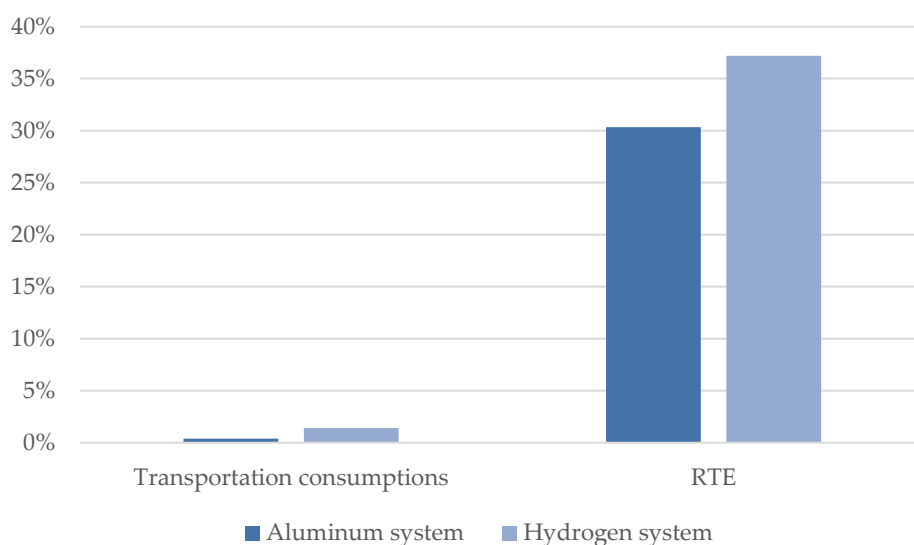


Figure 20. Comparison of transportation consumptions and RTE of aluminium-based and hydrogen-based storage systems.

#### 4.2.2.6 Sensitivity analysis

Since the results are very dependent on different hypotheses as input data, it is recommended to perform some sensitivity analysis on key parameters.

The first one, that is also the one with higher uncertainty, is the generation efficiency of the aluminium-based power plant. In the base case it is assumed 0.7, according to values reasonably reached in highly integrated plants with SOFC, gas turbines and steam

turbines. In case of missing some of the elements (for example just using SOFC), that could be too expensive, efficiency is lower, while in case of optimization values up to 0.8 could be reached. Therefore, a sensitivity analysis from 50% to 80% of generation efficiency has been carried out, resulting in increasing RTEs from 22% to 34% and decreasing specific emissions from over 600 to about 400 g/kWh (Figure 21).

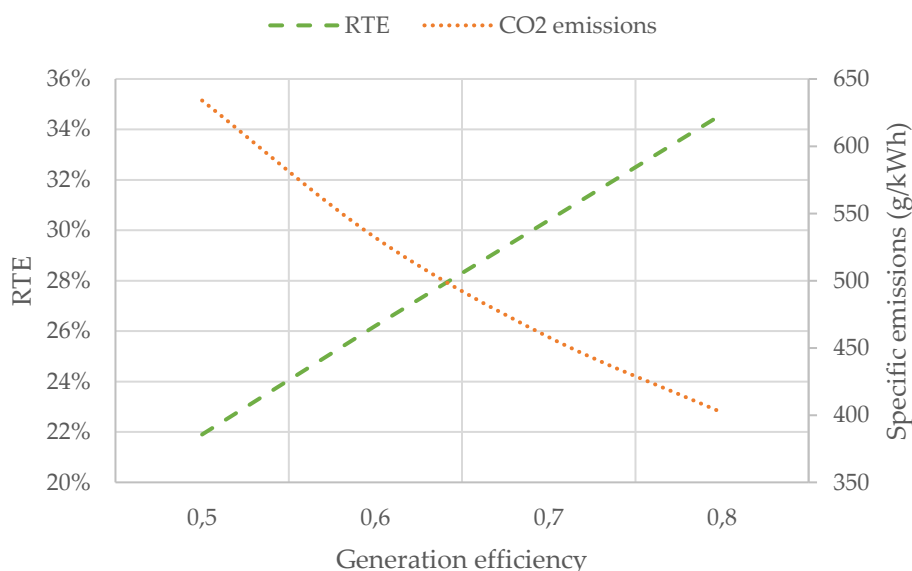


Figure 21. RTE and specific emissions at different efficiencies of the Al-to-power generation unit.

Another interesting aspect to consider is the comparison of Al and H<sub>2</sub> based systems in terms of transportation consumptions. In fact, this could be one of the biggest advantages for a solid-based system. The radius of the district has been changed in the range 20-250 km and the corresponding transportation consumptions have been found, calculated as fraction of fuel for transport compared to the total amount produced at the beginning of the process. As can be seen in (Figure 22), aluminium system shows generally much better performances, relating bigger advantages with increasing size of the district; it remains in the explored field under 3% compared to about 9% losses of the hydrogen system with very large size (250 km).

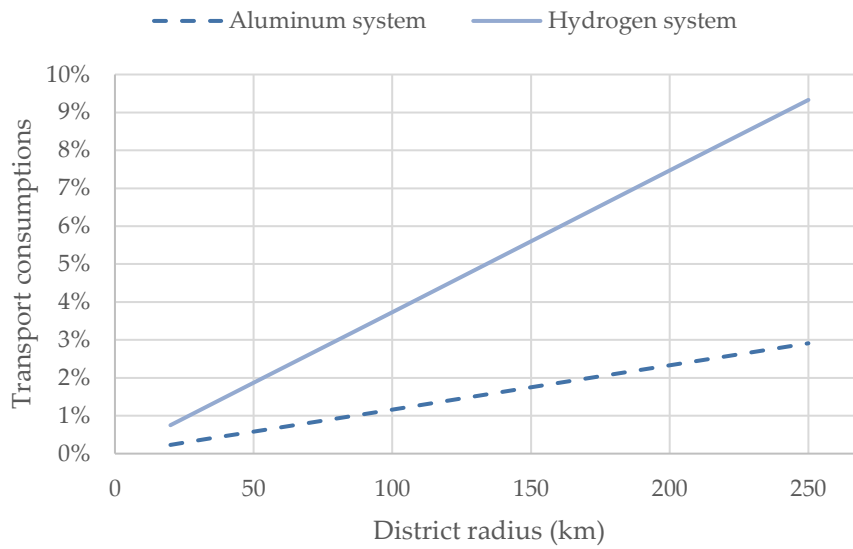


Figure 22. Comparison of transportation consumptions with different sizes (radii) of the district.

The same effect reflects in the RTE, as it remains quite constant for Al while it decreases much more for H<sub>2</sub> (Figure 23). Anyway, it must be said that hydrogen system keeps showing a higher RTE in all the explored field, even though it is more influenced by the size of the district.

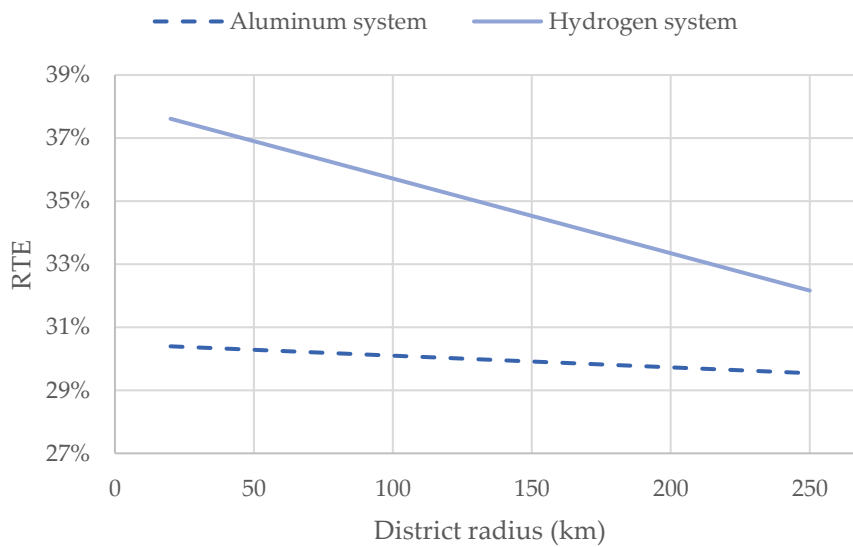


Figure 23. Comparison of RTEs with different sizes (radii) of the district.

## 5 Al-to-power plant model

In this section the aim is to build models of Al-to-power cogeneration plants in Aspen Plus and simulate their performances in different conditions, with the purpose to optimize the electrical and thermal efficiency.

The reference scheme is the one proposed by Barelli et al., already cited previously [17], and mainly consists in a SOFC+GT+ST plant (solid-oxide fuel cell + gas turbine + steam turbine), the one that should deliver high electrical efficiencies and working at medium-high temperatures (components deal with temperatures always lower than 1000°C). The model is built with different blocks and operating conditions, with the integration of heat recovery units and optimization of the working principle of each component. The main sections of the plant are schematically represented in Figure 24 with the same color code that will be used in the Aspen Plus model.

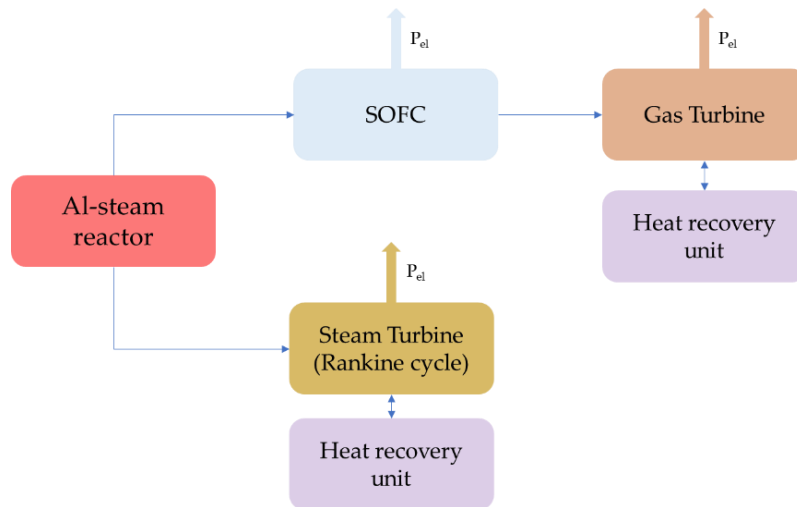


Figure 24. Schematic of the main sections of the Al-to-power plant.

### 5.1 Components description

#### 5.1.1 Reactor

The first component to be analyzed is the reactor. Since the reaction under consideration is strongly exothermic, it is necessary to remove heat from it in order to maintain the temperature of reaction fixed (for example at 900°C). If the reactor is considered adiabatic and isolated, the temperature of reaction would in fact reach values over 2000°C (value

found simulating the stoichiometric reaction in an adiabatic equilibrium reactor) with the triggering of a combustion flame that is not acceptable.

An efficient way to cool the reactor is to exploit the heat of reaction for two purposes: 1) to vaporize the inlet water needed for the Al-steam reaction; 2) to act as steam generator for a bottom Rankine cycle, producing electricity. Anyway, such a reactor is not trivial to be built; conceptually, it could be imagined as depicted in Figure 25. The component 1 is the real aluminium-steam reactor, operating at ambient pressure or slightly pressurized (3 bar) and in which the temperature must be kept fixed. This reactor could be immersed in a pressurized steam generator (3) fed by water pumped from the Rankine cycle and producing high temperature and pressure steam for the steam turbine. Another section of the component could be assigned to the generation of steam as reactant, depicted with number 2, that must operate at low pressure, the same one as the reactor.

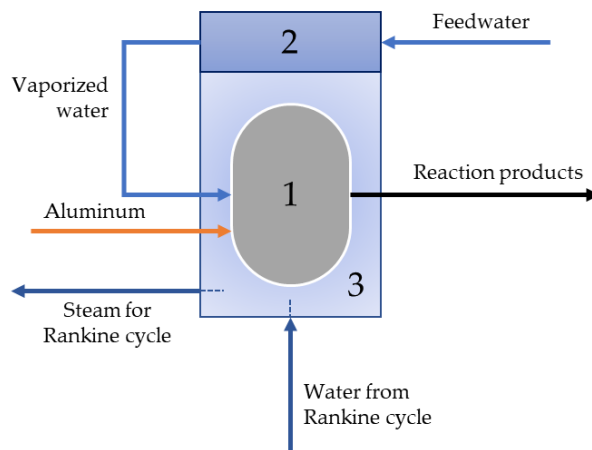


Figure 25. Conceptual scheme of a water-cooled isothermal Al-steam reactor. 1: reactor; 2: vaporizer for reacting water; 3: steam generator for Rankine cycle water.

Another aspect to consider in the reactor is that one of the products is solid (alumina). It is important to foresee a system that removes alumina from the reactor so that the outlet pipe only contains gaseous substances (hydrogen and surplus steam). Since it is a separation of a solid from a gas, it could be a mechanical separator. At the reaction temperature of 900°C alumina is produced in microparticles, making possible the continuous use of the reactor (theoretically avoiding any clogging effect) [17].

### 5.1.2 Steam Rankine cycle

The steam cycle converts part of the thermal energy of the reaction in useful mechanical energy. A stream of water is pumped at high pressure to the heat source, consisting in the

reactor itself, where it is completely vaporized and superheated up to a certain value (superheating is guaranteed because the temperature inside the reactor is always much higher than the requested temperature for the turbine inlet). The steam is then passed through a standard steam turbine that converts part of its enthalpy in mechanical work, reducing temperature and pressure. Finally, water is condensed in a cooler, that can also consist in a heat exchanger if thermal recovery is possible, and the cycle re-starts from the pump (Figure 26).

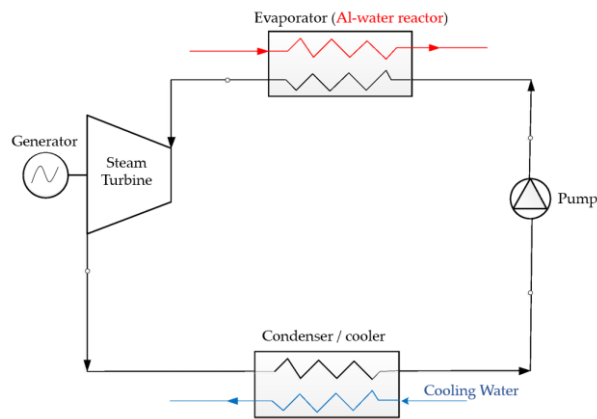


Figure 26. Schematic of a typical Rankine cycle.

### 5.1.3 Solid oxide fuel cell

The solid oxide fuel cell (SOFC) produces electrical energy taking advantage of the chemical energy contained in the hydrogen exiting the reactor. A SOFC has been selected as main power generator because of its relatively high operating temperature (700-850°C), not dissimilar to the temperature of Al-steam reaction, meaning that thermal integration is guaranteed. Moreover, the gas exiting the SOFC are still at a sufficient high temperature to transform their enthalpy into additional power in a gas turbine.

The working principle of a SOFC is depicted in Figure 27, in which DC electricity is produced thanks to the electrochemical oxidation of hydrogen (anode) by oxygen (cathode), with transport of  $O^{2-}$  species through the electrolyte.

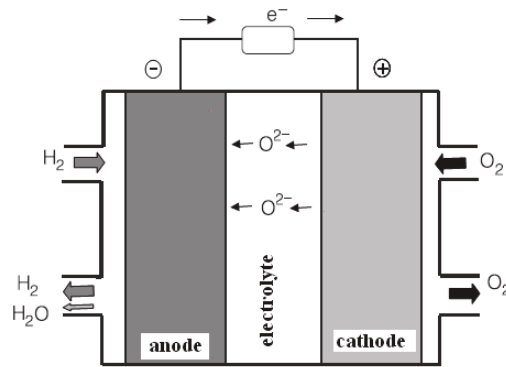


Figure 27. Schematic representation of a SOFC.

In our case, the anode is fed with the gas mixture exiting the Al-steam reactor (after the separation of the solid phase, the alumina), consisting in hydrogen with some residual water deriving from an over-stoichiometric excess or from a possible incomplete reaction. The cathode is fed with ambient air, acting as a coolant medium for the stack and providing the stoichiometric oxygen. Air is raised at the system pressure of 3 bar by a compressor, and its temperature is increased in a heat exchanger exploiting the exhausts from the following turbine.

#### 5.1.4 Gas turbine section

The exhausts of the SOFC still have some potential energy content due to their temperature and their chemical composition. In fact, the fuel cell does not consume 100% of the input hydrogen, but only a fraction, according to a parameter usually defined fuel utilization (FU). Common values for the FU are around 0.8. Thus, at the exit of the SOFC hydrogen is still present, together with high temperature steam, so that it is possible to perform a combustion of the residual gas in an afterburner (in air) to increase the temperature of the flow. The gases are then expanded in a microturbine that discharges its exhausts at ambient pressure.

## 5.2 Model building

The model built on Aspen has the layout reported in Figure 28.

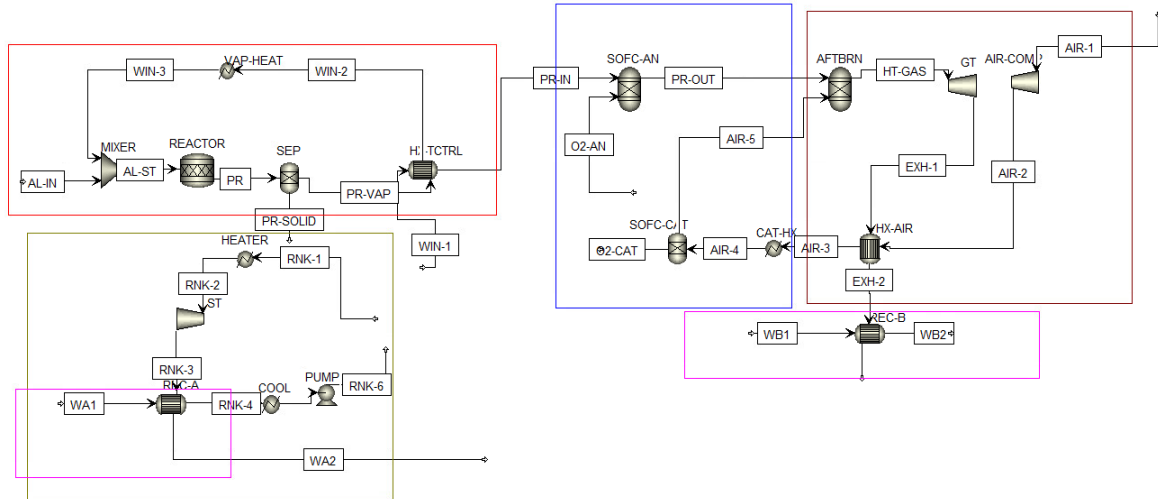


Figure 28. Layout of the Al-fed power plant model in Aspen Plus.

The main sections are the following:

- Reactor section, in the red box, modeling the component already illustrated in Figure 25.
- Power generation from the heat extracted from the reactor, in the green box, implementing a Rankine cycle.
- Heat recovery section, in the purple box, in which hot water is produced in heat exchangers.
- SOFC section, in the blue box, comprehensive of anode and cathode.
- Power generation from SOFC exhausts and air pre-treating, in the brown box, including an afterburner and a gas turbine, a compressor and a heat exchanger working on inlet air.

### 5.2.1 Reactor model

The reactor must be fed with aluminium and steam. A stream of feedwater at ambient temperature (WIN-1) is passed through the heat exchanger HX-TCTRL with the aim to control the temperature of the produced gases (PR-VAP) as they will be delivered to the SOFC anode. The stream WIN-2 is still liquid, and the rest of the energy required to vaporize it (up to a temperature of 350°C) is provided by the dummy heater “VAP-HEAT”. This component is not present in reality, but it is used to model the vaporization of the feedwater inside the reactor. Steam and aluminium powder are mixed together and enter the reactor, where hydrogen and alumina are produced at a reaction

temperature of 900°C. The block used to model the reactor is an isothermal stoichiometric one (RStoich), where the reaction is an input of the component imposed by the user, together with the reaction temperature and the fractional conversion of the fuel (Al). A separator is added to model the separation of the solid phase (made up of alumina), that actually should happen inside the reactor itself (Figure 29).

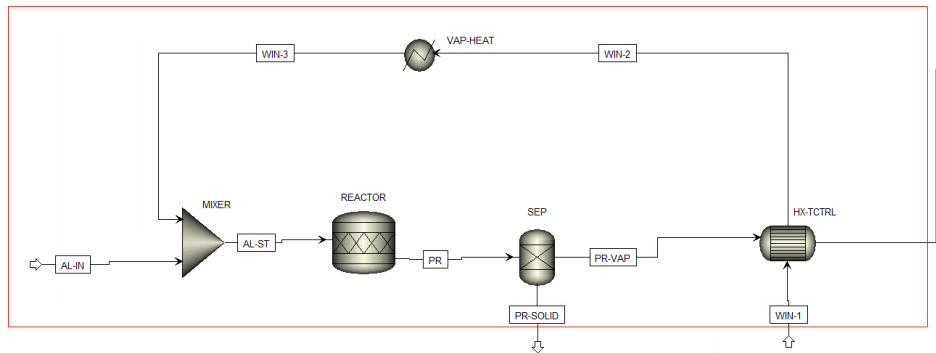


Figure 29. Reactor section - model in Aspen Plus.

### 5.2.2 Rankine cycle model

The steam Rankine cycle is implemented separately from the reactor. The parameter linking it with the aluminium-steam reaction is included in the fictional component “HEATER”, that models the heat exchange inside the reactor. This block provides a fixed amount of thermal energy to the water in the cycle, corresponding to the residual heat available in the reactor. This capacity can be easily calculated by subtracting from the heat released by the Al-steam reaction the one used to vaporize the feedwater (VAP-HEAT in the reactor section). Heat transfer is guaranteed because the temperature of the reactor is always much higher than the one at the inlet of the steam turbine.

The flow rate of water loaded to the circuit is calculated thanks to a design specification in order to produce steam at 550°C before the turbine. The high-pressure side of the circuit is at 100 bar, while the low-pressure side is at 1 bar; this is the pressure drop that the turbine exploits to recover mechanical work. At the same time, the turbine outlet temperature is 100°C, with water at its saturation point (vapor fraction in the order of few percentages, acceptable by a steam turbine). The condensation section is split in two stages: in the first one the saturated steam exchanges heat (REC-A) until it reaches a vapor fraction of 0.05 with an additional water flow (WA1, WA2) that, in this way, it is heated up to a significant value for the cogeneration application (e.g., 90°C), exploiting

the latent heat of water. To complete the condensation an auxiliary cooler is then inserted. A circulation pump is present to increase the pressure. The cycle is actually closed, but in Aspen it has been simulated as an open loop for convergency reasons (Figure 30).

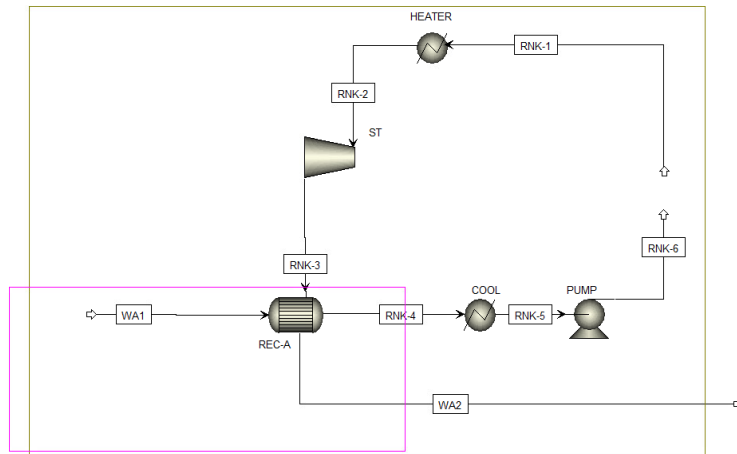


Figure 30. Rankine cycle section - model in Aspen Plus.

### 5.2.3 SOFC model

The SOFC is modeled separating anode and cathode functions (Figure 31): the anode is modeled by a “RGibbs” reactor, that minimizes the Gibbs free energy of the mixture of gases as input (hydrogen/steam and oxygen) performing the global reaction of oxidation of hydrogen ( $H_2 + \frac{1}{2}O_2 \rightarrow H_2O$ ), while the cathode is modeled as a “separator”, extracting the correct amount of stoichiometric oxygen to be delivered to the anode ( $O_2-CAT = O_2-AN$ ) from the flow of inlet air (AIR-4). The latter passes through the fictional heat exchanger CAT-HX that simulates the temperature increase of the air to reach thermal equilibrium with the SOFC (850°C). Applying a thermal balance on the stack, it is possible to impose the corresponding air flow that removes the excess heat implementing calculators and design specifications.

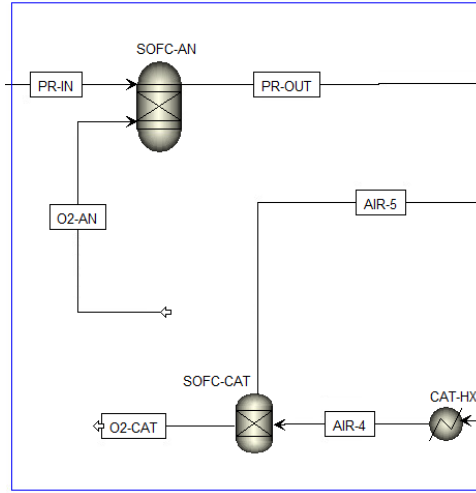


Figure 31. SOFC section - model in Aspen Plus.

The equivalent total current produced in the SOFC  $I_{TOT}$  can be found knowing the flow of hydrogen at the inlet of the anode  $\dot{n}_{H_2}$ , thanks to the Faraday's law of electrochemistry:

$$I_{TOT} = \dot{n}_{H_2} \cdot Z_{H_2} \cdot F \cdot FU \quad (15)$$

where  $Z$  is the charge number (for hydrogen  $Z = 2$ ),  $FU$  is the fuel utilization factor (assumed 0.8), and  $F = 96485 \text{ C/mol}$  is the Faraday constant. The stoichiometric oxygen needed at the cathode is also found using Faraday law (this time, with  $Z = 4$ ), as:

$$\dot{n}_{O_2} = \frac{I_{TOT}}{Z_{O_2} \cdot F} \quad (16)$$

Then, if a value of voltage of the cell is set (assumed  $V_c = 0.8 \text{ V}$ , avoiding the implementation of the polarization curve, out of the scope of this model), it is easy to calculate the electrical power produced by the unit  $P_{SOFC}$ :

$$P_{SOFC} = V_c \cdot I_{TOT} \quad (17)$$

By performing an energy balance of the SOFC, the extra heat that must be removed from excess air  $Q_{SOFC}$  can be computed considering the enthalpy of reaction  $\Delta H_r$  that can be found as net heat duty exchanged by the anode block:

$$Q_{SOFC} = |\Delta H_r| - P_{SOFC} \quad (18)$$

A design specification is then set to find the amount of external air that permits to extract the thermal power  $Q_{SOFC}$ , imposed in the fictional component CAT-HX. The separator

modeling the cathode sends the stoichiometric oxygen to the anode and the rest of air directly to the afterburner.

#### 5.2.4 Gas turbine section

Downstream the SOFC, an afterburner burns in air the residual hydrogen remained unreacted after the fuel cell, whose amount depends on the fuel utilization factor FU. The stream exiting the afterburner is composed of N<sub>2</sub> (more than 70%, deriving from air), H<sub>2</sub>O and O<sub>2</sub> and reaches temperatures in the range 900-1000°C. A microturbine expands the hot gases from 3 bar to ambient pressure, recovering mechanical work. A compressor is used to extract atmospheric air and feed it to the SOFC cathode, after a heat recovery unit (HX-AIR in Figure 32), in which the outlet temperature of the preheated air is fixed at 650°C. A final recuperator (REC-B) recovers heat in order to provide thermal energy to an additional stream of water up to 90°C.

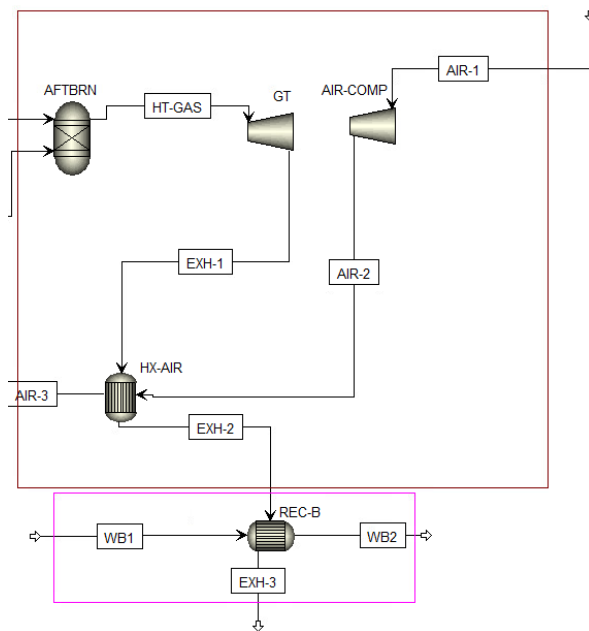


Figure 32. Microturbine section - model in Aspen Plus.

#### 5.2.5 Operating parameters of the reference case

The reference mass flow rate of aluminium as input (AL-IN) is 200 g/s. The other reactant, water (WIN-1), is fed to the mixer in an over-stoichiometric ratio of 33% (266 g/s), imposed in Aspen Plus by means of a “calculator” block. In the first heat exchanger, this flow of water heats up until the temperature of the exit gases lowers to 750°C (fixed by a “design specification” in Aspen). The heater “VAP-HEAT” provides thermal energy in

order to vaporize this flow of water to a temperature of 350°C, ready to enter the reactor. The latter is modeled by an isothermal reactor in which a conversion yield is imposed (1 if the ideal reaction is fully realized, <1 if not all the aluminium oxidized – in the reference case a full conversion yield is considered) at a fixed temperature of 900°C and at a pressure of 3 bar (common pressure to all the components until the gas turbine). It is worth noticing that in theory pressure has no effect on the equilibrium composition, according to Le Chatelier principle (number of moles of gases do not vary during the reaction). Produced gases (hydrogen and excess steam) at 900°C are separated from the solid oxides and, as already mentioned, their temperature is lowered to 750°C before entering the anode of the SOFC. Operating temperature of the SOFC has been fixed to 850°C, working with a fuel utilization (FU) of 0.8. Voltage of the SOFC cell has been considered fixed (a polarization curve is not implemented in this first stage) to 0.8 V. The afterburner acts as an adiabatic reactor with Gibbs free energy minimization (reactor “RGibbs” in Aspen Plus). The microturbine has a discharge pressure of 1 bar (expansion ratio of 3), isentropic efficiency of 0.9 and mechanical efficiency of 0.98. The same parameters are valid for the compressor, with compression ratio of 3. The mass flow of air passing through the compressor is calculated by a design specification in such a way that the thermal balance of the SOFC is closed. After a heat recovery section that increases its temperature to 650°C, the oxygen required for the electrochemical oxidation (imposed by a calculator block) is fed to the cathode, the rest is fed to the afterburner for the combustion of the residual hydrogen. Regarding the Rankine cycle, the input flow rate of water, pumped at 100 bar, is calculated by a design specification so that the available residual heat from the reaction (represented by a fixed “heat duty” of the component “HEATER”) provides steam at around 550°C, ready to be fed to the steam turbine. The latter, with isentropic efficiency of 0.85 and mechanical efficiency of 0.98, expands the steam down to 1 bar. The first condenser (REC-A) acts as a thermal recovery unit, able to provide heat to an external flow of water up to 90°C. The amount of water that can be heated up is calculated by a design specification in order to set the vapor fraction at the outlet of the REC-A to 0.05 (so that the temperature of the condensing steam inside it is always higher than the one of the external flow of water). An additional cooler completes the condensation and cooling of the water to the ambient conditions. A similar method is employed for the second heat recovery system (REC-B) involving a gas-water heat

exchanger. The flow rate of water at 90°C is calculated by a design specification setting the outlet temperature of exhausts to 120°C.

## 5.3 Results

### 5.3.1 Efficiency metrics

Main indicators of the plant must be found in each configuration that has been studied. The starting point is maintained constant in each run: the input material is 200 g/s of aluminium fed to the reactor. The energy content of this material flow can be evaluated in two ways, depending on how the latent heat of vaporization of water is accounted, so that a lower heating value (LHV) and a higher heating value (HHV) of aluminium can be fixed. The latter corresponds to the specific energy of the material, equal to 31 MJ/kg as discussed in the thermodynamic analysis and is comprehensive of all the energy forms involved in the Al-steam reaction. It considers the reacting water already in form of steam, so that no heat of vaporization is subtracted. Instead, the LHV takes into account that for the Al-water reaction at high temperature a vaporization process must be realized, and this energy is subtracted from the total energy delivered by the reaction (this reflects the fact that water is generally available in ambient conditions and energy must be spent to vaporize it to the desired temperature). LHV of aluminium can be set to 17.87 MJ/kg; the energy flow entering the system is found multiplying the LHV or HHV by the mass flow rate and it is considered the only input energy for the plant.

The choice to use LHV or HHV is arbitrary. However, it plays an important role when determining the efficiency of the system, since one is almost the double of the other. The convention employed in this work is to use LHV for electrical efficiency and all the efficiencies in layouts that do not extract useful heat from the condensation of water, while HHV is possibly used to calculate thermal and global efficiencies in the case the condensation of water provides useful heat: in this case, in fact, if the reference were the LHV, the efficiency could result higher than 1. If  $P_{net}$  is the net electrical power produced by a plant, and  $\dot{m}_{Al}$  the mass flow of aluminium (200 g/s), the electrical efficiency is calculated as:

$$\eta_{el} = \frac{P_{net}}{\dot{m}_{Al} \cdot LHV_{Al}} \quad (19)$$

Regarding the thermal recovery, the useful product is a flow of hot water at 90°C. Therefore, if  $\Phi_{tot}$  is the total useful thermal power,  $\dot{m}_{w,tot}$  is the total flow rate of useful water produced at 90°C,  $c$  is the specific heat of water (considered 4.19 kJ/kgK, a mean value between 15°C and 90°C),  $\Delta T_w$  is the temperature increase (considering water available at 15°C, the temperature increase is 75°C), the thermal efficiency can be calculated with respect to the HHV (since heat could be transferred by condensing water) as:

$$\eta_{th} = \frac{\Phi_{tot}}{\dot{m}_{Al} \cdot HHV_{Al}} = \frac{\dot{m}_w c \Delta T_w}{\dot{m}_{Al} \cdot HHV_{Al}} \quad (20)$$

A parameter of global efficiency can be calculated on the basis of HHV considering both electric and thermal output:

$$\eta_{gl} = \frac{P_{net} + \Phi_{tot}}{\dot{m}_{Al} \cdot HHV_{Al}} \quad (21)$$

### 5.3.2 Complete plant

The complete plant is the one including SOFC, microturbine and steam turbine power generation. Moreover, thermal recovery is maximized, taking advantage of the heat of condensation in the Rankine cycle and the heat of the exhaust gases. The main results regarding temperature and mass flow rates involved are reported in the system diagram of Figure 33.

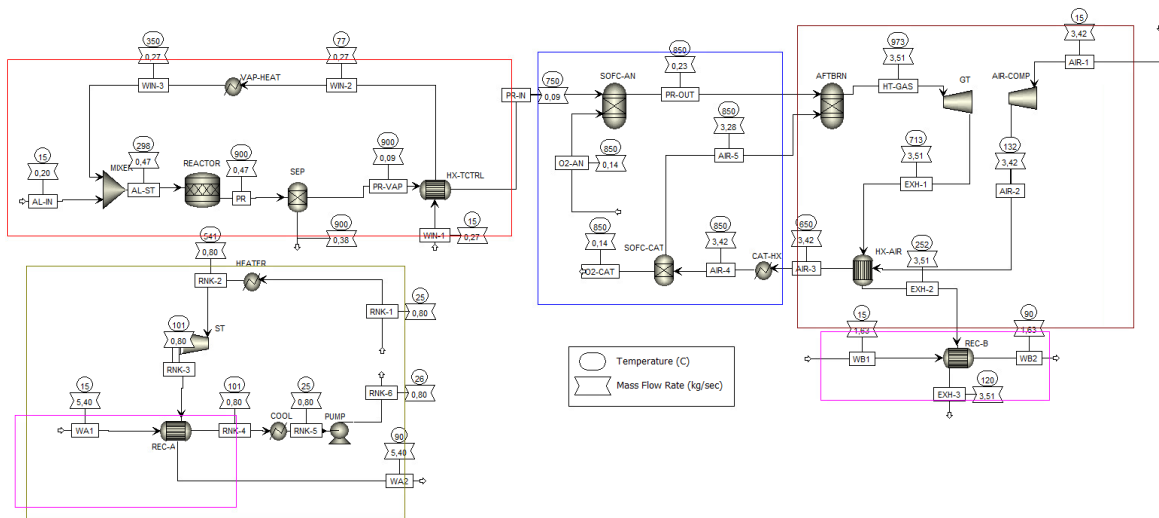


Figure 33. Optimized SOFC+GT+ST plant: system diagram and results.

The reaction takes place with an excess of water of 33%, and with unitary yield (all aluminium is supposed converted to alumina).

The net electrical production can be calculated in this case as:

$$P_{net} = P_{SOFC} + (P_{GT} - P_{comp}) + (P_{ST} - P_{pump}) \quad (22)$$

since the air compressor and the pump are auxiliary consumptions. Electricity consumed by circulation pumps for the heat recovery circuits and for the supply of water to the reactor are neglected, since they do not work at high pressure (max. 3 bar of the reactor feeder). Thermal production is found by summing up the effect of the two recuperators (REC-A, REC-B).

With the input parameters reported in Table 13, the plant provides 2.76 MW of electrical power and recovers 2.21 MW of thermal power with an electrical efficiency of 77.2% (Table 14). Global efficiency of 60.1% is calculated on the basis of HHV, and it is defined as the total energetic output (electrical and thermal) divided by the maximum energy input of aluminium (HHV).

Table 13. Input parameters for plant simulation.

INPUT PARAMETERS	
<b>Aluminium mass flow rate</b>	0.2 kg/s
<b>Reacting water excess</b>	0.33
<b>Reacting water flow rate</b>	0.266
<b>Temperature of reaction</b>	900 °C
<b>Reaction yield</b>	1
<b>Pressure of the main circuit</b>	3 bar
<b>SOFC fuel utilization</b>	0.8
<b>Expansion ratio of the microturbine</b>	3
<b>Steam turbine inlet temperature</b>	550 °C
<b>Higher/Lower pressure of Rankine cycle</b>	100/1 bar
<b>Vapor fraction after condensing recuperator</b>	0.05
<b>Setpoint temperature of produced hot water</b>	90 °C

Table 14. Results of the plant simulation.

OUTPUT PARAMETERS	
Total electric power output	2760 kW
Total thermal power output	2207 kW
Electrical production from SOFC	1373 kW
Electrical production from microturbine	714 kW
Electrical production from Rankine cycle	673 kW
Amount of hot water produced	7.03 kg/s
Produced hydrogen in the reactor	898 m <sup>3</sup> /h
Electrical efficiency (base LHV)	77.2 %
Electrical efficiency (base HHV)	33.4 %
Thermal efficiency (base HHV)	26.7 %
Global efficiency (base HHV)	60.1 %

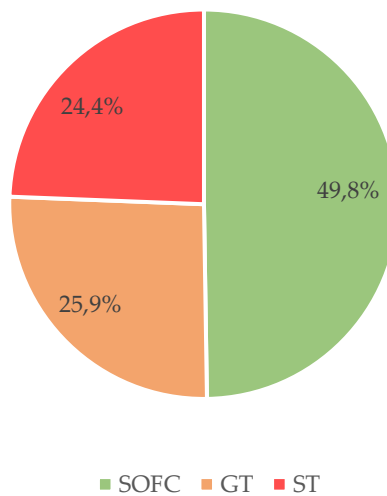


Figure 34. Contribution to the total power output of the three generation systems.

The reactor yield set to 1 makes possible the production of almost 900 m<sup>3</sup>/h of hydrogen with 200 g/s Al input, corresponding to 1247 ml<sub>H<sub>2</sub></sub>/g<sub>Al</sub>, confirming the high theoretical volumetric density of aluminium for the storage of hydrogen.

As depicted in Figure 34, half of the contribution to the total power derives from the fuel cell, directly exploiting hydrogen in an electrochemical way. The other half is practically equally divided into the contribution of the microturbine and the steam turbine.

The most important sources of unavoidable energy expenses, appearing as losses in the system are:

- Energy to heat up reactants: aluminium and water need to be brought to the reaction temperature of 900°C starting from ambient conditions. Part of the energy contained in the aluminium is directly spent to run this process. This is the most important contribution of lost energy.
- Wasted energy: thermal energy contained in flows released to the ambient is considered lost. First, one of the products of the reaction is solid (alumina), and is extracted from the reactor at the high temperature of 900°C. In theory, this would allow to harness heat from the material but, since it is very unlikely to have such a complex thermal recovery system, it is considered a loss. The second flow of energy wasted to the ambient is the one related to the secondary cooler in the Rankine cycle, in which condensation of water is completed. Finally, the release of hot exhaust gases to the ambient after the microturbine and the heat recovery section is the last thermal waste.
- Electrical energy of auxiliaries: in particular, in the scheme the considered electricity spent is the one for the compressor and the pump, already taken into account to calculate the net power output.

### **5.3.3 Effect of water excess**

The performance of the plant is strongly dependent on the amount of water required in the reactor. In fact, a strong excess would require high amount of energy for the vaporization of the flow itself, reducing the availability of excess heat for the Rankine cycle. At the same time, a higher excess of water increases the mass flow rate of the gases passing through the microturbine, possibly increasing its power output.

For the SOFC, the fraction of steam at the anode inlet becomes higher when increasing the reacting water, thus influencing the cell voltage, that reduces, while the current do not change, according to Faraday law (since the absolute flow of hydrogen do not change). The molar fraction of water at the anode inlet can be calculated in function of the water excess  $e$  as:

$$y_{H_2O,an} = \frac{e}{1 + e} \quad (23)$$

The Nernst voltage at the inlet fuel channel of each cell depends on the molar concentration of the species (in particular in this case, of water), with the trend reported in Figure 35 and Figure 36:

$$E_{Nernst} = -\frac{\Delta\bar{g}(T, p_0)}{ZF} - \frac{RT}{ZF} \ln\left(\frac{y_{H_2O}}{y_{H_2} \cdot y_{O_2}^{0.5}} \cdot \left(\frac{p_0}{p}\right)^{0.5}\right) \quad (24)$$

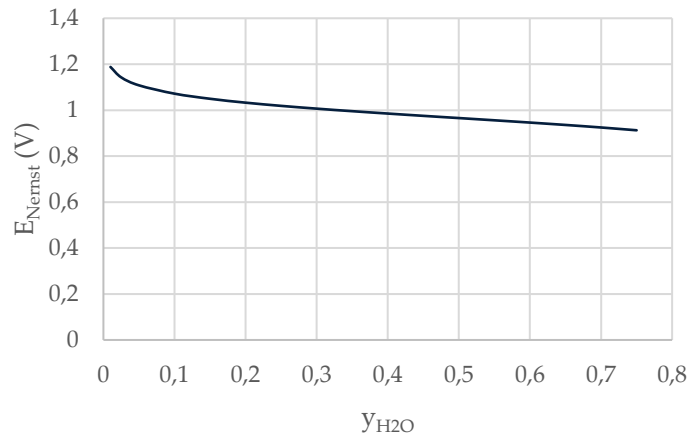


Figure 35. Dependence of the Nernst voltage with the concentration of H<sub>2</sub>O at the anode inlet.

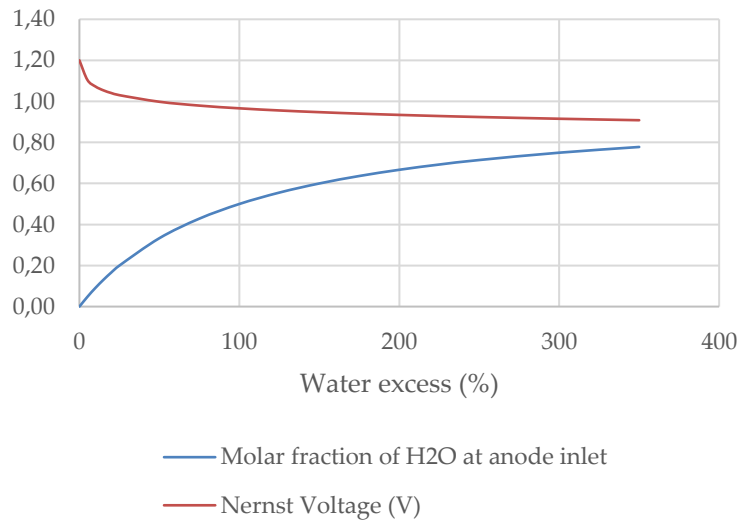


Figure 36. Molar fraction of hydrogen at anode inlet and Nernst voltage depending on the water excess.

Operating voltage in SOFC can be assumed to follow a linear polarization curve, because of the mainly resistive behavior of the system:

$$V_{op} = E_{Nernst} - ASR \cdot i \quad (25)$$

where ASR is the area-specific resistance (a lumped parameter taking into account concentration, ohmic and diffusion overvoltage) and  $i$  is the current density.

Having set the reference layout at  $e = 0.33$ , meaning  $y_{H_2O,an} = 0.25$ , the electrical power delivered by the SOFC at a water excess  $e$  can be calculated scaling the reference one with the operating voltage at the new concentration:

$$P_{SOFC,e} = P_{SOFC,ref} \cdot \frac{V_{op,e}}{V_{op,ref}} = P_{SOFC,ref} \cdot \frac{E_{Nernst,e} - ASR \cdot i}{E_{Nernst,ref} - ASR \cdot i} \quad (26)$$

In theory, ASR also depends on the concentration of the species; in fact, if a high concentration of water is present its value increases due to a more problematic diffusion of hydrogen into H<sub>2</sub>O. However, the effect cannot be easily quantified if without a proper diffusion model, therefore in this case the value of ASR (and so the product  $ASR \cdot i$ ) is considered constant, and the effect of water concentration is fully assigned to the decrease of Nernst voltage. The product  $ASR \cdot i$ , representing a voltage drop, can be calculated in the reference condition as:

$$ASR \cdot i = E_{Nernst,ref} - V_{op,ref} \quad (27)$$

and kept constant to calculate the SOFC power for different water excess.

The power delivered by SOFC, microturbine and steam cycle, derived from the Aspen Plus simulation are shown in Figure 37.

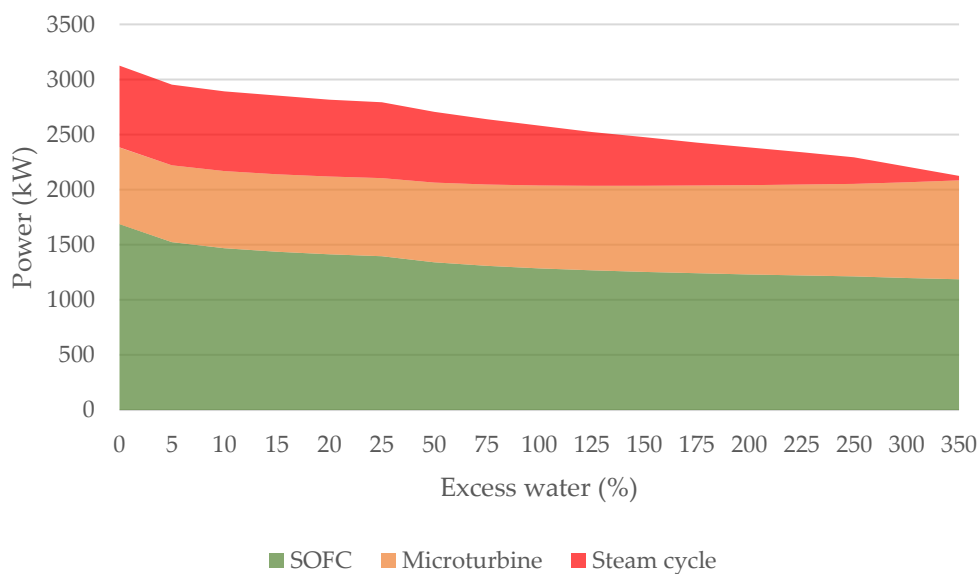


Figure 37. Electric power delivered by SOFC, GT and ST in function of the water excess.

As clearly visible, steam cycle is particularly affected by the water excess, with strongly decreasing deliverable power. At an excess water of 350%, the steam turbine cannot produce any more power. In fact, increasing the water excess leads to increasing energy required to vaporize the feedwater to the reactor, in expense of the thermal energy that can be transferred to the steam cycle; at a certain point, corresponding to  $e=350\%$ , all the thermal energy released by the Al oxidation is used internally to vaporize the feedwater.

At the same time, the power output of the GT slightly increases with water excess, thanks to the increase in mass flow rate passing through the turbine.

The effect on the SOFC, as already mentioned, is to decrease the output power, but not in a drastic way.

It is possible to conclude that the convenience of the hybrid SOFC+GT+ST power plant is confirmed until low values of water excess are employed. Over 350% excess, the steam cycle is completely useless since no additional thermal power is delivered by the reaction. Results on electrical power and thermal power output are depicted in Figure 38, highlighting an almost linear decrease in both thermal and electrical power, with a slightly lower rate regarding electrical one, thanks to the compensation due to the microturbine. The initial spike in the electrical power is due to the SOFC, exhibiting much higher production with pure hydrogen.

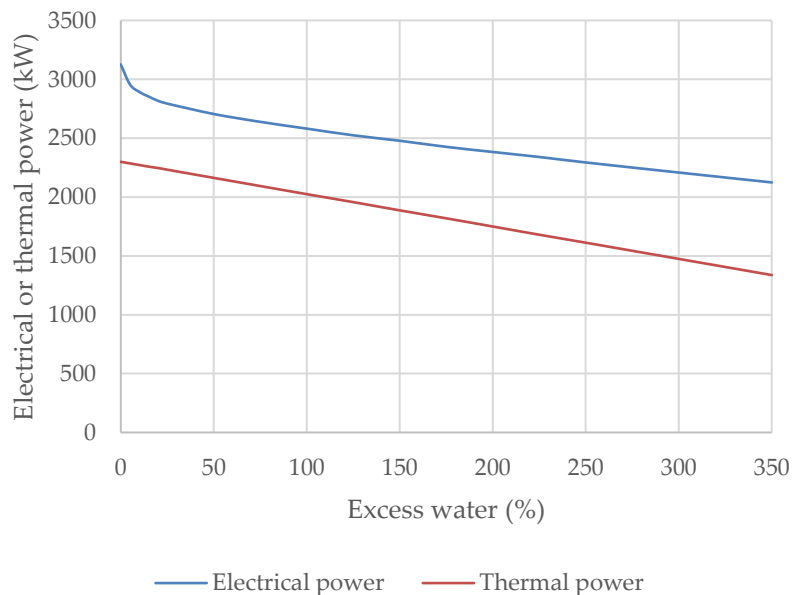


Figure 38. Electrical and thermal power of SOFC+GT+ST plant in function of water excess.

### 5.3.4 Effect of reaction temperature

A sensitivity analysis on reaction temperature is performed, in order to evaluate if this parameter is strongly influencing the performance of the system. Since the optimal temperature of reaction of Al-steam oxidation from thermodynamic and kinetic viewpoint is not standard yet, an interval in the range 750-1200°C has been investigated. Modifying the reaction temperature has effects only on the thermal balance of the reactor and, consequently, on the available heat to the steam boiler in Rankine cycle. In fact, the components downstream the reactor are not affected by this modification, since the temperature at the inlet of the fuel cell is controlled and fixed by the heat exchanger (HX-TCTRL), so that SOFC, GT and secondary heat recovery are not influenced by a temperature change in the reaction chamber. The effect on the power output of steam cycle (blue curve) and amount of produced hot water (red curve) can be seen in Figure 39.

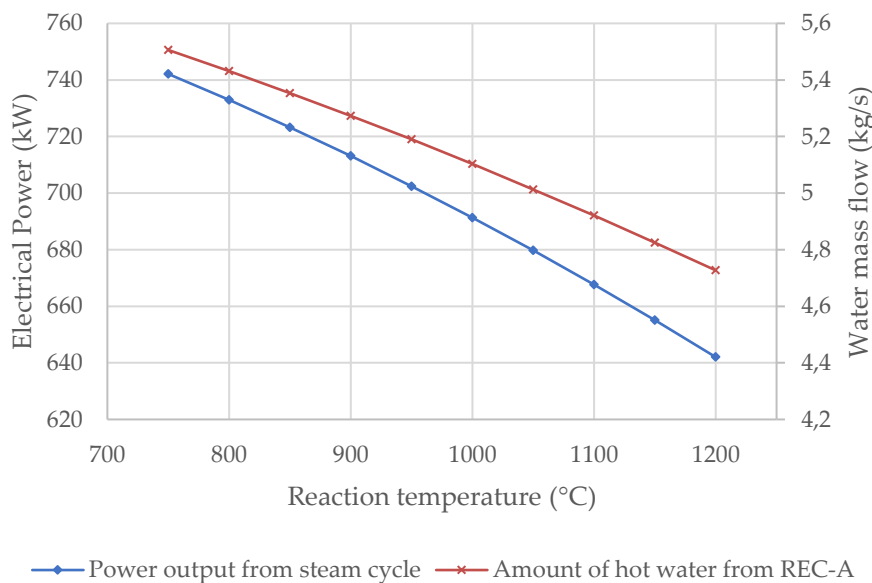


Figure 39. Effect of reaction temperature on the power output of steam cycle and primary heat recovery.

An increase in the reaction temperature reflects in a decrease of ST power output and the bottom thermal recovery. However, in the analyzed range, the decrease is quantified in -13% in the Rankine cycle efficiency. The global plant electrical efficiency decreases by just 3%. Thus, since increasing the reaction temperature is probably convenient to reach a complete oxidation of aluminium, then the operation can be safely done without incurring in a drastic efficiency decrease of the plant.

### 5.3.5 Comparison with simpler layout (SOFC-GT only)

The plant considered until now, though with a very high electrical efficiency, has also a high degree of complexity. Integration of SOFC with gas turbines is a technology already studied and demonstrated. Instead, it is not trivial to construct a continuous reactor in which the thermal energy is recovered to drive a Rankine cycle; in fact, the reactor would need to sustain different pressures: a high-pressure section to work as boiler of the Rankine cycle (e.g., 100 bar), and a lower one related to Al-water reaction (e.g., 3 bar). To date, such a configuration has not been proposed yet. Moreover, the power produced from the steam turbine strongly decreases for increasing amount of reacting water, making its presence less important. Therefore, it could be interesting to study a simpler layout excluding the Rankine cycle from the system.

In this configuration (Figure 40) power is produced in the SOFC-GT system only, while the extra heat of reaction is exploited to heat up water. In this way, the electrical efficiency of the plant is reduced, but a higher amount of thermal power can be recovered.

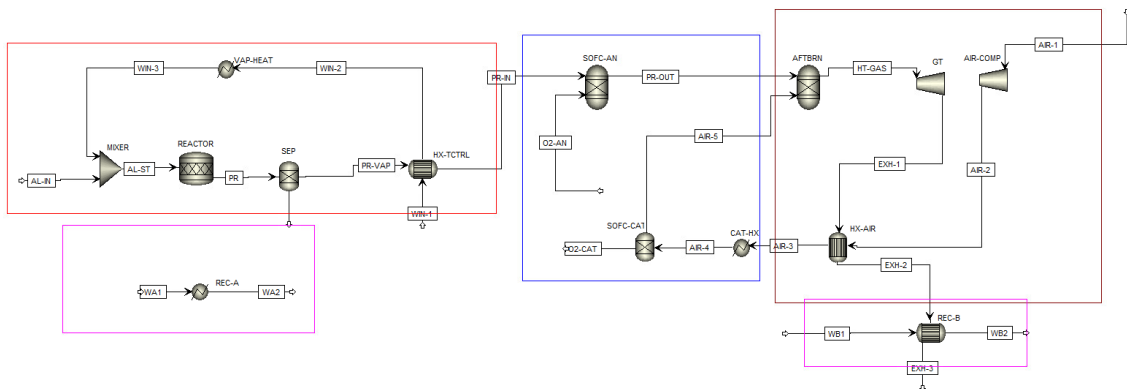


Figure 40. Simpler layout: SOFC-GT plant.

With the same input parameters of the reference case, this plant offers an electrical power of 2.09 MW and a thermal recovery of 3.03 MW. The electrical efficiency is reduced to 58.4%.

The effect of increasing the reacting water is in this case not monotonic: after an initial steep drop due to the decrease in SOFC efficiency, the total power increases again thanks to the effect of GT (increase of the flow rate of gases in the turbine), having a more important weight than the slight decrease in performance of the SOFC. Instead, the

thermal energy recovered decreases almost linearly since the amount of heat required to vaporize the reacting water is linearly dependent on the water excess (Figure 41).

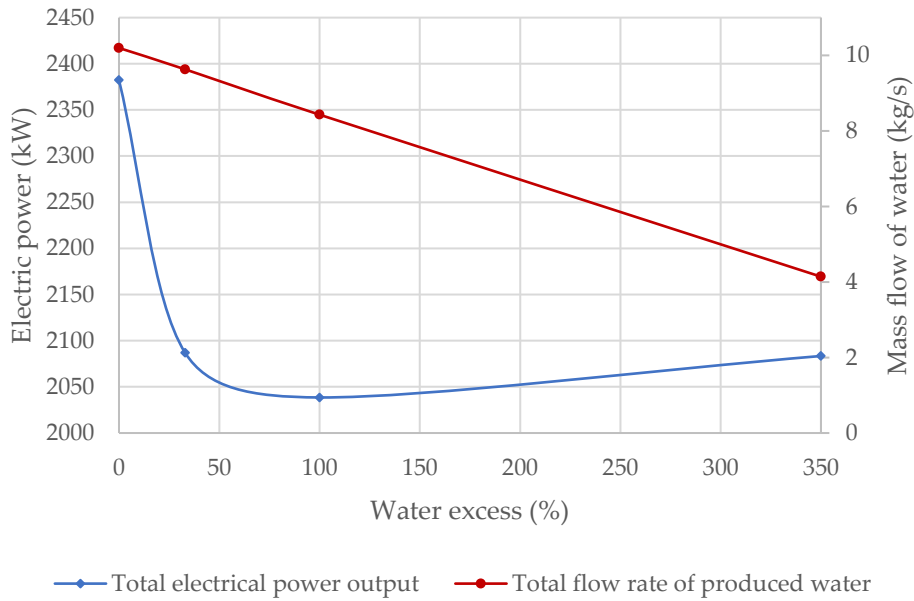


Figure 41. Effect of water excess in SOFC-GT system.

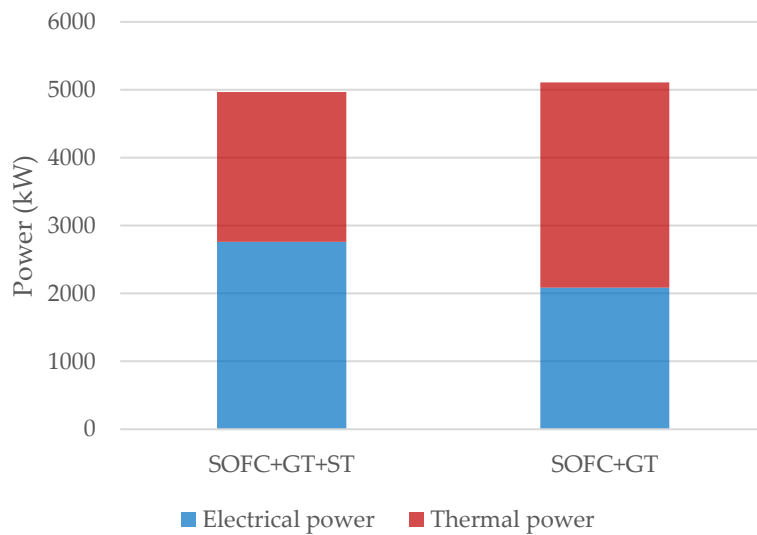


Figure 42. Comparison of SOFC+GT system with SOFC+GT+ST system.

The comparison with the previous configuration is represented in Figure 42, clearly showing that the simpler configuration provides less electric power but increases the weight of thermal power. The sum of electric and thermal power is almost constant in the two schemes, with a slightly higher value for the SOFC-GT because the excess reaction

heat is completely recovered, while in SOFC-GT-ST the recovery happens in the condensation stage of Rankine cycle, where not all the latent heat is retrieved (in fact, an additional cooler was inserted in that layout).

In conclusion, simpler SOFC-GT configuration is convenient with respect to more efficient SOFC-GT-ST one when:

- The plant has to cover high thermal requests.
- Water excess in the reactor is high.
- Lower capital costs are a constraint.

## 6 Experimental analysis

The main focus of this experimental section is the evaluation of hydrogen production in the reaction of aluminium with water steam. An evaluation of the reactivity of the sample during air oxidation is also performed to compare the different oxidizing media.

After a review of the experimental literature on Al-steam reaction, the experimental setup will be presented together with the methodology. A sub-paragraph will be dedicated to each test, and finally a discussion and comparison of the results is reported.

### 6.1 Literature references

Many researchers have already studied, both theoretically and experimentally, the Al-H<sub>2</sub>O reaction, but mainly at low temperatures [48][49]. In fact, the idea of reacting aluminium with water at room temperature (or slightly more) is very attractive but, as discussed before, brings two main issues – the necessity to use catalysts and the impossibility to exploit the heat of reaction (since it is released at too low temperature) – leading to very low RTE. Some other researchers evaluated the reaction driven at very high temperature (>1500°C), but in this case it can be considered a pure combustion, producing a high amount of heat but not exploiting the heating value of the hydrogen, because in current aluminium burners it is considered as an exhaust gas vented in the atmosphere.

An attractive choice is to study the reaction at intermediate temperatures, higher than the melting point of the metal (660°C) but lower than the ones that would create a combustion flame. According to literature, it is advisable not to go over 1200°C in order to avoid risks of violent reaction, as it can be considered the temperature at which combustion takes place. In the intermediate temperature range, it would be possible to efficiently exploit the heat of reaction and easily recover hydrogen (or further exploit it to produce electricity in a fuel cell).

Barelli et al. [50] studied the isothermal Al-steam reaction at temperatures below and upon the melting point, evaluating the effect of temperature and steam mass flow rate. They concluded that oxidation of Al in H<sub>2</sub>O improves as temperature rises; in particular a big increment can be seen after the melting point. Below it, conversion efficiency could

not overcome 7.55%. Increasing the temperature, the conversion efficiency rises exponentially, especially after 800°C showing a conversion improvement from 20% to 70%, reached at 900°C. Moreover, the reaction shows an initial peak of hydrogen production in the first minutes, then the reaction continues at a lower rate for more than 1 hour, suggesting a slow reaction mechanism. The best conversion efficiency they found is 73.13%, obtained at 900°C.

Shmelev et al. [51] studied the reaction of molten aluminium with steam in a burner device at high temperatures (up to the melting point of alumina, i.e., more than 2000°C), with reactor yields up to 40% in case of simple aluminium, or up to 100% if KOH is included in the melt.

The wide range of results seen in different papers justifies an experimental campaign to further assess the oxidation of aluminium in various conditions. In fact, many different experimental setups have been investigated in literature, and often the results cannot be comparable for this reason. Moreover, no references were found on controlled isothermal reaction at medium-high temperatures (800-1000°C) other than the aforementioned paper from Barelli et al.

## **6.2 Experimental setup**

The experimental session has been realized in the DENERG laboratories of Politecnico di Torino, hosted in Environment Park in Turin, a technological park working and researching on environmental innovation. The available test bench for our analysis has been the one usually employed for chemical looping processes, as the methods and components are quite similar to our case. Nevertheless, the bench had never been employed to run experiments with steam (wet mode operation), therefore it was necessary to perform some preliminary configuration and tests to confirm the correct functioning also with the use of steam, that is one of the two fundamental reactants in the Al wet cycle. The block diagram in Figure 43 represents the main sections and components of the test bench.

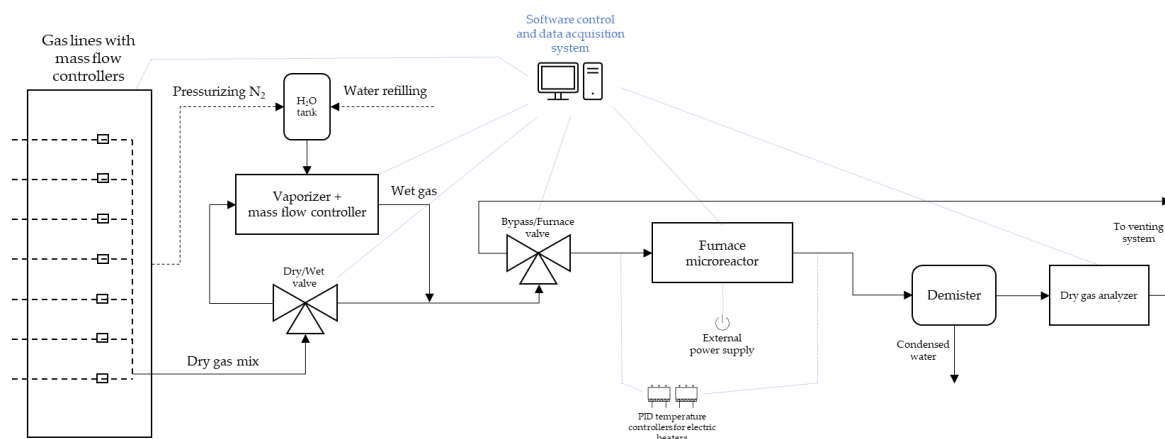


Figure 43. Experimental setup used for Al-steam reaction.

A series of 7 pressurized gas lines are available from the laboratory network, with the possibility to work with Ar, H<sub>2</sub>, CH<sub>4</sub>, CO, CO<sub>2</sub>, N<sub>2</sub>. Each one is equipped with pressure regulators and mass flow controllers, of the type proportional-integral-derivative (PID). The water is contained in a tank pressurized by nitrogen, derived directly from the laboratory network before the pressure and mass flow controllers; the tank is equipped with a safety valve, a venting valve and a water refilling system. Water is sent to a steam evaporator made of electric heating plates, linked to a controller that allows to set the desired temperature of the produced steam (a typical value is 120 °C) and its amount. The operation of the bench in dry or wet mode is decided by a 3-way valve that sends the dry gas to the humidification section or bypasses it: if the valve is in wet mode, the gas passes through the vaporizer, in which an amount of steam is injected (expressed as percentage of the total flow). The humidified flow can now enter a microreactor/furnace, after passing through a second valve that permits to bypass the furnace itself in case of necessity. All the pipelines after the humidifier are insulated and heated by electrical resistances, in order to avoid the condensation of water (Figure 44a).

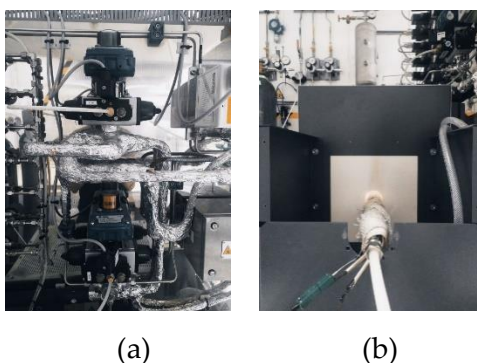


Figure 44. Experimental setup: 3-way valves and heated pipes (a) and outlet section of the microreactor (b).

The microreactor consists in a Carbolite Gero 3000 tube furnace (with alumina tubes) with working temperatures up to 1600-1700 °C, controlled by an external unit for the power supply. At the input and output of the reactor the temperature is monitored by means of two thermocouples connected to electrical resistive heaters (Figure 44b); these temperature is the input to the PID controllers that increase or decrease the electric power of the resistances to avoid condensation. The testing sample can be inserted in an alumina or quartz boat crucible positioned at the center of the tubular furnace, where the set point of temperature is guaranteed. However, the solution that was adopted here is a “tube-in-tube” configuration, where the sample is placed inside a smaller tube (with internal diameter of 8 mm) that is then put inside the bigger tube (internal diameter of 32 mm) embedded in the reactor furnace.

Downstream the reactor, the mix of gases and steam passes through a condenser, consisting in a steel demister followed by a much finer water filter just before the input to the gas analyzer. In this test bench there would be the availability of an additional chiller, not needed in the experiments that were performed due to the low water flow rates involved, therefore this section is bypassed. Actually, some preliminary tests have been performed including a silica-filled tube acting as an additional water trap, that proved to be oversized. The dry gas flow is finally sent to the analyzer (Emerson Rosemount), that can measure the concentration of the different chemical species during time (only hydrogen is of interest in our tests), and then it is sent to the venting system.

Besides this main section, the test bench has the availability of a TGA (Thermo-Gravimetric Analysis) with embedded DTA (Differential Thermal Analysis) that will be used to test the functionality of the main section by performing a comparison oxidizing aluminum with air. The TGA cannot work with water, therefore it cannot be used to study the Al-steam reaction. The working principle of the TGA is to evaluate the mass evolution of a sample during a thermal process; during oxidation, we expect the mass of the sample to increase, since oxygen is bonded to the molecule, while during reduction the mass should decrease. TGA can reach temperatures as high as 1600°C, and oxidizing (air) or inert atmospheres (Argon) can be employed.

The whole system is controlled by software: one is dedicated to temperature set points of the furnace, the other to the mass flow rates. The software allows to operate in manual or automatic mode: in the latter it is possible to predispose the different steps to configure a

“recipe”, like temperature ramps, mass flow variations, or dry/wet valve openings.

Before performing the tests with aluminium, a final configuration of the experimental setup must be found. This is done by performing some chemical looping cycles with other materials (ceria-zirconia, SFNM perovskite, iron oxides), not reported in this Thesis.

### 6.3 Methods

In the program, the flow rate of dry gas (N<sub>2</sub>) is fixed at the beginning and does not change during the experiment of aluminium oxidation. The amount of water is defined as molar percentage of the total flow. This means that, to maintain the dry gas flow rate constant, the total flow increases when water is sent. However, all the water is condensed and removed before entering the analyzer, that evaluates the concentration of hydrogen in the dried flow. Being  $\dot{V}_{H_2}$  the unknown flow rate of hydrogen,  $\dot{V}_{N_2}$  the flow rate of the nitrogen carrier, and  $y_{H_2}$  the molar fraction of hydrogen depicted by the analyzer, the following relation holds:

$$\dot{V}_{H_2} = y_{H_2} \cdot (\dot{V}_{N_2} + \dot{V}_{H_2}) \quad (28)$$

from which it is possible to calculate the flow rate of hydrogen as:

$$\dot{V}_{H_2} = \dot{V}_{N_2} \cdot \left( \frac{1}{y_{H_2}} - 1 \right) \quad (29)$$

With the flow rate  $\dot{V}_{H_2}$  at each second, the total volume of hydrogen produced in a test  $V_{tot,H_2}$  can be easily calculated integrating the flow in time:

$$V_{tot,H_2} = \int_{t_i}^{t_f} \dot{V}_{H_2} dt \quad (30)$$

The mass of hydrogen  $m_{H_2}$  can be found by multiplying the latter by the standard hydrogen density ( $\rho_{H_2} = 0.0898 \text{ g/l}$ ). This mass must derive from the conversion of aluminium; the amount of aluminium reacted is found using the reaction stoichiometry ( $m_{Al,r} = m_{H_2}/0.111$ ). In this way, it is possible to calculate the conversion yield ( $\varepsilon_{conv}$ ), comparing the reacted aluminium to the total loaded aluminium ( $m_{sample}$ ), and the generation yield in volume of hydrogen per unit mass of sample ( $\varepsilon_{gen}$ ).

$$\varepsilon_{conv} = \frac{m_{Al,r}}{m_{sample}} \quad ; \quad \varepsilon_{gen} = \frac{V_{tot,H_2}}{m_{sample}} \quad (31)$$

The steam mass flow can be evaluated starting from the volumetric percentage input passing through the calculation of the total moles of gas+steam sent into the reactor:

$$\dot{m}_{H_2O} = \left( \dot{V}_{N_2} \cdot \frac{y_{H_2O}}{1 - y_{H_2O}} \right) \cdot \frac{\bar{M}_{H_2O}}{\bar{v}_{STD}} \quad (32)$$

Where  $y_{H_2O}$  is the input steam concentration,  $\bar{M}_{H_2O}$  the water molar mass,  $\bar{v}_{STD}$  the standard molar volume (22.414 l/mol).

Calibration of the analyzer have been performed as soon as a detectable deviation is noted in the results, including both the zero and the span calibration. At the end of each calibration a period of time is reserved to clean up the circuit thanks to a N<sub>2</sub> purge. During the tests, attention had to be paid to avoid any variation of flow rate, since the analyzer proved to be very sensible to them, reporting higher values of concentration during the first minutes after an increase in flow rate and vice versa.

## 6.4 Preliminary tests in microreactor

### 6.4.1 Microreactor – 1<sup>st</sup> test

The first test in tube-in-tube reactor have been performed to check the functionality of the bench. First, the internal tube made of alumina (8 mm of internal diameter) was cleaned and measured, to correctly place the sample inside at the center. An amount of 2.35 g of alumina spheres (3 mm diameter, Sigma Aldrich ), acting as supporting material, was chosen in order to fill 8 cm in the center of the tube, where reaction temperature is guaranteed. The supporting material for the powder was also used in the reference of Barelli et al. to avoid agglomeration of reaction products and so, in theory, to optimize the surface of reaction. Then, they were manually mixed with aluminium until it covered uniformly the external surface (Figure 45), finally the weight of aluminium was calculated by subtraction of the “white” alumina spheres from the total weight of the mix. In this way we found a mass of 45 mg of Al.

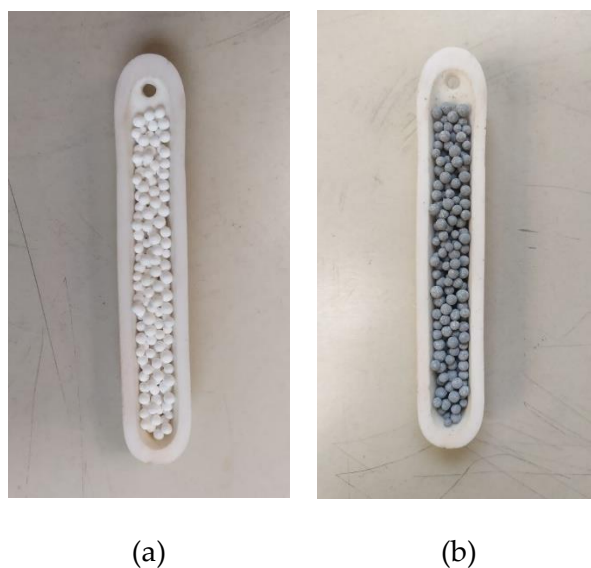


Figure 45. Alumina spheres before (a) and after (b) the mixing with aluminium.

The mixed spheres were placed at the center of the ceramic tube using quartz wool pieces to keep the sample in position, to form a reaction bed. Finally, the loaded ceramic tube was inserted into the furnace (Figure 46).



Figure 46. Tube-in-tube reactor – output section.

The test foresaw the evaluation of water oxidation at the temperature of 900°C. Reaction parameters were selected to be close to the reference ones (e.g., the work of Barelli [50]), with a flow rate of 400 ml/min of N<sub>2</sub>, humidified at 50% (corresponding to 19.3 g/h of steam) during oxidation. While reaching the setpoint temperature in the furnace, the analyzer has been calibrated in a range 0-10% H<sub>2</sub>, then a 30 min purge in N<sub>2</sub> was performed before starting the oxidation sending water. The test did not provide the

expected results, with only some oscillations of the H<sub>2</sub> concentration that cannot be attributed to hydrogen production from the sample.

### 6.4.2 Microreactor: 2<sup>nd</sup> test

To check if the problem was the sample, a second test in the tube-in-tube reactor was carried out using a different aluminium powder: it appeared much finer and volatile, with a declared maximum particle size of 5 µm. The same procedure of loading and weighing as test 1 has been performed, and this time the amount of aluminium adhered to the surface of the spheres was only 20 mg. This weight is less than half the amount of the 1<sup>st</sup> test with the same weight of spheres, probably due to the much higher volatility of the new powder.

The aim of the test was to replicate exactly the previous tentative in the isothermal oxidation of Al at 900°C but with a slightly lower water concentration (30%). Actually, after some minutes of oxidation in which no significant hydrogen production is seen, the furnace temperature has been increased to 1000°C and then reduced to 600°C to evaluate if the temperature variation could induct a hydrogen production.

The results, shown in Figure 47, reveal some small oscillations in the hydrogen concentration, in the order of less than 300 ppm (0.03%). It is likely that these peaks can just relate to natural oscillations of the instrument, more than a real production of hydrogen. Therefore, also this second powder did not provide meaningful results in the test.

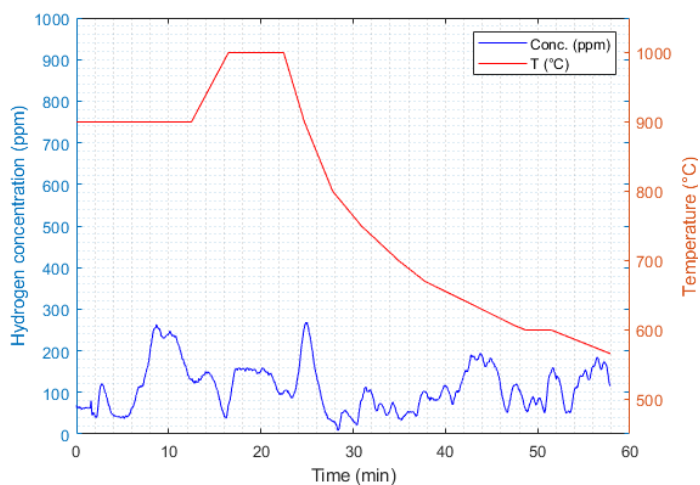


Figure 47. Results of the second test on aluminium in the reactor showing no significant hydrogen production.

The appearance of the sample at the end of the test (Figure 48) proves that the transformation into alumina has probably happened, due to the white color of all the mix (spheres+sample); however, the fact that negligible amount of hydrogen has been detected suggests that the oxidation could have occurred before the start of the steam injection due to some oxygen infiltration. Another option is that, being the mass of the sample so small, it could have been dispersed in the reactor or dragged by the gases.



Figure 48. Appearance of the sample at the end of the second test.

The next tests will be performed with some changes allowing to better control the atmosphere in the reactor and to increase the mass of the sample, using a different method of placing it inside the tube.

### **6.4.3 Microreactor: 3<sup>rd</sup> test**

In this new test two important variations have been implemented:

- 1) Aluminium was directly inserted as powder in a swab of quartz wool (Figure 49), closed and positioned at the center of the tube. No more alumina spheres as supporting media were used, as they proved to be difficult to handle (the material load on the spheres was too limited, and their removal from the tube was complicated).
- 2) The temperature of oxidation was not constant anymore, and a temperature ramp has been realized in order to test the material from 500°C to 900°C with continuous temperature increase while sending water. Before, the sample has been kept in inert atmosphere (N<sub>2</sub>) until the start of the temperature ramp with water.



Figure 49. Sample of aluminium in the quartz wool for tube-in-tube reactor testing.

The tested sample mass (first batch, with higher mean particle size) was 101.3 mg, the dry gas flow rate 400 ml/min (of N<sub>2</sub>) and the oxidation was performed in 30% H<sub>2</sub>O, corresponding to a steam mass flow rate of 8.27 g/h. According to literature [28], the presence of H<sub>2</sub>O strongly influences the behavior of the reaction, but increasing the concentration does not lead to significant changes; practically, from 30% to 100% H<sub>2</sub>O the behavior is very similar, with differences only in the range 650-850°C and in the peak corresponding to the melting point. Therefore, a concentration of 30% has been selected for the test assuming it is sufficient for a coherent reaction mechanism and not too high to risk possible accumulation in the circuit.

The sample was heated up to 500°C in N<sub>2</sub> (400 ml/min) with a temperature ramp of 20 K/min and stayed at this level for 5 minutes. After, water was sent and temperature was increased with a ramp of 10 K/min, until 900°C.

This time, the results of oxidation are evident, with two significant peaks in correspondence with the phase changes (Figure 50). From literature, peaks are expected at around 550°C (transformation to  $\gamma$ -alumina) and 660°C (melting point). In our case, peaks appear at a higher temperature (600°C and 710°C) but spaced as expected. The reason could be that the temperature revealed by the furnace controller is the one of the ceramic heater, while the sample itself is subjected to a delay in the order of some minutes. Practically, if the x-axis is shifted of -50°C, the peaks fall exactly where expected (550°C and 660°C); this means that probably the temperature of the sample is in delay with respect to the temperature of the furnace of about 5 minutes.

## Experimental analysis

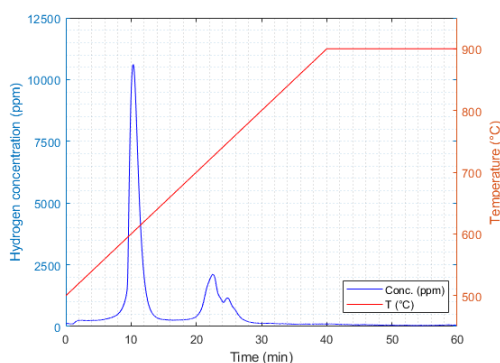


Figure 50. Results of the test in the reactor (Al-H<sub>2</sub>O) with temperature ramp.

Integrating the flow rate of hydrogen that can be calculated starting from the concentration, it is found a total amount of 13.66 ml of H<sub>2</sub> (1.23 mg) produced during the test leading to a yield of 135 ml/g, that is a quite low value. Relating the total volume with temperature (applying the correction of 50°C delay) the result is a cumulative curve in which the two steps of oxidation are evident (Figure 51). Therefore, the reaction of simple aluminium powder with steam is confirmed to occur, even at temperatures below the melting point. On the other hand, the results show a low reactivity at higher temperatures (after 750°C the curve flattens a lot). Since, from stoichiometry of reaction, the potential production of hydrogen is much higher than what produced with this sample mass, the oxidation at the end of the test is not completed.

The reason for the reaction stop has been proven to be the positioning of the sample in the tube. In fact, without a supporting medium, it moved from its initial position into a spot at much lower temperature due to gas drag, where reaction could not proceed. This fact led to an addition of a supporting bar into the tube, to keep the sample in position.

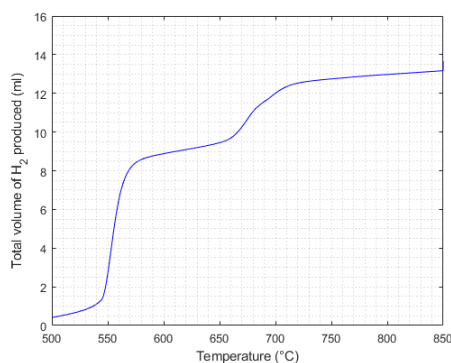


Figure 51. Integrated flow of hydrogen during the test with respect to (corrected) temperature.

## **6.5 TGA tests – oxidation in air**

After the first preliminary tests in the reactor, useful to optimize the experimental setup, aluminium oxidation in air has been tested in thermogravimetric analysis (TGA). Literature references are numerous for this topic, therefore the tests could represent a good mean to verify the reactivity of the sample and to check the compliance and repeatability of results.

### **6.5.1 Temperature programmed oxidation (TPO) in air**

In the first test, a sample of 31.8 mg of aluminium, placed in a small alumina crucible, has been tested in a TPO (temperature programmed oxidation), during a temperature ramp. The sample has been heated in two stages: in the first one, from the ambient temperature to 300°C, with a rate of 20 K/min, no reactivity is expected, and therefore it has just been heated in inert atmosphere (100 ml/min of Ar). It was kept at 300°C for 15 min in Ar, considering this temperature as the effective starting point of the experiment. The second stage of heating is the one in which oxidation is expected: the material reaches 1500°C starting from 300°C through a linear ramp, in an oxidizing atmosphere composed of a mixture of 50% Ar and 50% air, maintaining constant the total flow rate of 100 ml/min. In this way, the total fraction of oxygen (the only oxidizing agent) in the flow is 10%, the rest is inert (50% Ar, 40% N<sub>2</sub>). The temperature ramp has been set to 10 K/min. Once 1500°C are reached, the sample is kept at this temperature in the same oxidizing atmosphere for 5 minutes, in which the oxidation is expected to finish, if not already completed before. Finally, to bring back the sample to ambient temperature, a decreasing ramp of 20 K/min is set, in inert atmosphere.

The temperature program and the results of the mass variation of the sample during time in the TGA are reported in Figure 52.

## Experimental analysis

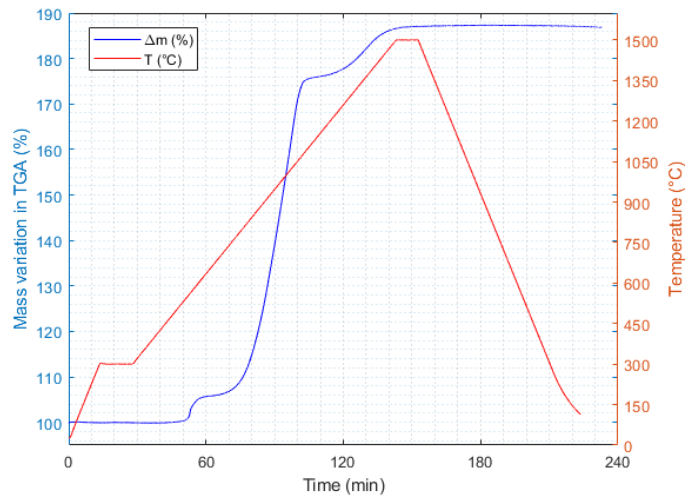


Figure 52. TGA results of aluminium oxidation in air (temperature ramp and % mass variation in time).

The mass variation of the sample is reported as percentage of the initial mass of the sample, and it is due to the addition of oxygen to the material during oxidation. The final mass percentage variation has been found in 187.1%, confirming the expected result from theory. Moreover, three steps are evident, corresponding to the three phase variations previously explained in 3.1.2. Once the temperature of 1500°C is reached, the sample does not increase its mass anymore, because the oxidation is completed. Of course, it remains constant also during the descending ramp. The time needed for the complete oxidation during this kind of temperature ramp can be estimated as 90 min (from min 50 to min 140 of the experiment).

Converting the graph in terms of temperature-mass, the relation of reaction rate with temperature is more evident (Figure 53). The onset of the first sharp increase is around 530°C, proceeding until 580°C. Then, no effect is present near the melting point (660°C), as expected during air oxidation, while the second rapid mass increase is between 750°C and 1050°C. To this point, the oxidation of the material is complete for 85%; the third and final stage is the ramp that concludes at 1500°C.

## Experimental analysis

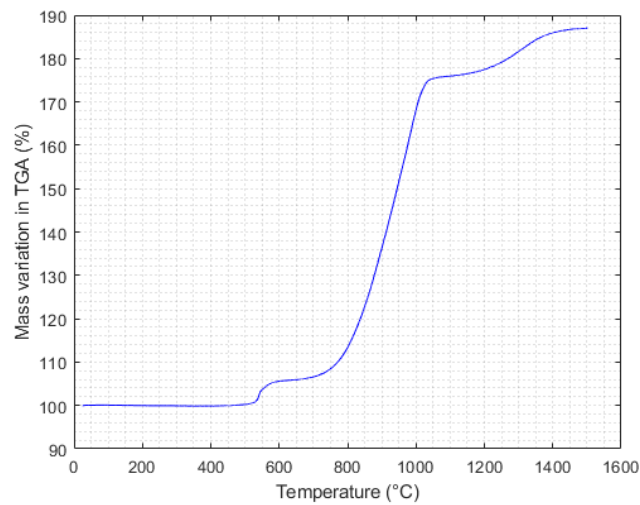


Figure 53. TGA results of aluminium oxidation in air (temperature vs mass variation).

The corresponding DTA results are reported in Figure 54.

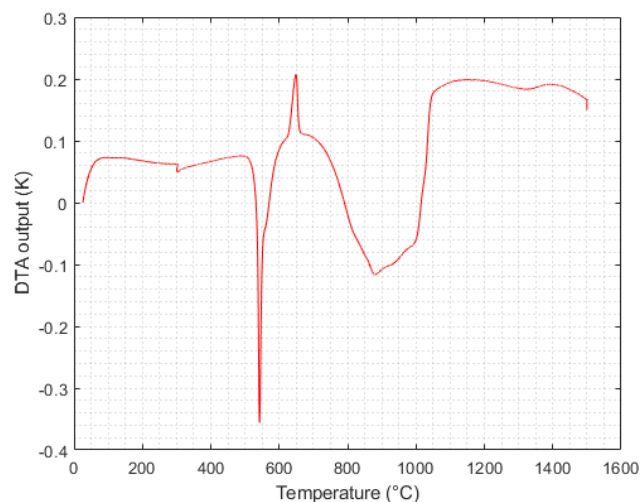


Figure 54. DTA results of aluminium oxidation in air (negative values for exothermicity).

In the graph, the various phase transitions are evident. In particular, at 540°C an exothermic peak is related to the transition to  $\gamma$ -alumina from the amorphous one. This peak is related to the first stage of oxidation visible in the TGA. The melting of aluminium is associated to an endothermic peak in DTA at 650-660°C, without a corresponding one in the TGA. Then, another – more gradual – exothermic stage is visible, corresponding to the second stage of oxidation; this corresponds to the gradual transition from  $\gamma$  to  $\theta$  alumina.

A visual inspection of the sample confirms the oxidation, passing from the grey powder of aluminium to the white solid of alumina. The reaction product appears as a hard and compact conglomerate of particles (Figure 55).

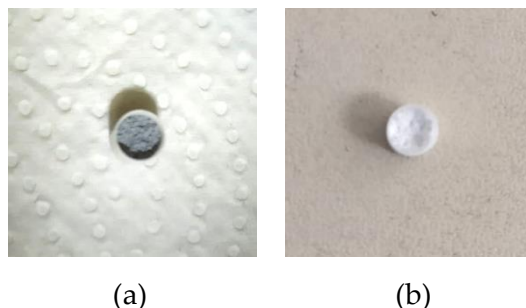


Figure 55. Aspect of aluminium sample before (a) and after (b) the air oxidation in TGA.

### **6.5.2 Isothermal test in air**

Following the TPO air oxidation performed in the TGA, and since almost no results were obtained in the isothermal oxidation at 900°C in the microreactor (in steam, with alumina spheres), a similar test has been carried out in TGA, with the aim to evaluate the reaction in air in isothermal mode. If the results of this test are negligible, it is possible to say that the aluminium oxidation has a better kinetics if temperature is changed dynamically during the reaction. The sample (40 mg) has been heated up in inert atmosphere (same as the TPO test) until 900°C, then it was subjected to a flow of air (10% O<sub>2</sub>) for 1 h. In this way, oxidation starts at 900°C and before this temperature the sample is still unreacted.

The results shown in Figure 56 reveal that an oxidation occurs, with higher reactivity in the initial part, and then decreasing in time. The first mass increase that can be seen from 30 to 50 min could be due to infiltration of air into the instrument, leading to some oxygen-driven oxidation before the setpoint temperature. The final plateau is instead due to the switching to the non-oxidizing atmosphere after 1 hour of test.

The focus on the oxidation period (1 h, Figure 57) shows a first stage in which, in less than 5 minutes, the sample gains 10% of its weight. After this (exothermal, as proved by a DTA analysis) peak, the reaction rate reduces continuously in time, to the point that, after 1 h, the oxidation is far from complete, with a 20% weight gain.

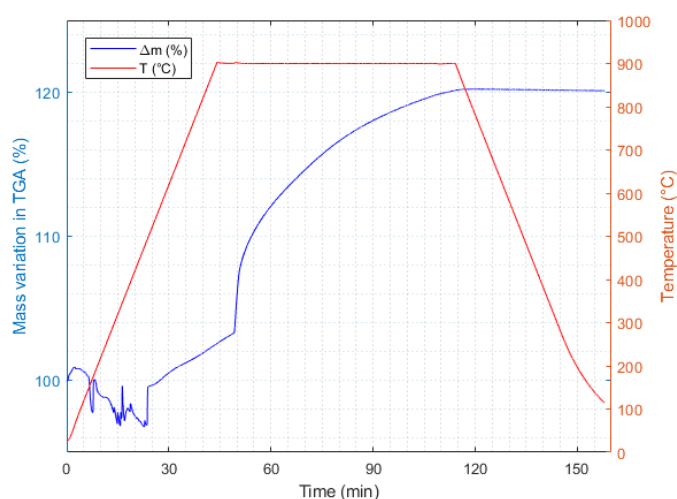


Figure 56. Temperature program and results of isothermal air oxidation in TGA.

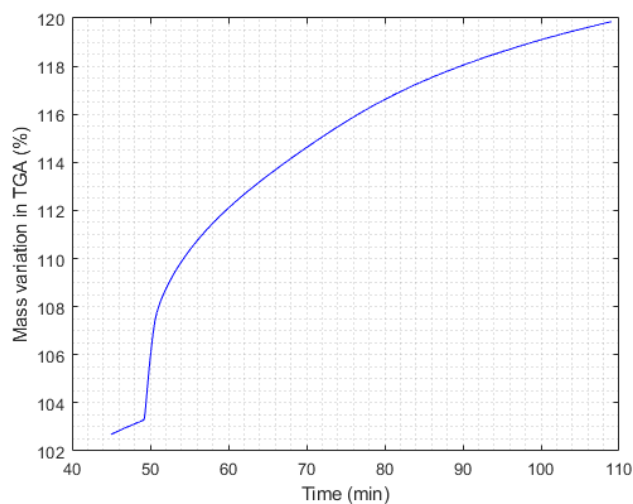


Figure 57. Focus on isothermal oxidation section: TGA results.

## 6.6 Tests in microreactor

Thanks to the good results of TGA and to a rearrangement of the experimental setup, the experiments collected in this section were considered successful, providing results in both isothermal and TPO using water steam as oxidant in the microreactor.

### 6.6.1 Isothermal water oxidation - 900°C

A mass of 127 mg of aluminium has been tested in the reactor proceeding with an isothermal oxidation in H<sub>2</sub>O, at a temperature of 900°C. To remove the highest possible amount of residual water in the circuit, the system is flushed with nitrogen at 400°C for

about 15 minutes (at this temperature water is easily vaporized and the sample still does not react meaningfully). Then, a ramp at 20 K/min is imposed to reach 900°C, for a time interval of 25 min always with the dry circuit, in 400 ml/min of N<sub>2</sub>. In this section of the experiment, analyzing the results it is evident that some residual water is still present in the circuit, since hydrogen has been produced, but the amount cannot be controlled. After reaching 900°C, the circuit is switched from dry to wet, and a 30% concentration of water is sent for 3 hours. In Figure 58 the evolution of H<sub>2</sub> concentration in the outlet flow is reported together with the temperature of the furnace.

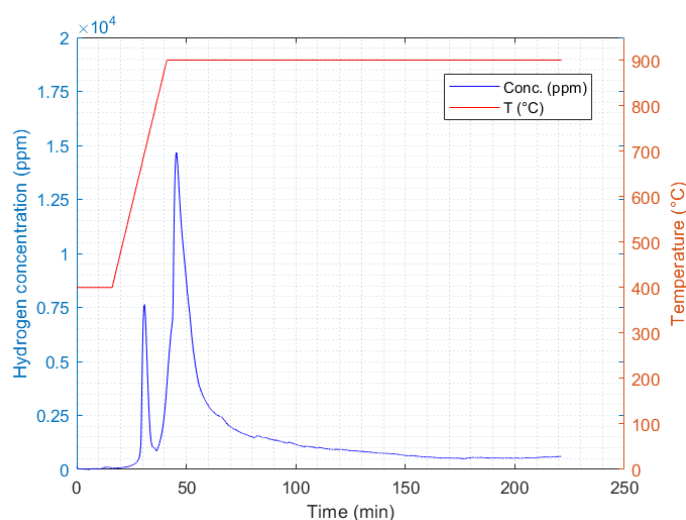


Figure 58. Concentration and temperature in the isothermal water oxidation in microreactor.

A first (unwanted) peak of production is present between the microstructural change of Al (550°C) and the melting point (660°C), due to some residual water, impossible to remove from the circuit. Then, once 900°C are reached, another (higher) peak is present, corresponding to the start of isothermal oxidation, as water is sent.

Isothermal oxidation proceeds initially with a high reaction rate, when water starts to be fed in the reactor. Then, hydrogen continues to be produced, but at a lower and lower rate, however the production is not negligible: around 500 ppm are still detected by the instrument. They cannot be related with a calibration error since at the end of the test, after flushing the circuit with nitrogen, the concentration reached again the zero, confirming that the concentration of hydrogen after 3 hours was still due to a production from the sample.

The total volume of H<sub>2</sub> produced is 130.65 ml, leading to a generation yield of 1028.8

ml/g, and with a conversion yield of 83%, the best result in all the tests in microreactor, also because it was the longest one. The evolution of produced hydrogen can be seen in the graph of Figure 59.

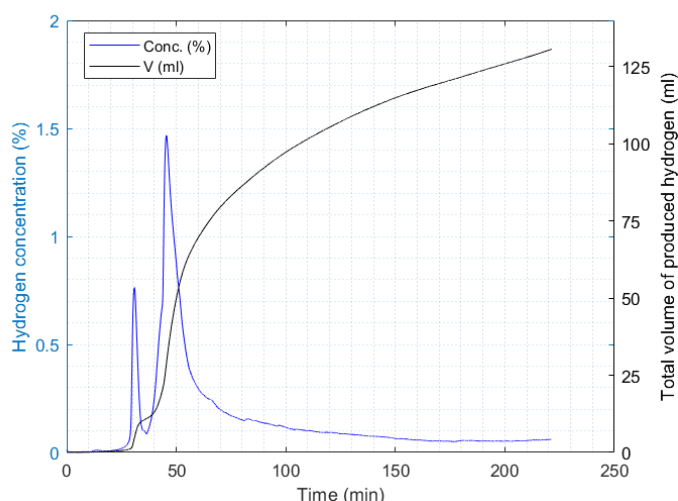


Figure 59. Concentration and evolution of hydrogen volume produced in the isothermal water oxidation in microreactor.

The effect of oxidation before the set point temperature is quantified evaluating the production until 900°C, where some residual uncontrolled water made possible the reaction. Before the isothermal oxidation, the sample was oxidized for its 10% and 15.51 ml of H<sub>2</sub> were produced. This means that, actually, the amount of hydrogen produced during the isothermal oxidation should be reduced of this quantity, lowering it to 115.14 ml.

### 6.6.2 TPO in water

Since the experimental setup is finally established and gives repeatable and coherent results, the following test is a temperature-programmed oxidation in the microreactor. A sample of 108 mg is brought to 450°C in inert atmosphere, then a temperature ramp of 10 K/min is set, up to 1000°C, for a duration of 55 minutes, using the “vapo” circuit (30% H<sub>2</sub>O concentration). At this final temperature, the oxidation should be almost complete. Anyway, the sample is kept at 1000°C sending water still for 1 hour.

Results of the test are reported in Figure 60. Two peaks are evident during the phase changes of the material, below 700°C. Then, between 700 and 800°C the reaction rate is quite low, then a sharp increase can be noted, with the maximum detectable hydrogen

concentration in the analyzed flow of more than 3.5% at around 980°C, the highest result in all the tests. Performing the integral calculation, reported in Figure 61, it is possible to assess that the total volume of H<sub>2</sub> produced is 102.03 ml, with a generation yield of 945 ml/g and a final aluminium conversion of 76% after around 2 h of oxidation.

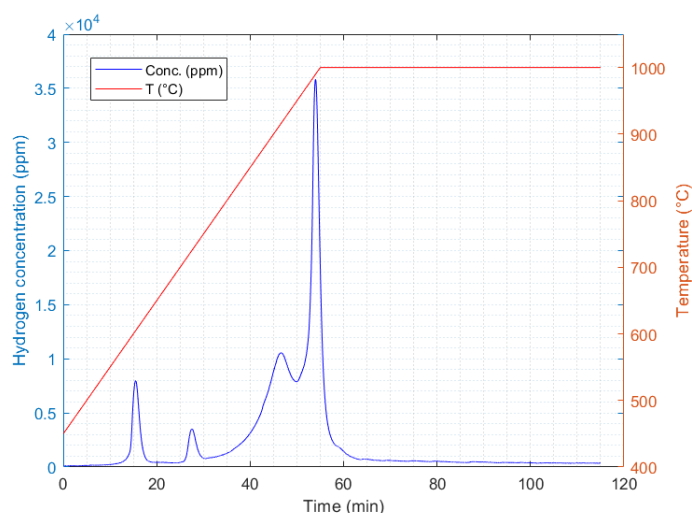


Figure 60. TPO in microreactor: H<sub>2</sub> concentration and temperature ramp

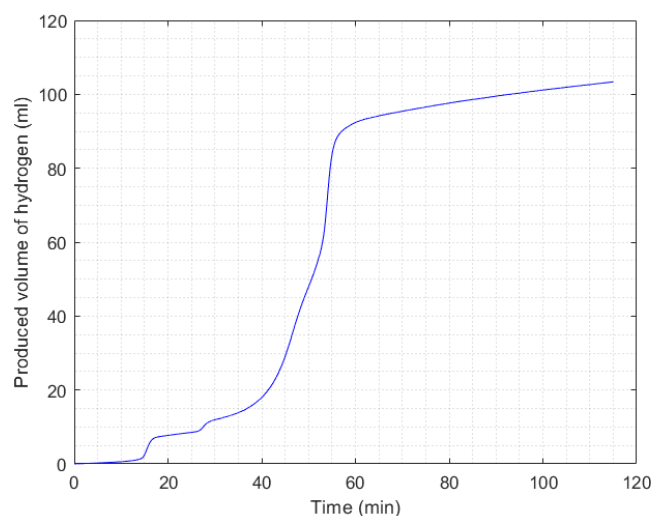


Figure 61. TPO in microreactor: produced volume of H<sub>2</sub>.

### 6.6.3 Isothermal water oxidation - 950 and 1000°C

To evaluate the isothermal performance of the material, it would be necessary to guarantee that no water is sent into the system before the setpoint temperature is reached. Unfortunately, the experimental setup has proven to be not sufficiently hermetic to water infiltration or accumulation, so that an uncontrollable amount sent during the

## Experimental analysis

ramp cannot be avoided. Therefore, to reduce to the minimum this effect, the temperature ramp of the furnace has been set to the maximum (so that the time passed below the setpoint is minimized), also because it is no more of interest what happens below 1000°C in ramp, since it has been effectively studied in the previous TPO.

Following the same procedure, the isothermal oxidation is evaluated both at 950°C and 1000°C. A sample of 127 mg (chosen in order to have comparable results with the 900°C oxidation, done with the same mass) is kept in inert atmosphere during the temperature ramp, with the maximum power sustained by the furnace. Once setpoint is reached, circuit is switched to wet and 30% water is sent for 1 hour.

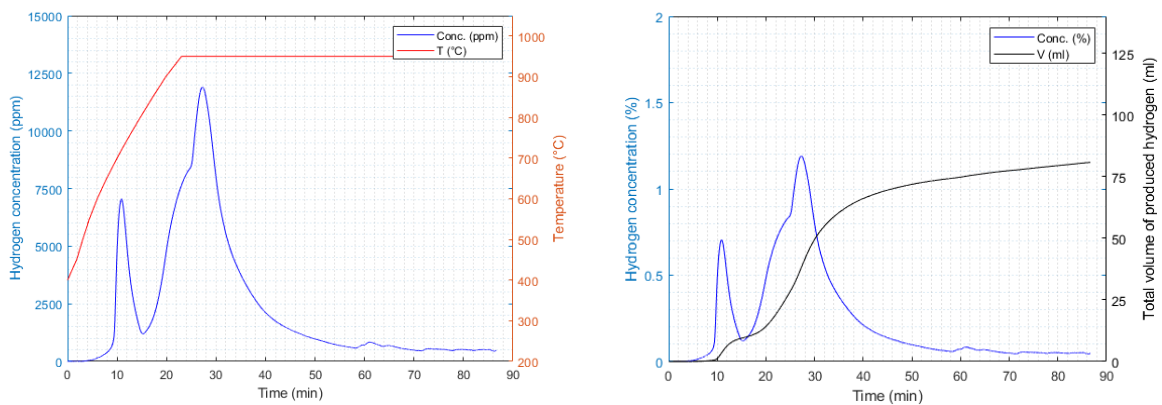


Figure 62. Results of isothermal oxidation in water at 950°C.

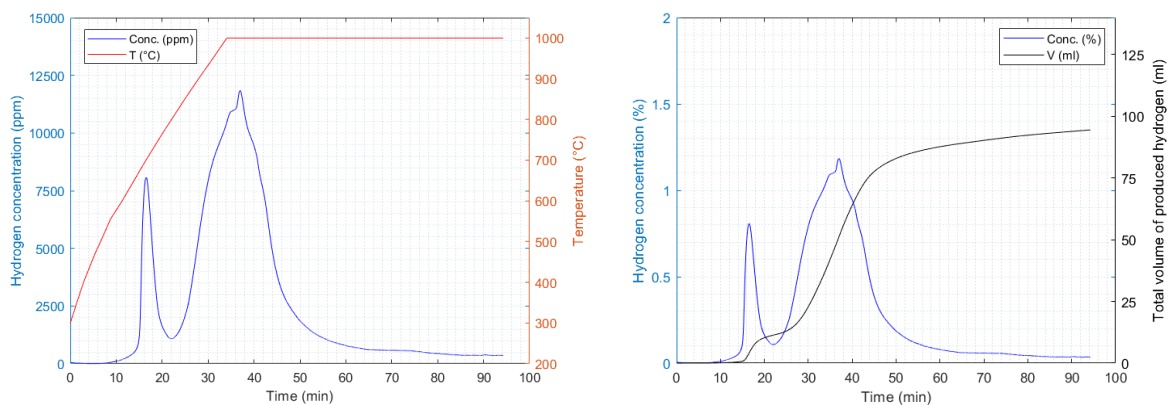


Figure 63. Results of isothermal oxidation in water at 1000°C.

As clearly visible in Figure 62 and Figure 63, the production of hydrogen during the temperature ramp could not be avoided due to the experimental setup. It is possible to assess that, during the ramp and before fixing the temperature, the sample was oxidized to its 15% (950°C) and 24% (1000°C). However, a peak during the sending of water is visible, increasing the rate of reaction when the circuit is switched to wet.

Final yield of the test was 52.2% (644.6 ml/g) at 950°C and 60.4% (747.5 ml/g) at 1000°C, showing that the reaction proceeds faster at higher temperature.

#### 6.6.4 TPO in water – sample with finer particle size

This last test had the objective to evaluate the effect of particle size, using the second batch of aluminium powder with much finer appearance (particle size < 5 µm). Since the TPO has been the test with the most accurate results among the ones performed in microreactor, the second batch has been tested in TPO with the same parameters (heating rate, reaction times, methods) as the previous one (6.6.2). Tested sample mass was 113 mg. Results (Figure 64) show two clear peaks, one before the melting point (with higher magnitude) and one around the setpoint temperature of 1000°C.

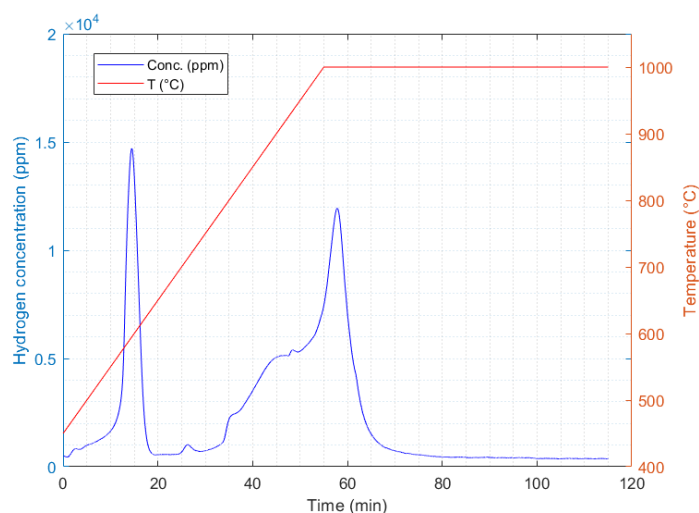


Figure 64. TPO with the second batch, with finer aluminium powder.

Total hydrogen production has been 103.93 ml, with a reaction yield of 920 ml/g and a conversion of 74%.

## 6.7 Discussion

The experimental analysis showed the possibility of performing aluminium oxidation at high temperature without using any particular treatments, catalysts, or other activation techniques. Reaction times are comparable to what found in literature, with long time required for complete the oxidation of all the samples.

TGA, performed in air, confirmed that the isothermal reaction is much slower than the temperature ramp, with many hours required to complete the process. Experiments in

TGA exactly reflect what expected from literature.

Experiments in microreactor have been trickier being difficult to avoid the presence of residual water in the circuit. In this framework, the most realistic test has been the one in temperature ramp, in which the different phases of aluminium oxidation are very clear. From literature, the expectation was to complete the reaction at  $T \approx 1000^\circ\text{C}$ , while in our test, with a total duration of about 2 h, oxidation reached only 74%. Actually, the sample kept producing hydrogen at  $1000^\circ\text{C}$  in a non-negligible way, therefore it is probable that the process would have been completed if 2-3 more hours were available. Anyway, the yield of this test is the best obtained among all the attempts if compared on the same interval of time. This confirms that, also for water oxidation, performing temperature ramp is more effective than the isothermal oxidation.

### 6.7.1 Effect of temperature in isothermal oxidation

The effect of temperature in isothermal oxidation has been analyzed performing the same test at  $900^\circ\text{C}$ ,  $950^\circ\text{C}$  and  $1000^\circ\text{C}$ . The results, collected in Table 15, show a similar conversion yield for  $900^\circ\text{C}$  and  $1000^\circ\text{C}$  tests (total duration considered is 80 minutes, comprehensive of a first uncontrolled part in ramp and a second isothermal part). Instead, at  $950^\circ\text{C}$  the reaction seems slightly slower.

Table 15. Integral results of isothermal oxidation in water at different temperatures.

T ( $^\circ\text{C}$ )	V <sub>tot</sub> (ml)	Conversion (%)	Yield (ml/g)
900	100.86	64.2	794.2
950	81.86	52.2	644.6
1000	94.93	60.4	747.5

To compare the evolution of hydrogen in time for the three temperatures, three different graphs can be considered. In the first one (Figure 65) it is reported the complete oxidation peak, comprehensive of the time spent in temperature ramp and in isothermal mode. The results have been taken starting from the point in which 1000 ppm are reached (considered the start of the peak), for a duration of 1 h. It can be seen that at  $900^\circ\text{C}$  the peak seems higher, and the reaction seems to continue with a higher pace, while peaks at  $950^\circ\text{C}$  and  $1000^\circ\text{C}$  reach the same maximum value, as they also stabilize to a very similar value in the second part of the test.

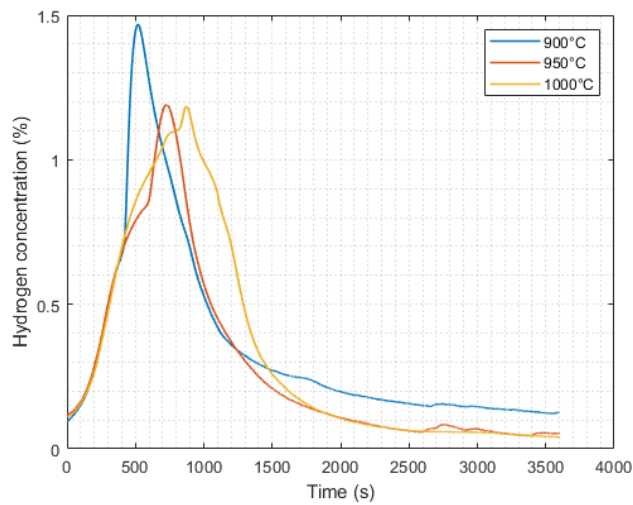


Figure 65. Comparison of isothermal oxidation in water at 900°C, 950°C and 1000°C – full peak.

In Figure 66 a focus of the isothermal part is reported, that is, starting from the point in which a controlled flow of water is injected at the setpoint temperature, and tracing the trend for the next 45 minutes. In this way the peak occurs at the same point in time for all three experiments.

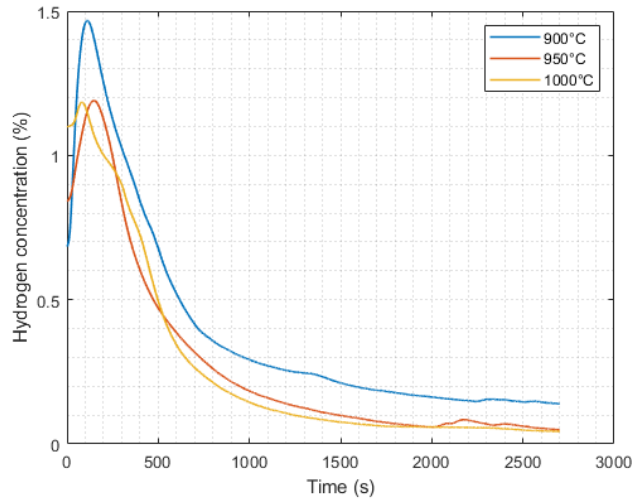


Figure 66. Comparison of isothermal oxidation in water at 900°C, 950°C and 1000°C – isothermal peak only.

Finally, the integral corresponding to the evolution of hydrogen volume is also computed, as reported in Figure 67. The first part of oxidation is superimposable for all three cases, confirming the repeatability of the experiment. Then, similar profiles are found for 950°C and 1000°C reaction, with higher yield for the latter, and with a very slow reaction after the first peak is done. Instead, at 900°C the reaction proceeds initially

slower than 1000°C, but in the second part the rate is much higher than the other two cases, with a higher global result.

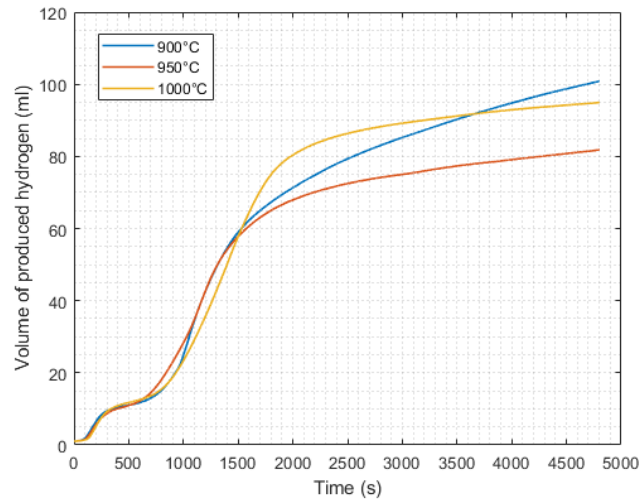


Figure 67. Comparison of isothermal oxidation in water at 900°C, 950°C and 1000°C – integral values of produced hydrogen volume.

An interesting aspect is that in the first part before/near the melting point only one peak is visible, differently than the results of the TPO (6.6.2) that showed two peaks. This could be due to the different heating rate of the tests, with the TPO performed at 10 K/min while the isothermal one at the highest rate achievable by the furnace, that is variable depending on temperature but in the range of 20-30 K/min. Another possibility is that the uncontrolled water concentration in the isothermal tests during the ramp is too low to make visible a peak during the melting of the metal, as expected from literature (peak corresponding to melting is only present at sufficiently high water concentration).

### 6.7.2 Effect of particle size

The effect of particle size has been evaluated during a TPO. Data on the maximum diameter related to the coarse powder could not be found, while the fine powder was guaranteed with average particle size  $< 5 \mu\text{m}$ . A visual inspection (Figure 68) shows that the first batch appears much more agglomerated and coarser than the second one, that is much more volatile.



Figure 68. Appearance of the coarse powder (a) and fine powder (b).

A comparison of the two tests, with the hydrogen concentration during time, is reported in Figure 69.

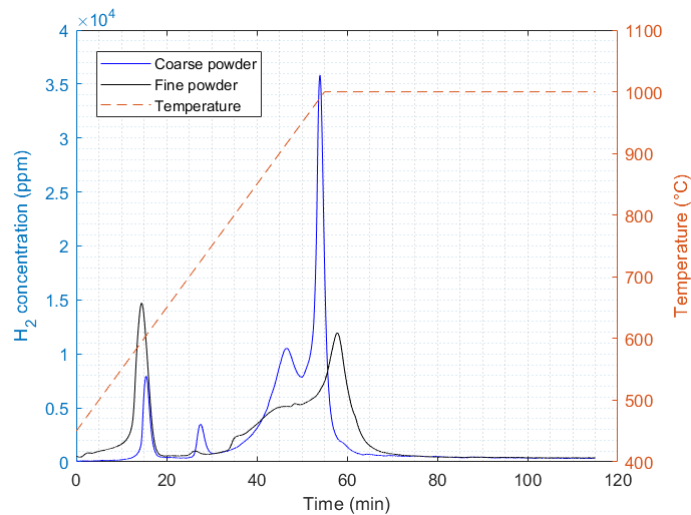


Figure 69. Comparison of detected H<sub>2</sub> concentration from the TPO of coarse and fine powder.

The evolution of hydrogen in time is quite different in the two cases. Considering the coarse powder, the test reflects what expected, with the presence of 2 initial peaks (one related to the microstructural change in solid phase, the other related to the process of melting) with lower magnitude with respect to the main one, placed between 900°C and 1000°C. Instead, for the fine powder the first oxidation peak is even bigger than the one at higher temperature. The maximum value of the first concentration peak is almost the double of the one detected in the coarse powder, and its duration is longer. Moreover, the sample started its oxidation at much lower temperatures, with H<sub>2</sub> concentrations >1000 ppm already before 500°C. This fact proves a better reactivity of fine powder when the sample is in solid phase. After this temperature, another difference is that with the fine powder the peak corresponding to melting is practically negligible. Finally, a more

gradual oxidation proceeds until a second peak is visible, delayed and with much lower magnitude (about 1/3) compared to the coarse powder. After reaching the setpoint temperature, the production rates of the two powders are practically superimposable. At the end of 1 h of isothermal oxidation, both samples continued to produce hydrogen, with decreasing detected concentration (slightly lower than 400 ppm at the end of the test). Therefore, two different stages can be distinguished: in the first one (during temperature ramp and some minutes of isothermal oxidation, for a total of 70 minutes) the behavior of the two batches has substantial differences (Figure 70a), while after this point the two curves show a very similar trend (Figure 70b).

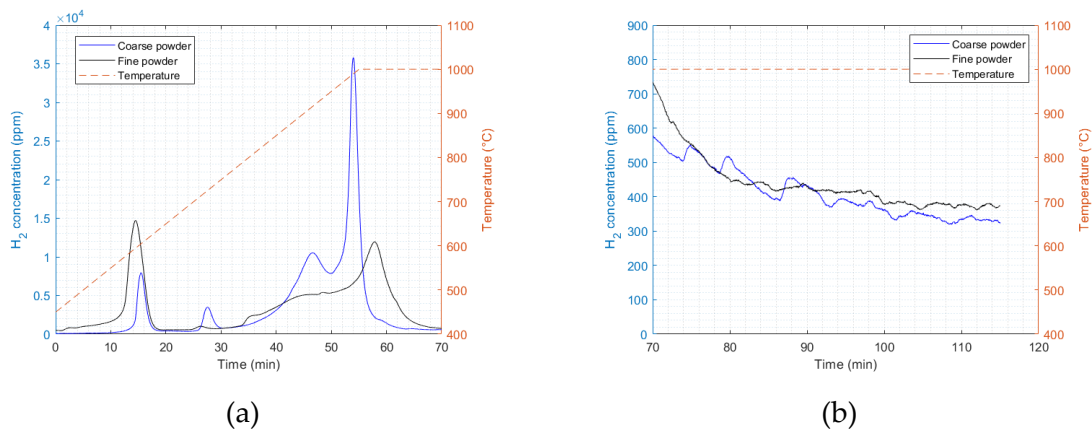


Figure 70. First (a) and second (b) stage of the TPO for the two different batches of Al powder.

The evolution of the volume of produced hydrogen, normalized by the sample mass, is shown in Figure 71. After 20 minutes, corresponding to a temperature of 650°C (sample is still solid) the fine powder already produced 221 ml<sub>H<sub>2</sub></sub>/g, corresponding to a conversion of 18%. Instead, coarse powder produced in the same period only 69 ml<sub>H<sub>2</sub></sub>/g, corresponding to a conversion of 6%.

Globally, the production of hydrogen is very similar in both the tests, with a conversion rate of 76% (coarse powder) and 74% (fine powder). Therefore, the real advantage of using a fine powder is not to have a higher global production, but to assure much better performances at low temperatures when the sample is still solid.

At higher temperatures (800-1000°C) coarse powder seems to have a higher reaction rate. Considering the interval between 40 and 60 minutes, the mean reaction rate is 0.572 ml/(g·s) for the coarse powder and 0.379 ml/(g·s) for the fine powder.

## Experimental analysis

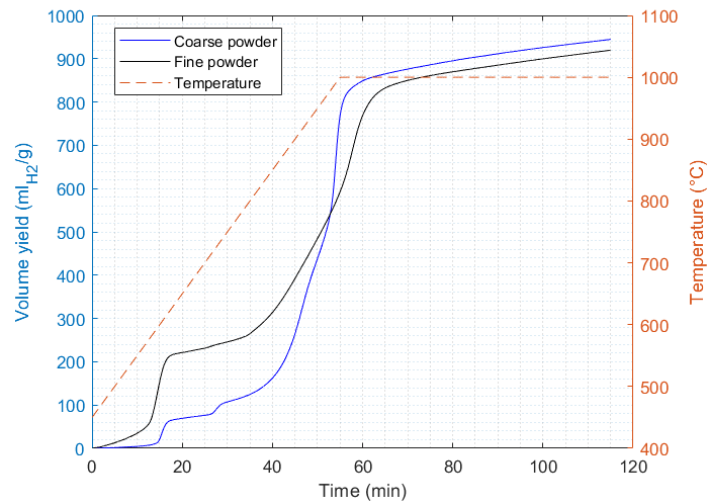


Figure 71. Comparison of calculated hydrogen volumetric yield from the TPO of coarse and fine powder.

The fact that the fine powder performed worse at high temperature could be due to the large oxidation already happened in solid phase, that created bigger particles of alumina, nullifying the positive effect of having fine powders. In theory, a fine powder in liquid phase would still contain small particles of solid alumina derived from the external oxide layer naturally present (since alumina melts at 2072°C) that could act as effective reaction sites. Instead, if the oxide grows, the surface area available for the reaction could reduce due to possible agglomeration. Anyway, further studies are needed (e.g., isothermal oxidation of fine powder at high temperature) to verify what is the real effect of reducing the particle size when reacting molten aluminium.

## 7 Conclusions

In this study, a comprehensive assessment of aluminium as energy storage material was presented. By performing a thermodynamic analysis, both the dry cycle and the wet cycle of aluminum have been studied, focusing on the latter. The demonstrated theoretical energy density of 23.3 kWh/l confirmed that aluminium is one of the most promising electrofuel for a zero-carbon compact energy production and storage. In order to reach high electrical efficiencies, the oxidation of Al with water has proven to be an effective process, exploiting the production of hydrogen from the reaction and its efficient utilization in fuel cells.

The case study on a regional level demonstrated the effectiveness of the material for P2P processes, in the context of long-term energy storage. The comparison with the more standard hydrogen-based P2P showed a slightly lower RTE (30.3% compared to 37.2%) but, if transportation consumption is taken into account, the hydrogen-based P2P rapidly decreases its RTE while aluminum-based one is almost non-sensitive. However, if current standard production methods for aluminium in smelters are considered, a non-negligible amount of CO<sub>2</sub> is emitted in the whole P2P (around 400 g/kWh stored), acting as the bottleneck of the process. The development of CO<sub>2</sub>-free production methods, already a viable technical solution, must be incentivized and pursued.

The model of an aluminum-based cogenerative power plant has been proposed and simulated in Aspen Plus. The plant, comprehensive of three generation section (SOFC, gas turbine and steam turbine), reached an electrical efficiency of 77.2% in the base configuration. The effect of varying the mass flow of reacting water has been simulated: with increasing excess of water, SOFC and steam turbine decrease their power output, while the microturbine slightly increases its one. The global effect is to decrease the electrical production, up to a point where the recovery steam cycle cannot produce power anymore (at a water excess of 350%). The effect of varying the temperature of reaction was also studied, showing low sensitivity of the system performances to this parameter (only -3% of global electrical efficiency increasing the temperature from 750°C to 1200°C). The experimental analysis focused on the production of hydrogen by the reaction of aluminium with H<sub>2</sub>O at temperatures of 900-1000°C. After some preliminary test carried out to optimize the experimental setup, both isothermal and TPO test were performed.

## Conclusions

The best results were obtained in TPO, showing that the oxidation of micron-sized aluminum powders in water steam shows different stages. The first one is related to a solid phase change of the material, the second corresponds to the melting point, and the third is placed at higher temperatures (starting from around 800°C, up to 1000°C). Isothermal tests have been more difficult to perform correctly due to the presence of residual water in the circuit, but they also provided meaningful results. Isothermal tests at 900°C, 950°C and 1000°C showed different behaviors, with efficient hydrogen production especially at 900°C (a yield of 1028.8 ml/g and a conversion of 83% was calculated during a 3 h test). Aluminium was also tested in TGA in order to assess the reaction with oxygen, finding the results expected from experimental literature and proving the reactivity of the powder. The last test in microreactor showed the effect of changing the particle size: a smaller mean particle diameter relates to increased peak of oxidation when the sample is solid (about 3 times more hydrogen is produced in this phase), while after the melting point the highest production rate seems to be the one with the coarser powder.

As aluminum is not considered a developed electrofuel yet, research should continue to investigate the various aspects linked to the production and utilization of this energy-dense metal. Some interesting and requested research pathways could be:

- The optimization of the aluminium production methods in smelters. Current production based on Hall-Héroult process still cannot be considered CO<sub>2</sub>-free even if the input electricity is completely green: research on inert anodes, wettable cathodes and other related technology is crucial for the development of a carbon-free aluminum supply chain.
- The life cycle assessment of the material. Using aluminum as energy vector would require building an infrastructure that must be evaluated for the entire lifecycle of each component, to check the actual circularity of the process.
- Experimental analysis on Al-water reaction using commercial-grade aluminium, at different reaction parameters. The optimization of Al-H<sub>2</sub>O reaction is the first step needed to make possible the construction of a hypothetical first reactor. The construction of reaction models for different conditions would be another important topic, in order to drive the experimental research.

## 8 References

- [1] H. Ritchie, M. Roser, and P. Rosado, "CO<sub>2</sub> and Greenhouse Gas Emissions," *Our World in Data*, 2020. <https://ourworldindata.org/co2-and-other-greenhouse-gas-emissions> (accessed Nov. 08, 2022).
- [2] International Energy Agency, "World Energy Outlook 2022," 2022.
- [3] A. P. M. Velenturf and P. Purnell, "Principles for a sustainable circular economy," *Sustainable Production and Consumption*, vol. 27. Elsevier B.V., pp. 1437–1457, Jul. 01, 2021. doi: 10.1016/j.spc.2021.02.018.
- [4] T. M. Alabi, F. D. Agbajor, Z. Yang, L. Lu, and A. J. Ogungbile, "Strategic potential of multi-energy system towards carbon neutrality: A forward-looking overview," *Energy and Built Environment*. KeAi Communications Co., 2022. doi: 10.1016/j.enbenv.2022.06.007.
- [5] M. J. Palys and P. Daoutidis, "Power-to-X: A review and perspective," *Comput Chem Eng*, vol. 165, p. 107948, Sep. 2022, doi: 10.1016/J.COMPCHEMENG.2022.107948.
- [6] H. Ababneh and B. H. Hameed, "Electrofuels as emerging new green alternative fuel: A review of recent literature," *Energy Conversion and Management*, vol. 254. Elsevier Ltd, Feb. 15, 2022. doi: 10.1016/j.enconman.2022.115213.
- [7] J. M. Bergthorson, "Recyclable metal fuels for clean and compact zero-carbon power," *Progress in Energy and Combustion Science*, vol. 68. Elsevier Ltd, pp. 169–196, Sep. 01, 2018. doi: 10.1016/j.pecs.2018.05.001.
- [8] M. Baumann, L. Barelli, and S. Passerini, "The Potential Role of Reactive Metals for a Clean Energy Transition," *Advanced Energy Materials*, vol. 10, no. 27. Wiley-VCH Verlag, Jul. 01, 2020. doi: 10.1002/aenm.202001002.
- [9] European Commission, "Critical Raw Materials for Strategic Technologies and Sectors in the EU - a foresight study," 2020. doi: 10.2873/865242.
- [10] J. M. Bergthorson *et al.*, "Metal-water combustion for clean propulsion and power generation," *Appl Energy*, vol. 186, pp. 13–27, Jan. 2017, doi: 10.1016/j.apenergy.2016.10.033.
- [11] L. Yaqoob, T. Noor, and N. Iqbal, "An overview of metal-air batteries, current progress, and future perspectives," *J Energy Storage*, vol. 56, p. 106075, Dec. 2022, doi: 10.1016/j.est.2022.106075.

## References

- [12] A. G. Olabi *et al.*, “Metal-air batteries—a review,” *Energies*, vol. 14, no. 21. MDPI, Nov. 01, 2021. doi: 10.3390/en14217373.
- [13] J. M. Bergthorson *et al.*, “Direct combustion of recyclable metal fuels for zero-carbon heat and power,” *Appl Energy*, vol. 160, pp. 368–382, Dec. 2015, doi: 10.1016/j.apenergy.2015.09.037.
- [14] E. I. Shkolnikov, A. Z. Zhuk, and M. S. Vlaskin, “Aluminum as energy carrier: Feasibility analysis and current technologies overview,” *Renewable and Sustainable Energy Reviews*, vol. 15, no. 9, pp. 4611–4623, Dec. 2011. doi: 10.1016/j.rser.2011.07.091.
- [15] A. Senanu Samuel and Solheim, “Biocarbon in the Aluminium Industry: A Review,” in *Light Metals 2021*, L. Perander, Ed., Cham: Springer International Publishing, 2021, pp. 649–656.
- [16] A. S. Yasinskiy, S. K. Padamata, P. V. Polyakov, and A. V. Shabanov, “An update on inert anodes for aluminium electrolysis,” *Non-ferrous Metals*, vol. 48, no. 1, pp. 15–23, 2020, doi: 10.17580/nfm.2020.01.03.
- [17] L. Barelli *et al.*, “Reactive Metals as Energy Storage and Carrier Media: Use of Aluminum for Power Generation in Fuel Cell-Based Power Plants,” *Energy Technology*, vol. 8, no. 9, Sep. 2020, doi: 10.1002/ente.202000233.
- [18] “REVEAL storage,” 2022. <https://www.reveal-storage.eu/> (accessed Nov. 15, 2022).
- [19] “Reaction of Aluminum with Water to Produce Hydrogen A Study of Issues Related to the Use of Aluminum for On-Board Vehicular Hydrogen Storage,” 2008.
- [20] NIST, “NIST Chemistry WebBook.” <https://webbook.nist.gov/chemistry/> (accessed Nov. 17, 2022).
- [21] S. S. Zumdahl and S. A. Zumdahl, *Chemistry*. Houghton Mifflin, 2007.
- [22] A. Qiyuan Chen and W. Zeng, “Calorimetric determination of the standard enthalpies of formation of gibbsite,” 1996.
- [23] M. Y. Haller, D. Carbonell, M. Dudita, D. Zenhäusern, and A. Häberle, “Seasonal energy storage in aluminium for 100 percent solar heat and electricity supply,” *Energy Conversion and Management: X*, vol. 5, Jan. 2020, doi: 10.1016/j.ecmx.2019.100017.
- [24] M. Digne, P. Sautet, P. Raybaud, H. Toulhoat, and E. Artacho, “Structure and stability of aluminum hydroxides: A theoretical study,” *Journal of Physical Chemistry B*, vol. 106, no. 20, pp. 5155–5162, May 2002, doi: 10.1021/jp014182a.

## References

- [25] Z. Y. Deng, J. M. F. Ferreira, Y. Tanaka, and J. Ye, "Physicochemical mechanism for the continuous reaction of  $\gamma$ -Al<sub>2</sub>O<sub>3</sub>-modified aluminum powder with water," *Journal of the American Ceramic Society*, vol. 90, no. 5, pp. 1521–1526, May 2007, doi: 10.1111/j.1551-2916.2007.01546.x.
- [26] N. S. Shaitura, O. O. Laricheva, and M. N. Larichev, "Studying the Mechanism of the Low-Temperature Oxidation of Microsized Aluminum Powder by Water," *Russian Journal of Physical Chemistry B*, vol. 13, no. 2, pp. 231–244, Mar. 2019, doi: 10.1134/S1990793119020088.
- [27] M. A. Trunov, M. Schoenitz, X. Zhu, and E. L. Dreizin, "Effect of polymorphic phase transformations in Al<sub>2</sub>O<sub>3</sub> film on oxidation kinetics of aluminum powders," *Combust Flame*, vol. 140, no. 4, pp. 310–318, Mar. 2005, doi: 10.1016/j.combustflame.2004.10.010.
- [28] M. Schoenitz, C. M. Chen, and E. L. Dreizin, "Oxidation of aluminum particles in the presence of water," *Journal of Physical Chemistry B*, vol. 113, no. 15, pp. 5136–5140, Apr. 2009, doi: 10.1021/jp807801m.
- [29] D. Davis, F. Müller, W. L. Saw, A. Steinfeld, and G. J. Nathan, "Solar-driven alumina calcination for CO<sub>2</sub> mitigation and improved product quality," *Green Chemistry*, vol. 19, no. 13, pp. 2992–3005, 2017, doi: 10.1039/c7gc00585g.
- [30] W. T. Choate and B. A. Incorporated John S Green, "U.S. Energy Requirements for Aluminum Production Historical Perspective, Theoretical Limits and Current Practices," 2007.
- [31] P. Goel, D. Dobhal, and R. C. Sharma, "Aluminum–air batteries: A viability review," *Journal of Energy Storage*, vol. 28. Elsevier Ltd, Apr. 01, 2020. doi: 10.1016/j.est.2020.101287.
- [32] D. Raptis, A. K. Seferlis, V. Mylona, C. Politis, and P. Lianos, "Electrochemical hydrogen and electricity production by using anodes made of commercial aluminum," *Int J Hydrogen Energy*, vol. 44, no. 3, pp. 1359–1365, Jan. 2019, doi: 10.1016/j.ijhydene.2018.11.202.
- [33] A. Z. Zhuk, V. I. Borzenko, E. A. Buzoverov, P. P. Ivanov, and E. I. Shkolnikov, "Comparative analysis of hydrogen production technologies: Hydrothermal oxidation of the 'carbonless' aluminum and water electrolysis," *Renew Energy*, vol. 197, pp. 1244–1250, Sep. 2022, doi: 10.1016/j.renene.2022.08.023.
- [34] H. Ersoy *et al.*, "Hybrid Energy Storage and Hydrogen Supply Based on Aluminum—a Multiservice Case for Electric Mobility and Energy Storage Services," *Adv Mater Technol*, vol. 7, no. 8, Aug. 2022, doi: 10.1002/admt.202101400.

## References

- [35] M. Teichert, M. Y. Haller, and F. Sick, "Aluminium redox cycle in comparison to pressurized hydrogen for the energy supply of multi-family houses," *Applications in Energy and Combustion Science*, vol. 13, Mar. 2023, doi: 10.1016/j.jaecs.2022.100098.
- [36] F. Franzoni, M. Milani, L. Montorsi, and V. Golovitchev, "Combined hydrogen production and power generation from aluminum combustion with water: Analysis of the concept," *Int J Hydrogen Energy*, vol. 35, no. 4, pp. 1548–1559, Feb. 2010, doi: 10.1016/j.ijhydene.2009.11.107.
- [37] M. S. Vlaskin, A. O. Dudoladov, O. A. Buryakovskaya, and G. N. Ambaryan, "Modelling of aluminum-fuelled power plant with steam-hydrogen enthalpy utilization," *Int J Hydrogen Energy*, vol. 43, no. 9, pp. 4623–4631, Mar. 2018, doi: 10.1016/j.ijhydene.2018.01.023.
- [38] W. Yang *et al.*, "Efficiency analysis of a novel electricity and heat co-generation system in the basis of aluminum–water reaction," *Int J Hydrogen Energy*, vol. 42, no. 6, pp. 3598–3604, Feb. 2017, doi: 10.1016/j.ijhydene.2016.08.207.
- [39] Wikipedia, "List of aluminium smelters." [https://en.wikipedia.org/wiki/List\\_of\\_aluminium\\_smelters](https://en.wikipedia.org/wiki/List_of_aluminium_smelters) (accessed Apr. 05, 2023).
- [40] N. Bloxsome, "Karmøy in full production." <https://aluminiumtoday.com/news/karmoy-in-full-production> (accessed Apr. 05, 2023).
- [41] S. Sgouridis, M. Ali, A. Sleptchenko, A. Bouabid, and G. Ospina, "Aluminum smelters in the energy transition: Optimal configuration and operation for renewable energy integration in high insolation regions," *Renew Energy*, vol. 180, pp. 937–953, Dec. 2021, doi: 10.1016/j.renene.2021.08.080.
- [42] N. Depree, R. Düssel, P. Patel, and T. Reek, "THE 'VIRTUAL BATTERY'-OPERATING AN ALUMINIUM SMELTER WITH FLEXIBLE ENERGY INPUT."
- [43] DOE, "Energy requirements for hydrogen gas compression and liquefaction as related to vehicle storage needs," 2009. [Online]. Available: [http://www.eere.energy.gov/hydrogenandfuelcells/hydrogen\\_publications.html#h2\\_storage](http://www.eere.energy.gov/hydrogenandfuelcells/hydrogen_publications.html#h2_storage)
- [44] H. Basma and F. Rodríguez, "Fuel cell electric tractor-trailers: Technology overview and fuel economy," 2022. [Online]. Available: [www.theicct.org](http://www.theicct.org)
- [45] J. M. Ogden, "HYDROGEN DELIVERY MODEL FOR H2A ANALYSIS: A SPREADSHEET MODEL FOR HYDROGEN DELIVERY SCENARIOS," 2004.

## References

- [46] C. Springer and A. Hasanbeigi, "Emerging Energy Efficiency and Carbon Dioxide Emissions-Reduction Technologies for Industrial Production of Aluminum," 2016.
- [47] Our World In Data, "Carbon intensity of electricity, 2022," 2023. <https://ourworldindata.org/grapher/carbon-intensity-electricity> (accessed Apr. 28, 2023).
- [48] G. N. Ambaryan, M. S. Vlaskin, A. O. Dudoladov, E. A. Meshkov, A. Z. Zhuk, and E. I. Shkolnikov, "Hydrogen generation by oxidation of coarse aluminum in low content alkali aqueous solution under intensive mixing," *Int J Hydrogen Energy*, vol. 41, no. 39, pp. 17216–17224, Oct. 2016, doi: 10.1016/j.ijhydene.2016.08.005.
- [49] Y. Yavor, S. Goroshin, J. M. Bergthorson, D. L. Frost, R. Stowe, and S. Ringuette, "Enhanced hydrogen generation from aluminum-water reactions," *Int J Hydrogen Energy*, vol. 38, no. 35, pp. 14992–15002, Nov. 2013, doi: 10.1016/j.ijhydene.2013.09.070.
- [50] L. Barelli, L. Trombetti, A. Di Michele, L. Gammaitoni, J. Asenbauer, and S. Passerini, "Aluminum Steam Oxidation in the Framework of Long-Term Energy Storage: Experimental Analysis of the Reaction Parameters Effect on Metal Conversion Rate," *Energy Technology*, vol. 10, no. 9, Sep. 2022, doi: 10.1002/ente.202200441.
- [51] V. Shmelev, H. Yang, and C. Yim, "Hydrogen generation by reaction of molten aluminum with water steam," *Int J Hydrogen Energy*, vol. 41, no. 33, pp. 14562–14572, Sep. 2016, doi: 10.1016/j.ijhydene.2016.05.277.